Development of a Robust and Integrated Methodology for Predicting the Reliability of Microelectronic Packaging Systems

by

Ali Fallah-Adl

A Dissertation Presented in Partial Fulfillment
of the Requirements for the Degree
Doctor of Philosophy

Approved November 2012 by the
Graduate Supervisory Committee:

Amaneh Tasooji, Chair
Stephen Krause
Terry Alford
Hanqing Jiang
Ravi Mahajan

ARIZONA STATE UNIVERSITY

May 2013

ABSTRACT

Ball Grid Array (BGA) using lead-free or lead-rich solder materials are widely used as Second Level Interconnects (SLI) in mounting packaged components to the printed circuit board (PCB). The reliability of these solder joints is of significant importance to the performance of microelectronics components and systems. Product design/form-factor, solder material, manufacturing process, use condition, as well as, the inherent variabilities present in the system, greatly influence product reliability. Accurate reliability analysis requires an integrated approach to concurrently account for all these factors and their synergistic effects. Such an integrated and robust methodology can be used in design and development of new and advanced microelectronics systems and can provide significant improvement in cycle-time, cost, and reliability.

IMPRPK approach is based on a probabilistic methodology, focusing on three major tasks of (1) Characterization of BGA solder joints to identify failure mechanisms and obtain statistical data, (2) Finite Element analysis (FEM) to predict system response needed for life prediction, and (3) development of a probabilistic methodology to predict the reliability, as well as, the sensitivity of the system to various parameters and the variabilities. These tasks and the predictive capabilities of IMPRPK in microelectronic reliability analysis are discussed.

DEDICATION

This dissertation is dedicated to my parents for their unconditional love, encouragement and support, whom without their guidance, I would not be the person I am today.

I would also like to dedicate this dissertation to my wonderful wife for her endless love, strength, continuous encouragement, motivation and patience every step of the way throughout the course of my graduate studies. Her presence, help and support had a great impact on this accomplishment.

Finally, this thesis is dedicated to all of those who believe in the value of learning.

ACKNOWLEDGMENTS

I would like to acknowledge my advisor, Professor Tasooji, for her guidance and leadership throughout this project and the opportunity she provided me to be a part of this great work.

Also, I would like to extend my appreciation to all my committee members, Prof. Krause, Prof. Alford, Prof. Jiang and Dr. Mahajan, for their time and effort in evaluating my PhD dissertation and providing their valuable feedback.

Special thanks to the following individuals from Arizona State University (School for Engineering of Matter, Transport and Energy) and Intel Corporation who helped me through this project: (ASU) Laticia Lara, Lakshmi Kari, Mr. David Smith, Mr. Zhang, Mr. Karl Weise and (Intel) Dr. Ravi Mahajan, Dr. Nachiket Raravikar, Mr. Richard Harries, Mr. Rene Sanchez and Mr. David Woodham. The guidance of Dr. John McFarland from Southwest Research Institute in the application of NESSUS to this work is greatly appreciated.

TABLE OF CONTENTS

CHAPTER Page

APPENDIX

LIST OF TABLES

Table Page

Table Page

LIST OF FIGURES

Figure Page

Figure Page

Figure Page

Chapter 1

INTRODUCTION

1.1 Introduction

Ball Grid Array (BGA) packages using lead-free or lead-rich solder materials have been extensively used as Second Level Interconnects (SLI) in mounting the microelectronic packages to the printed circuit boards (PCB). The reliability of these BGA solder joints is of significant importance to the performance of the microelectronics systems. Product design and form-factor, solder alloy composition, microstructure, and inherent variabilities in materials properties greatly influence the BGA reliability.

Increasing demand for the small and high performance electronic devices using surface mount technology (SMT) and Ball grid array (BGA) design highlights the importance of conducting research in BGA reliability. In recent years, a significant amount of research activities have been conducted to address these concerns and improve the reliability of the microelectronic packages [1-7].

Considering numerous system variabilities that are present in microelectronics packaging; such as design variations (e.g. Wire bond, Flip chip, etc.), product applications (e.g. consumer electronics, Automobile, Aerospace, etc.), materials / property differences (e.g. Lead free solder, lead rich solder, mold compound, adhesion layer, and other materials used in packages), geometry or configurations, etc., the need for a robust and integrated methodology for predicting the reliability and sensitivity of these packages becomes more significant.

In order to address the reliability and sensitivity concerns in the microelectronic packaging systems, and to quantify the impact of the random variables on the overall system reliability, the IMPRPK methodology is being proposed. IMPRPK is an Integrated Methodology for Predicting the Reliability of the microelectronics Packaging systems.

1.2 Problem statement

Product performance and reliability are not only impacted by manufacturing and operating/use condition, but the reliability of any mechanical or electrical system is also directly influenced by the inherent variables present in such systems. A minor change in system variables could cause a substantial change in the system performance and reliability [8]. The focus of this dissertation is to develop a methodology for quantifying the impact of different variabilities; such as variation in material, design/ form-factor and processing, use condition and defect size on reliability of packages. This methodology can then be used in package design and/or manufacturing as new products with different requirements in form factors, material/processing, etc. are deemed needed in response to a time-sensitive market.

What differentiates our approach from others is our focus in considering many variables/variabilities at once when studying their impact on reliability, while a general approach by others is to investigate the effect by evaluating the effect of single variable at a time.

1.3 Approach

In order to address the above mentioned reliability concerns, the IMPRPK approach was proposed to be used in predicting the reliability and sensitivity of the microelectronic packages exposed to many system variabilities. The BGA interconnect reliability case was used as a mean to validate this proposed approach.

IMPRPK approach is a probabilistic approach used in predicting the reliability and risk factors of the system, as a function of variation in the system. This approach will help design engineers to identify the culprit system parameters and manage/reduce the potential risks associated with them during the product design, development, and the early stages of the manufacturing, hence, resulting in significant cycle-time and cost reduction.

In developing IMPRPK methodology, three major tasks were focused:

- <u>Task I- Characterization:</u> The main elements of this task are:
    i. Obtain the variability data associated with geometry (design/dimensions and BGA solder array), microstructure (processing effect), material properties (effect of composition, processing), and defect size (voids and cracks size distribution). These data are then

used in constructing the statistical random variable distribution functions needed for probabilistic analysis.

  ii. Characterize untested end-of-Line (EoL) and tested (Accelerated Thermal cycled, ATC) samples to identify the failure modes and select the appropriate life prediction models for accurate reliability analysis.

- Task II- Finite Element Method (FEM): Create and analyze the global and local Finite Element Models (FEM) to obtain individual BGA loading condition under a given loading condition and external parameters. Integrating FEM with a probabilistic model provides the capability to predict materials responses when the variabilities are incorporated into the loading/external condition input to FEM model. The global FEM model which defines the whole package, utilizes the input boundary conditions of the package (e.g. thermal cycling, displacement and rotation of the package) to calculate the package level displacements of the system "global FEM response". The local FEM model (also known as sub-model) uses the package displacement values predicted by the global model as the inputs/boundary condition for calculating the state of stress, strain and energy in individual BGA interconnects, hence the "local FEM response". The system response from the local model is then used in combination with the life prediction models, such as. Coffin-Manson, Perkins, Darveaux, and/or others [4], [9-19] to predict the time-dependent failure and/or package life/survival.

- Task III- Probabilistic and reliability analysis: The probabilistic and reliability analysis is the significant element of this study. In this task the variability distribution data generated in task 1, in combination with the local responses from the FEM simulation developed in task 2, are integrated with a commercially available probabilistic methodology, to predict the effect of system variability/uncertainties on product reliability. This integrated methodology not only is applicable for reliability analysis, it is also intended for use in design and manufacturing optimization and process control. The applicability and efficiency of various probabilistic analysis techniques for the microelectronic packages were evaluated during the course of this study in order to identify and select the most appropriate method for microelectronic systems.

1.4 Effects included

The study presented here includes the critical microelectronic package parameters on BGA reliability. The parameters considered include, but are not exclusively limited to: material properties, constitutive model constants, package components, geometry and dimensions, defect distribution, and use conditions. The FEM predictions are then used in conjunction with Darveaux’s life prediction model to determine the BGA survival life under the set conditions selected above. Combining the system variabilities data in the form of statistical distribution obtained in task (i) with these deterministic models developed in task (ii) and a probabilistic approach, provides the information on failure probability of the system, as well as the sensitivity of the system to the applied changes to any of the input variables.

1.5 Effects not included

Some effects such as microstructure evolution and formation and growth of the intermetallic compounds (IMCs) were not evaluated during this work. Combination of these effects with different life prediction (e.g. Coffin Manson and Perkins, etc.) and probabilistic models such as Monte Carlo, first and second order reliability could be studied as a future work.

Chapter 2

LITERATURE REVIEW

2.1 Introduction

This chapter summarizes BGA reliability issues and the relevant failure mechanisms, life prediction models, and reliability approaches discussed by other investigators.

Understanding of the BGA reliability concerns will be beneficial in improving the package performance and service life. In this chapter the system and BGA level reliability of the microelectronic packages will be discussed and effect of the key parameters involved in BGA reliability will be reviewed.

2.2 Microelectronics system reliability

One approach in defining the reliability of a system is to focus on the difference between the strength of the materials used in that system and the stress levels of the system in a given operation state. Upon the stress value in the system exceeding the strength of the material, the failure will occur and therefore the system will not be reliable anymore. Determining the stress levels of the system (system response to the loading and process and use condition) are generally complicated and numeric codes (e.g. ABAQUS and ANSYS) are required in determining the stress levels.

Effects such as thermal mismatch between the package elements (especially at local level) and thermal cycling of the packages (combination of cyclic loading and creep deformation) influence the stress levels of the system [20-21].

Depending on the type of the deterministic model used in reliability analysis, the response of the system could be in the form of the stress, strain or energy.

The probabilistic approach will predict the probability of the system failure by incorporating the variabilities in material, geometry and process and use condition in deterministic model.

The probabilistic approach is the main core of this dissertation.

2.2.1 Deterministic model

In the complex systems (e.g. microelectronic package) with multiple materials, boundary and use condition, determining the system response is often difficult and requires numeric FEM codes (e.g. ABAQUS, ANSYS, etc.) for solving them.

In the past years, a significant amount of papers have been published in the area of the first (FC) and second level (BGA) interconnects and also Surface Mount Device (SMDs) reliability [3], [5], [7], [9-11] [17-19].

2.2.2 Probabilistic approach

Reliability of the microelectronic package is influenced by the reliability of its components [22]. Natural variabilities in material properties and process and use condition exist in the manufacturing process of the electronic packages. Ignoring the effect of these variabilities would result in inaccurate service life prediction of electronic packages. Performing the probabilistic analysis will integrate the impact of these variabilities on overall system reliability [3], [5-7], [11], [13], [19], [24], [26].

2.3 BGA reliability

BGAs as second level interconnects (SLI) provide the mechanical, thermal and electrical connection between the substrate and PCB (Printed Circuit Boards). Integrity of these BGAs as one of the weakest elements of package, would impact the overall reliability of the microelectronic package [17] [24].

Parameters such as loading mode (tensile vs shear), temperature and strain rate influence the reliability of the BGAs (Fig. 1) [25].

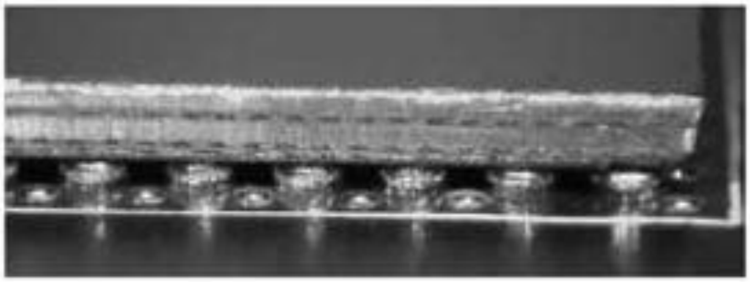

Fig. 1 Ball grid array (BGA) [23]

2.3.1 Failure models and mechanisms

Different failure modes commonly observed in the BGA solders include instantaneous brittle or ductile fracture and time-dependent failures such as Creep, fatigue, Thermo-Mechanical fatigue (TMF)influenced by operating conditions [27]. A summary of potential failure modes for BGA solders is provided in Fig. 2

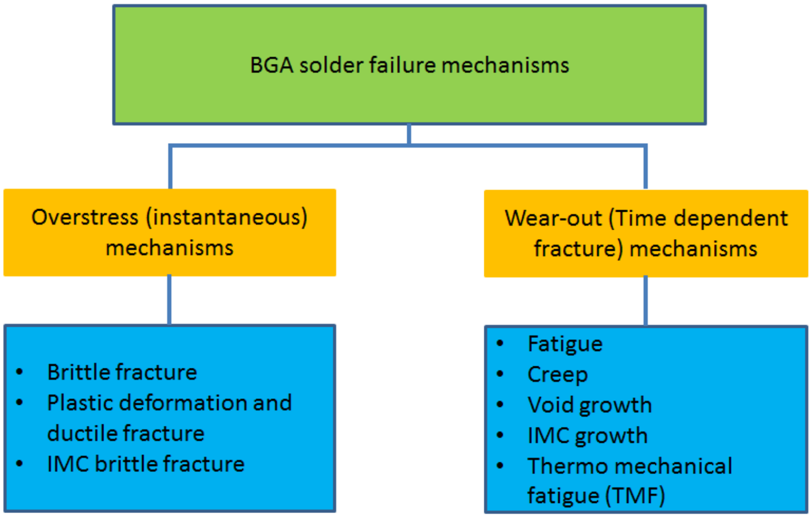

Fig. 2 Summary of the potential failure modes for BGA solders.

Synergistic effect of various mechanisms, e.g., creep-fatigue interactions, should be considered in BGA reliability analysis.

- The instantaneous failures generally occur due to the excessive tensile and/or shear loads and is a time independent failure. Depending on the type of BGA material e.g. ductile or brittle, different fracture surface will be observed. One of the common reasons of the brittle failure in the BGA solders in due to the formation of the brittle-natured intermetallic compounds forming in the tin-copper interface at elevated temperatures and/or reflow process [32][34]. Demonstration of different instantaneous failure modes related to the shear and pull tests and their results in the BGA solder failure are presented and discussed in detail in [28-29] and [31] respectively.

- Fatigue failure is the most recognized failure mechanism in the Second Level Interconnects (BGAs) and is caused by the low frequency cyclic load [30], [33]. The large difference in the coefficient of thermal expansion values between the silicon die (2.6 PPM/˚C) and organic FR4 substrate (18 PPM/˚C) in combination with cyclic temperature change is the root cause of the thermal fatigue failure. This effect is lower with using of the ceramic substrates [3].
- Fatigue failure has two stages, it starts with the crack initiation and follows by the penetration of the crack across the BGA until the solder joint becomes unstable and fracture occurs [17].
- The time dependent (and usually slow) permanent deformation of the BGA solders under the influence of stresses at elevated temperatures in the range or above the 50% of their absolute melting temperature (homologous temperature), occurs as a result of creep deformation. Considering the melting temperature of the SAC405 and Sn37Pb solders (217˚C and 183˚C respectively), these solders are subjected to the creep deformation even at room temperature (25˚C). This effect is even more significant for the Sn37Pb solders since they are

in about 65% of their absolute melting temperature at 25˚C [35]. Long dwell times during thermal cycling and/or duty cycle, especially, the high temperature hold time will increase the impact of the creep failure in the BGAs. Creep failure decreases the thermal fatigue life of the BGA solders by damaging and degrading the grain boundaries of the BGA solders via the nucleation, growth and combination of the cavities in grain boundaries (intergranular failure) [36-37].

The creep behavior in the BGA solders are controlled by two main mechanisms:

- Dislocation creep
- Diffusion creep

Both of these mechanisms are active at elevated temperatures and their main difference is in the level of stress and microstructural behavior. The dislocation creep is defined based on the dislocation motion within the crystal as a result of high stress levels while the diffusion creep is described based on the diffusion of vacancies as a result of applied stress. The diffusion creep mechanism will be active even at lower stress levels [35]. Fig. 3 shows a generic example of creep strain vs. time graph, reflecting the increase in creep rate with increasing temperature.

Prior to primary creep, there is a time independent material extension which could be either elastic or combination of elastic and time independent plastic. In the primary creep region the material deforms with a fairly high rate until the material reaches to the work hardening condition which will cause a decrease in the creep strain rate. Increasing the temperature of the material will cause a thermal based recovery phenomenon which will balance with the work hardening effect and will result a steady-state creep strain (second stage of the creep) in this stage the deformation is independent of time and strain. During the tertiary creep, grain boundary cavitation and coalescence is responsible for intergranular cracking and creep failure.

The ATC tested BGA’s were used to identify the failure modes in solder cracking.

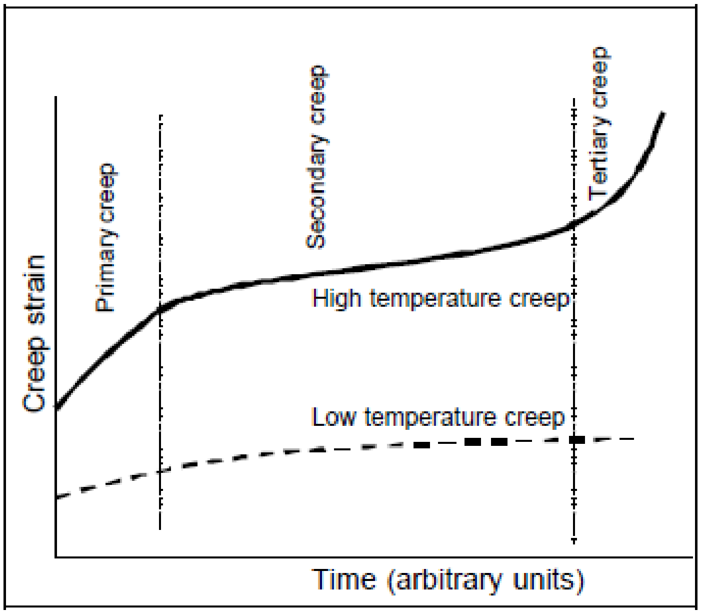

Fig. 3 Creep strain vs. temperature for the solders [35].

2.3.2 Parameters influencing reliability

Ball grid array solder reliability is the critical element influencing overall package reliability. Material properties (e.g. Chemical composition, microstructure, etc.), package design and form factor (flip-chip, wire-bond), product processing and use condition (e.g. temperature) [2], [38] are parameters that impact the service life and reliability of microelectronics packages. In addition to these parameters, the inherent variability present on these parameters play a significant role on the reliability. It is of utmost importance that we understand and predict the impact of all these parameters and variability on product performance in an efficient and timely manner, in quest to address the fast paced market entry requirement. The listing of various parameters and those considered in this study is provided in Table. 1

Table. 1 Various parameters considered in this study

Parameters	Details	Applied in this study
Design	Flip Chip	Yes
	Wire bonded	Yes
	Dimensions and thicknesses	Yes
Material	Solder microstructure	No
	Solder properties	Yes
Processing	Temperature	Yes
	Defect size	Yes
	Reflow temperature	No
Application and use	Temperature	Yes
	Dwell time	Yes

2.3.2.1 Material

2.3.2.1.1 Chemistry

Chemical composition plays a substantial role in the reliability of the BGAs. Composition, microstructure, ductility and intermetallic compounds are some of the key material parameters influencing the BGA reliability.

Common solder materials used for First Level Interconnect (FLI) C4 bumps and Second Level Interconnect (SLI) BGAs are Sn37Pb (lead-rich) and Sn-Ag-Cu lead-free alloys (e.g., SAC405, etc.). The great wetting properties in combination with adequate creep, thermal fatigue, enhanced fluidity and relatively low melting temperature and vapor pressure made Tin based alloys a perfect choice for the microelectronic applications [33], [39-40], [42]. Two major classes of interconnect solder alloys used in microelectronics industry are:

- Lead based solder material
- Lead free solder material

The binary phase diagram of the SnPb solder material is shown in Fig. 4, where Sn37Pb is the eutectic composition alloy of Sn and Pb and the melting temperature of this alloy is about 183°C.

Utilizing the lead based soldering alloys in microelectronic industry has a long history and in the past 50 years the tin-lead solders were widely used in manufacturing of the electronic devices [39], [43]. In 2000, only in the U.S., 11500 tons of lead was consumed in manufacturing of the solders [41]. This was only 0.7% of the total lead consumption during that year.

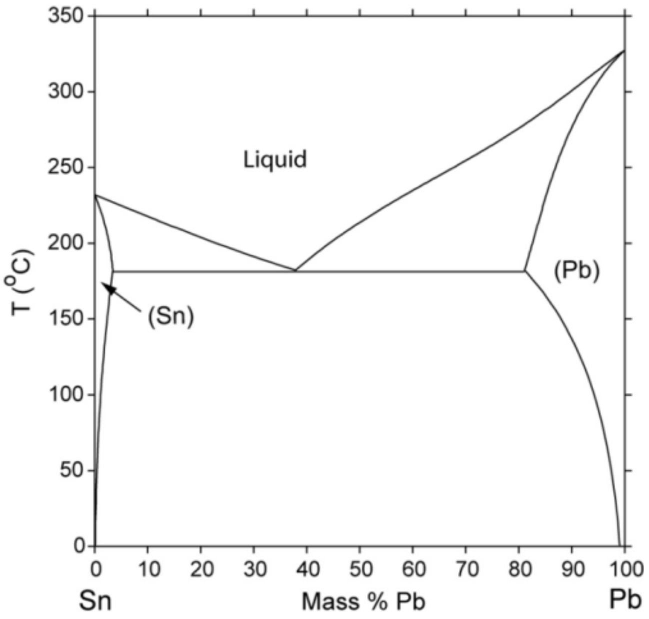

Fig. 4 Binary phase diagram for the eutectic Sn37Pb alloy [44]

Considering the great properties of the tin-lead solder alloys, the use of these solder alloys has been dropped in the recent years due to the toxic effect of the heavy metals on human health. Heavy metals such as lead could cause serious brain damages and because of this concern majority of the countries have passed bills to reduce and eliminate the use and disposing of the products containing the heavy metals [41] [43] [45]. Starting the July 2006, European Union has forbidden the use of the lead based electronics and therefore the Sn37Pb solders must be replaced with the alternative alloys [1]. The global effort in lead reduction (and removal) from the consumer electronics and other applications, has motivated the need to find alternative substitutions for the lead based solders.

To address this concern, the new lead free solder alloys were introduced. There are more than 70 different composition available for the lead free solders [40] and among these options the eutectic tin (Sn), silver (Ag) and copper (Cu) alloys are the most common options. Fig. 5 shows the top view of ternary phase diagram for the lead free SAC solders. According to this figure, majority of the near eutectic SAC alloys are located in the area confined in red area. Based on the composition of these three elements, different alloys could be formed (e.g. Sn-Ag, Sn-Cu, SAC205, SAC305, SAC405, etc.) [43][46].

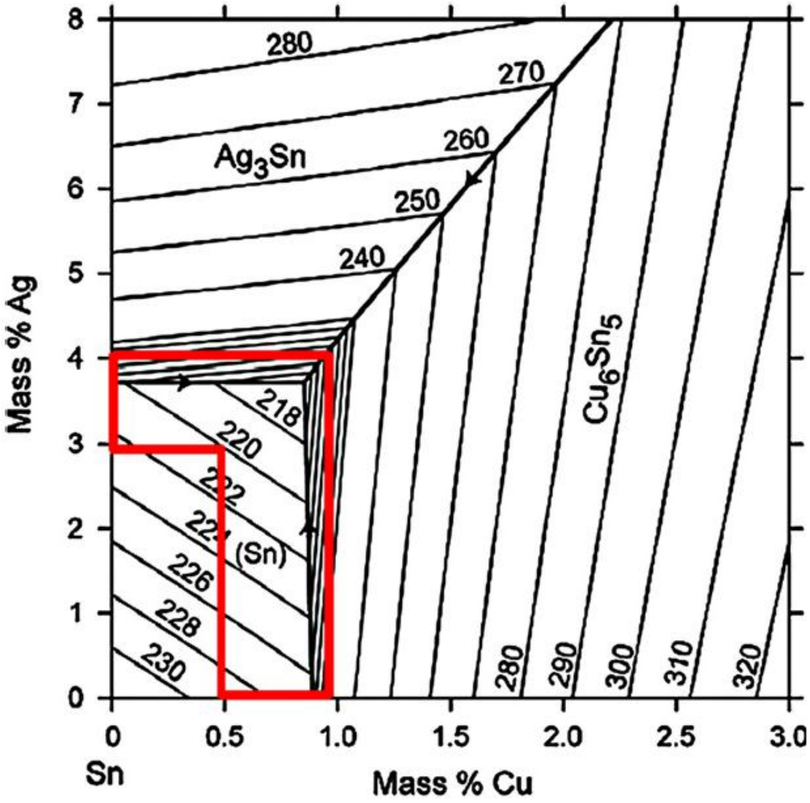

Fig. 5 Ternary phase diagram of the lead free solders (SAC) [44][47][48]

2.3.2.1.2 Microstructure

Microstructure of the BGA solders play a significant role in the BGA integrity and package reliability [50]. Depending on the BGA solder composition (e.g. SAC405, Sn37Pb, etc.), different inter metallic compounds (Ag_3Sn, Cu_6Sn_5) [36], [44], [50] could be formed within the base Tin matrix. Processing and use conditions influence the size of microstructural features such as grains and intermetallic compounds, impacting BGA solder properties such as the strength values. Well known Hall-Petch relation presented in equation (1) below, describes the effect of grain size on the yield stress of the crystalline metal, where the material strength increases with the inverse of the square root of the grain size d

$$\sigma_y = \sigma_0 + kd^{-1/2} \qquad (1)$$

In equation (1), σ_y is the yield stress, σ_0 is the friction stress needed to move individual dislocations, k is the constant (material dependent) and d represents the grain size [49], [51].

Microstructure evolution due to thermal exposure result in, grain size increase, and formation of micro voids and/or micro cracks [24].

Formation and coarsening of intermetallic particles as a result of elevated temperature is one of the factors in degrading the reliability of the BGAs [36].

The effect of the initial microstructure and its time dependent evolution during the use condition at elevated temperatures are generally not considered in life prediction models.

2.3.2.1.3 Statistical behavior

Many investigators have studied the stochastic behavior of the BGA solders, including, the impact of internal voids, cracks, temperature range, cycle frequency and etc. on properties [52-53]. Majority of these studies are experimental efforts and the effect of the internal voids were rarely included in the numeric (FEM) analysis. This study concluded that the probability of formation, position and the size of these voids in the electronic packages are absolutely random. Fig. 6 shows example of voids observed in BGA solder [53].Comparing the FEM and experimental results for the solders with and without voids have proven that the equivalent plastic and shear strain is not always larger for the solders with voids and factors such as position, frequency and size of the void will define the amount of the strain in the BGA solders [53-54].

It has also been reported that the effect of the voids in the lead free and lead based solder is not significant and could be neglected and only the voids larger than 50% of the solder joint area will reduce the integrity of the BGA solders [53].

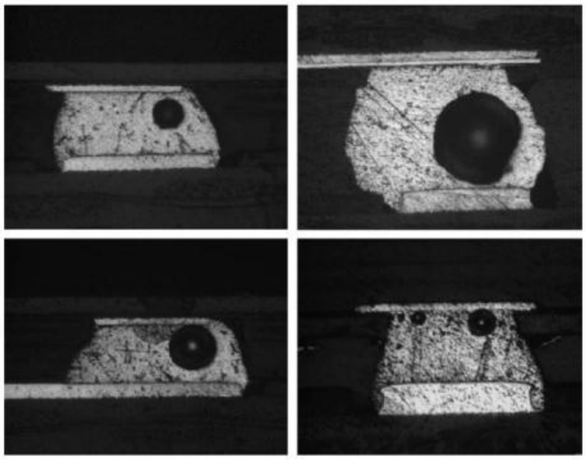

Fig. 6 Voids (with different size and position) from the time zero solder joints [53]

2.3.2.1.4 Solder DBTT effect

The Ductile Brittle Transition Temperature (DBTT), is the transition from ductile to brittle failure for a given loading mode and temperature as a result of constant or increasing strain rate. The ductile to brittle transition strain rate (DTBTSR) on the other hand is the strain rate level in which the ductile to brittle transition will occur in the BGA [25]. The ductile and brittle failure of the BGA solders as a result of tensile load is presented in Fig. 7 &8. According to these figures the bulk of the solder will mainly experience ductile failure whereas the interface failure will fail in brittle manner. Higher DTBTSR is the indicative of having a robust system with respect to impact loading. It is also shown that BGA aging can impact the ductile to brittle transition level [55-56].

Fig. 7 Ductile and brittle failure under the tensile test (this figure shows the different types of the failures (ductile, brittle and pad lift) [25]

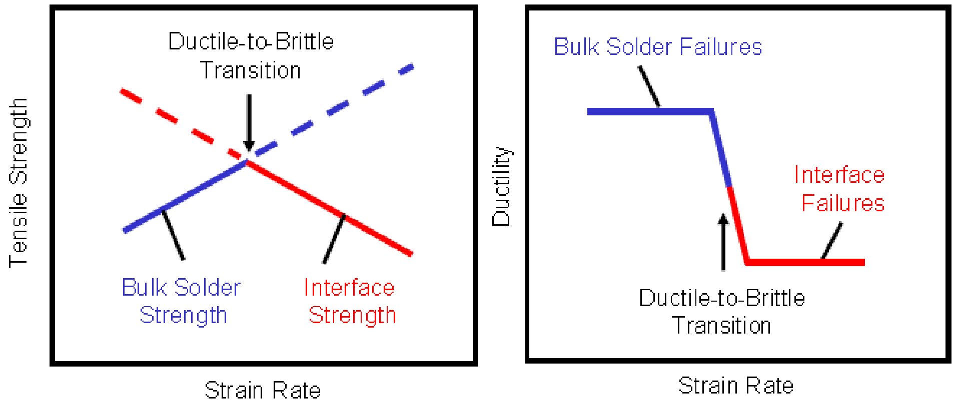

Fig. 8 Trend of tensile strength with strain rate (left) and trend of ductility with strain rate (right) [25]

The effect of the DBTT is more significant at low temperature thermal cycling which considering the high operation temperature of the consumer electronics (compared to DBTT) is not a concern.

2.3.2.1.5 Molding compound Tg effect

The glass transition temperature (Tg) of polymer and resin materials used in microelectronic systems (e.g., molding compound) has a crucial impact on microelectronic package reliability. The glass transition temperature is the reversible transition of the amorphous material from a hard and relatively brittle state to semi molten (rubber like) state. In the microelectronic packages, the amorphous materials (e.g. molding compound, underfill, die attach, etc.) have specific glass transition temperature. Generally the Coefficient of Thermal Expansion (CTE) values of these materials are low at lower temperatures (with higher elastic modulus) and it increases significantly above the glass transition temperature (Tg).

2.3.2.2 Geometry

2.3.2.2.1 Form factor

Parameters such as form-factor (e.g. wire bonded with molding compound vs. flip chip with under fill) in combination with the BGA layout in the package (e.g. full grit array vs. partial grit array) would influence the microelectronic package reliability. For instance, it has been reported that the fatigue failure in the partial grid array packages is much significant compared to the full grid array of solders [35][57]. BGA joints close to the edge of the silicon die have shown higher stress and strain values compared to the rest of the BGAs (see Fig. 9). This is due to high thermal mismatch between the silicon die and substrate.

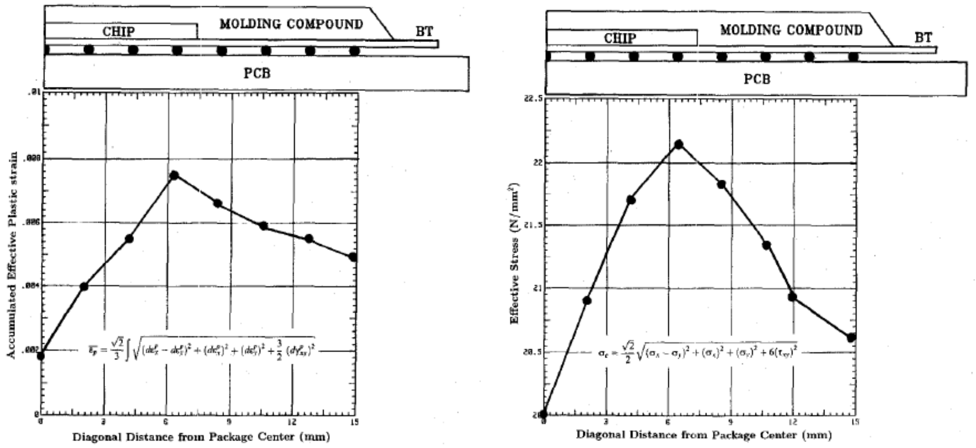

Fig. 9 Accumulated effective plastic strain (left) and Effective stress (right) [17]

Parameters such as package dimensions, solder standoff, pitch size, etc. will also impact the failure pattern of the packages. For instance the thickness of the silicon die and printed circuit board will impact the reliability of the BGA in opposite ways [23].

2.3.2.3 Processing and use condition

Understanding the details of the manufacturing process of the microelectronic packages in combination with specific requirements of use-condition is crucial for BGA integrity. Variations in process and manufacturing (e.g. Reflow, residual stress and cooling rate, etc.) in addition to device handling, on and off cycles and environmental effects (e.g. ambient temperature and humidity) are required to be incorporated in BGA reliability analysis.

2.3.2.3.1 Reflow

The formation of interconnects (e.g. BGA) in microelectronic packages takes place through the reflow process. Reflow process in combination with existing thermal mismatch between the package components could cause electrical discontinuity in the package [59]. The IMCs are the byproducts of the reflow process which prevents the further diffusion of the pad material into the solder joint by forming a brittle barrier layer [60].

2.3.2.3.2 Residual stress

Residual stresses are thermally induced stresses in the BGA. Package warpage and plastic deformation develop during the reflow/assembly process, due to the differences in the coefficient of thermal expansion of dissimilar materials, resulting in residual stresses forming at the solder joints [57-58], [61]. Fig. 10 shows the remaining deformation in the BGA solders as a result of the reflow process. This deformation at room temperature will induce the residual stress in the BGAs.

Selecting the package elements (especially epoxy materials) with similar CTE values would significantly reduce the level of residual stress in the packages. The residual stress has been recognized as one of the main reliability concerns in the microelectronic packages [57].

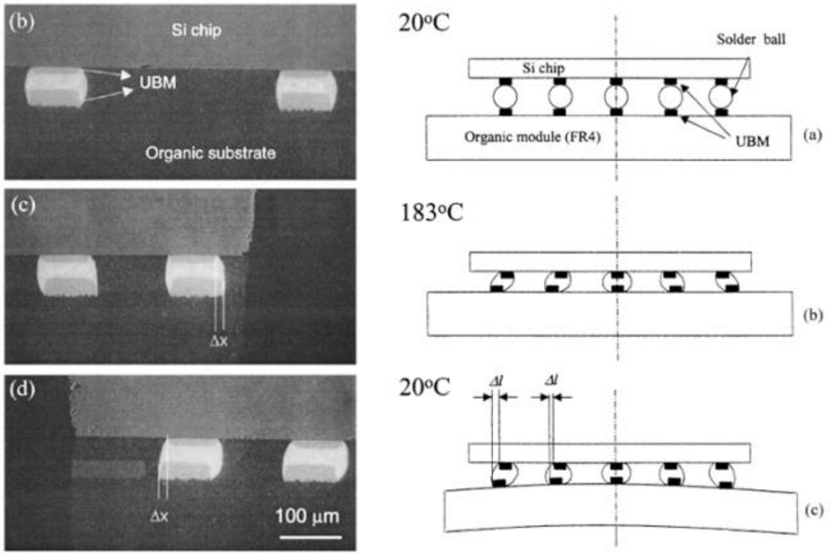

Fig. 10 Residual stresses in the BGA solders after the reflow as a result of the thermal mismatch between the silicon chip and FR4 board [33]

2.3.2.3.3 Cooling rate

Microstructure of the BGA is extremely sensitive to its processing steps. Cooling rate will influence the reliability and integrity of the BGAs by affecting the microstructure (different grain size and precipitate morphology) and altering their mechanical properties. Study by other investigators has revealed the effect of cooling rate and ATC cycle on fatigue life of the BGA solders, showing longer fatigue life for solders experiencing slower cooling rate [62]. Fig. 11 shows the effect of the cooling rate and heat treatment on the microstructure of lead-rich solders. In this Figure, slower cooling rates (lower than ~0.01˚C/s) in part (a) shows Sn and Pb lamellae’s while increasing the cooling rate will change the lamellae structure to globular structure with Pb rich particles with in the Sn rich phases.

Fig. 12 also shows the microstructure evolution as a result of cooling rate in the SAC405 solders. The effect of the cooling rate in the lead rich and lead free solders are discussed in [63], [65] and [64], [66] respectively.

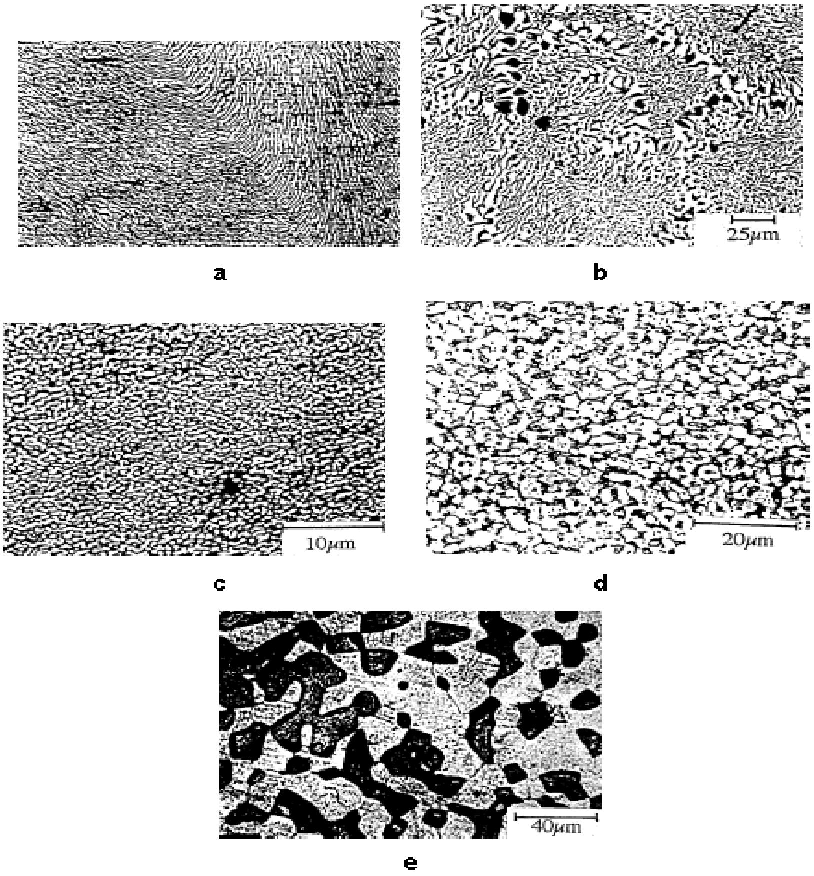

Fig. 11 Effect of the solidification and cooling rate on the Sn37Pb alloys (a) to (c) slow to rapid cooling rate, (d) annealing for 60 h at 85˚C (e) worked and annealed [63]

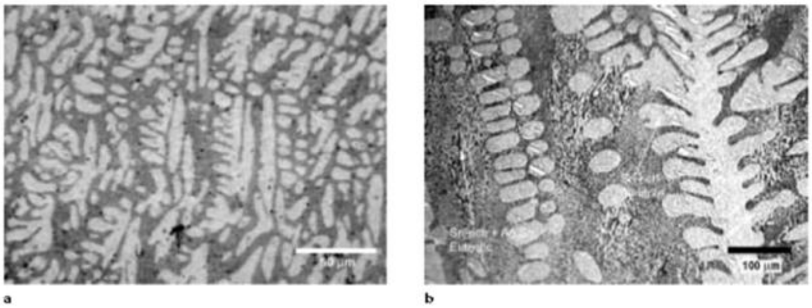

Fig. 12 Comparison between the water cooled (a) and air cooled (b) microstructure (Sn-3.5Ag) [64]

2.3.2.3.4 Thermal cycle

The typical microelectronic devices are subjected to thermal cycling during their normal operation and use condition. The reliability of packages exposed to such thermal cycling is evaluated using accelerated Thermal Cycle (ATC) tests, with hold time during the high and low temperatures of the ATC. Fig. 13 shows the comparison between the displacement-time graphs with and without hold times (Trapezoidal and Triangle respectively). Trapezoidal wave is generally used in ATC test.

The effects of the triangular and trapezoidal low cycle fatigue on microstructure evolution of SAC solder have been demonstrated in Fig. 14. According to this figure, including the upper and lower temperature hold times (Trapezoidal wave form) will increase the size of the intermetallic particles in BGA solders.

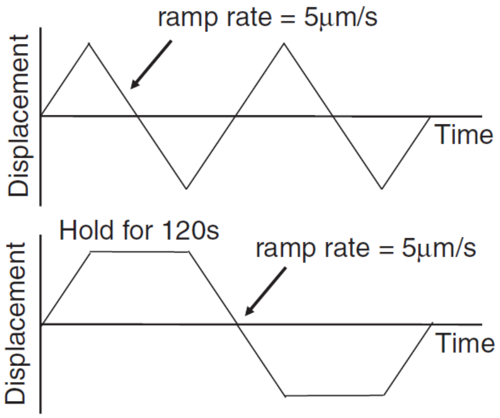

Fig. 13 Triangle (Top) and trapezoidal (Bottom) wave forms used in the fatigue tests [36]

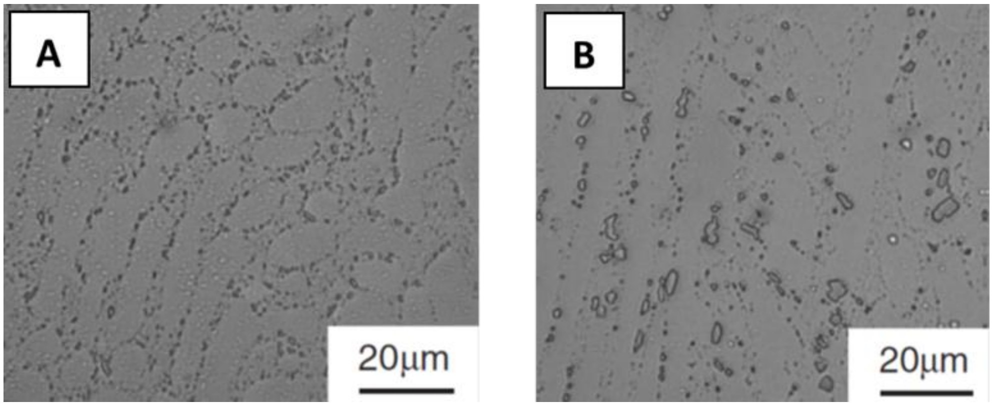

Fig.14 Effect of the dwell time on the microstructure (intermetallic particles) of the SAC solders (A) triangular low-cycle fatigue (B) Trapezoidal low-cycle thermal fatigue. [36]

Some investigators have reported insignificant temperature and hold time effect on lead-free SAC BGA solders crack length , while the effect was more significant in Sn37Pb solders [27], [36].

It is shown that thermal cycling can lead to reduced fatigue life of the solders, by altering their microstructure and formation of the IMC layers. A reduction in BGA fatigue life (by a factor of 6 to 8 times, after 1000 thermal cycles of aging) was reported by Pang JHL, Tan KH, Shi X, Wang Z [68]. The summary of the typical use condition and service life of different electronic package applications is presented in [24]

2.3.2.3.5 Aging effect

Aging will degrade the BGA reliability by altering the microstructure of the solder joints and formation of oxides at elevated temperatures [59]. It is also been shown that the BGA failure rate is higher for the thermal cycling and thermal shock aging compared to isothermal aging in both lead free and lead rich BGAs [14], [67]. Fig.15, 16, 17 demonstrate the morphology change in the lead free solders a result of different thermal aging process (isothermal, thermal cycling and thermal shock respectively) at 125˚C. These photomicrographs clearly show the increase in the thickness of the IMCs at the solder/copper-plate interface, with increased thermal aging temperature and time.

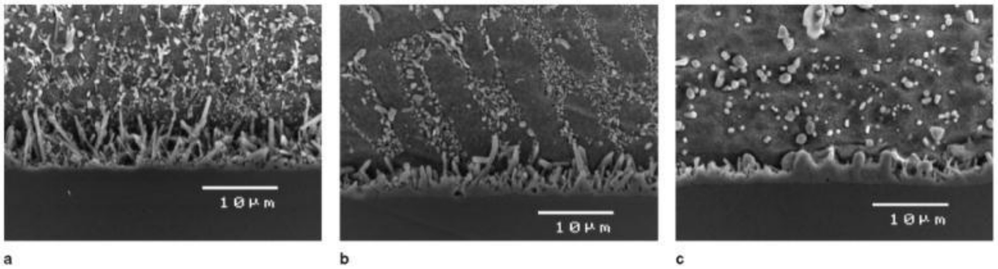

Fig. 15 IMC morphology change in lead free solder (during the isothermal aging) after (a) 0h (b) 119h (c) 262h [67]

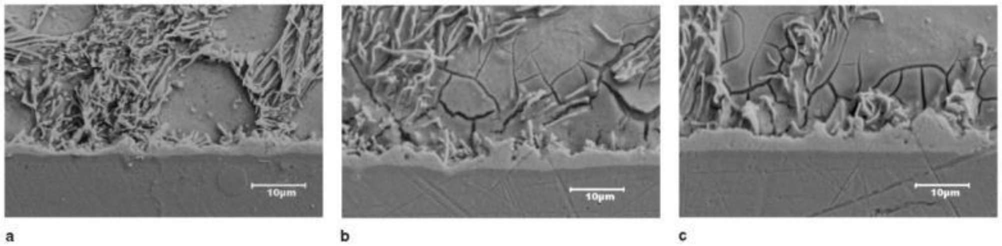

Fig. 16 IMC morphology change in the lead free solders subjected to thermal cycling (a) 500 cycles (b) 1000 cycles (c) 2000 cycles [67]

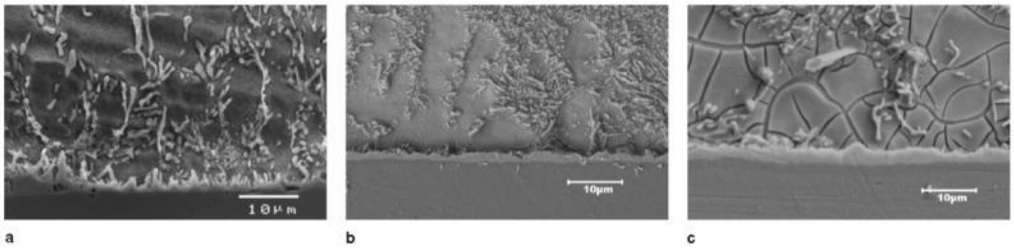

Fig. 17 IMC morphology change in the lead free solders subjected to thermal shock (a) 500 cycles (b) 1000 cycles (c) 2000 cycles [67]

Similar to lead free BGAs, the phase coarsening was also observed in Sn37Pb solders (Fig. 18). The phase coarsening in the Sn37Pb solders was significantly more compared to the SAC405 BGAs.

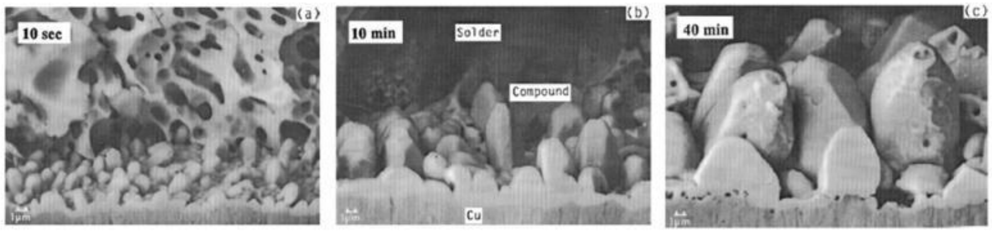

Fig. 18 Time dependent (200°C) IMC growth in the Sn37Pb solders (a) after 10 sec (b) after 10 min (c) after 40 min [33]

2.3.3 Deterministic models

Deterministic models are used to identify the response of the systems. Depending on the active failure modes in the system one of these models must be selected and utilized.

2.3.3.1 Fatigue

Fatigue is a type of failure which degrades the integrity of the BGA solders as a result of cyclic loads. The fatigue failure which is caused due to the alteration in temperature is called thermal fatigue. Different fatigue models will be reviewed in this section:

2.3.3.1.1 Various fatigue models

There are different empirical low cycle fatigue life models proposed by various investigators (e.g. Darveaux, Farooq, Perkins, Park, Engelmaier). Listing of different fatigue models along with their characteristics is shown in Table. 2 Even though these empirical life prediction models are commonly used, one should be considerate of the fact that the inaccuracy of these models in some cases could be as large as one order of magnitude [69]

Table. 2 Fatigue models and their classifications [72]

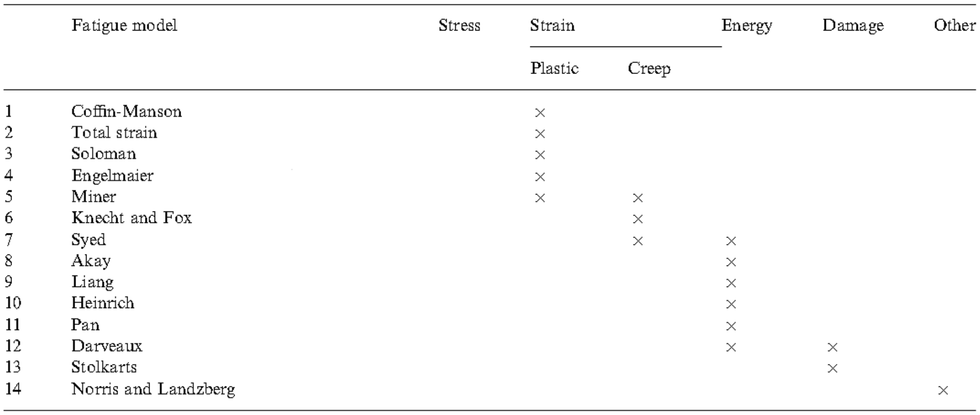

	Fatigue model	Stress	Strain		Energy	Damage	Other
			Plastic	Creep			
1	Coffin-Manson		×				
2	Total strain		×				
3	Soloman		×				
4	Engelmaier		×				
5	Miner		×	×			
6	Knecht and Fox			×			
7	Syed			×	×		
8	Akay				×		
9	Liang				×		
10	Heinrich				×		
11	Pan				×		
12	Darveaux				×	×	
13	Stolkarts					×	
14	Norris and Landzberg						×

Some of these models are further discussed in the following sections.

Coffin-Manson Model:

Coffin-Manson is the most recognized method in fatigue life prediction analysis. [9], [17], [24], [35-36], [70-71].

Equation (2) shows the general form of the Coffin-Manson fatigue model.

This relation was first proposed in 1950's and ever since then has been used in fatigue life prediction applications.

$$N_f = K{\varepsilon_p}^n \qquad (2)$$

In this relation, the N_f represents the number of cycles to failure and ε_p represents the plastic (inelastic) strain range and K and n are the constants of the model. Some investigators use N_f (50%) or the number of cycles to 50% failure for N_f in

Coffin-Manson equation. Thermal cycling and/or available fatigue data are generally used in determining the constants of the Coffin Manson equation (or the modified versions of the equation discussed below).

Since the Coffin-Manson is a general relation for the metals, various researchers have modified this equation to incorporate different parameters and interactions impacting fatigue behavior, and calculate the relevant constants [9-11]. Equation (3) shows the modified version of the Coffin-Manson relation for low cycle fatigue of the Sn37Pb solders [9]

$$N_f = \frac{1}{2}\left(\frac{\Delta\gamma}{2\varepsilon_f'}\right)^{(1/c)} \qquad (3)$$

Where,

N_f = mean cycles to failure

ε'_f = fatigue ductility coefficient ~ 0.325

C = fatigue ductility exponent=$-0.442-6*10^{-4}T_s+1.74*10^{-2}\ln(1+f)$

$\Delta\gamma$ = shear strain range

T_s = mean cyclic solder joint temperature, ˚C

f = cyclic frequency, $1\leq f\leq 1000$ cycles/day

The former equation was also reported by John Lau [9] with different constants.

The difference in reported constants for equation (3) by John Lau are:

T_s = mean cyclic solder joint temperature, ˚C = 52.5°C (liq to liq) and =35°C (air to air)

f = cyclic frequency, 1≤f≤1000 cycles/day = 200 cycles per day for liquid to liquid thermal shock and =30 cycles per day to air to air temperature cycling

C=-0.38122 for liquid to liquid thermal shock and =-0.40325 for air to air temperature cycling

Farooq [11] version of the Coffin-Manson equation representing 50% median life is given in equation (4)

$$N_f = K({\varepsilon_p}^{-2}) \qquad (4)$$

In this equation ε_p represents the maximum von Mises plastic strain range.

Perkins [10] version of the Coffin-Manson equation for the median fatigue life is represented in equation (5) below, where $\Delta\varepsilon_{in}$ represents the inelastic strain range per cycle

$$N_f = 82.4(\Delta\varepsilon_{in})^{-0.863} \qquad (5)$$

Darveaux life prediction model:

Darveaux’s life prediction model is based on combination of two terms. First term represents the required number of cycles for crack initiation, while the second term represents the crack growth after initiation.

Equation (6) demonstrates the general form of the Darveaux's model [12], [16].

$$\begin{aligned} &\text{Crack initiation} : N_0 = a\Delta W_{\text{ave}}^{b} \\ &\text{Crack growth rate} : \frac{\mathrm{d}l}{\mathrm{d}N} = c\Delta W_{\text{ave}}^{d} \\ &\text{Characteristic life} : N = N_0 + \frac{l}{\mathrm{d}l/\mathrm{d}N} \\ &\text{Failure-free life} : N_{\text{ff}} = \frac{N}{2}. \end{aligned} \tag{6}$$

In these set of equations the first term represents the number of cycles to initiation while the second term shows the crack growth rate.

The constants of the model (a, b, c and d) are generally calculated by fitting the experimental data on the number of cycles to crack initiation and crack growth rate generated for various energy values [73]. (*l*) Is the shortest distance in which the crack would extend before instantaneous or final fracture. In IMPRPK, (*l*) is equal to the diameter of the solder neck region. The typical constants of the Darveaux's model are provided in [4], [14-16], [74]. Table (3) shows the constants of the Darveaux's model for the lead free and lead rich solders.

Table. 3 Constants of the Darveaux's model for the lead free and lead rich solders (assuming the number of cycles to crack initiation=zero) [74]

Material\Parameters	**a**	**b**	**c**	**d**
SAC405	N/A	N/A	0.0068	1.4613
Sn37Pb	N/A	N/A	0.0044	1.3227

It has been reported that Darveaux's model will predict the BGA life with a 25% correlation error [12]. Study by other investigators [76] based on the independent comparison of data has shown much larger inaccuracies.

A volumetric average of the accumulated viscoplastic energy density (equation (7)) is used in Darveaux's equation.

The purpose of the volumetric averaging of the energy is to reduce the sensitivity of the energy values to element size and mesh density used in finite element models for predicting the energy density. The value of the strain energy is equal to the area confined inside the stabilized stress-strain hysteresis loop [75]. Many investigators have reported stabilized hysteresis loops after the first 3 cycles in ATC tests [87].

$$\Delta W_{\text{ave}} = \frac{\sum \Delta W \bullet V}{\sum V} \qquad (7)$$

<u>Perkins life prediction model</u>:

Perkins has used the following relation to calculate the median life of the solders [10]. This life prediction model relates the temperature, geometry and frequency information of the package to the median fatigue life. Equation (8) demonstrates the Perkins model.

$$N_f = \{\left(\frac{100}{\Delta T}\right)^{1.9} \left(\frac{f}{2}\right)^{\frac{1}{3}} e^{1414\left(\frac{1}{Tmax}-\frac{1}{373}\right)}\mathrm{G} \qquad (8)$$

$$G = 12439 - 70.1A - 434B - 1301C - 930D - 272E + 302CD$$

In this relation, (A) is the substrate size, (B) is the CTE mismatch between the board and substrate, (C) is the substrate thickness, (D) is the board thickness and (E) is the ball pitches.

Morrow fatigue life model:

Morrow fatigue life model presented by equation (9) is discussed in detail in references [24] and [52]: The variables in this model are:

$$N_f(50\%) = \frac{1}{2}\left[\frac{2\varepsilon_f}{\Delta W}\right]^{-\frac{1}{C}} \qquad (9)$$

ε_f=fatigue ductility coefficient

ΔW= cyclic visco-plastic strain energy (the confined area inside the cyclic stress-strain hysteresis loop

C= fatigue ductility exponent (-0.5 to -0.7 for common engineering metals)

Engelmaier-wild fatigue life model:

Engelmaier-wild fatigue life model (equation 10 & 11) is another modified version of the Coffin-Manson model that empirically incorporates the dwell time and frequency effect in fatigue life calculation [24]:

$$N_f(50\%) = \frac{1}{2}\left[\frac{2\varepsilon_f'}{\Delta D}\right]^{-\frac{1}{C}} \qquad (10)$$

Where,

ε_f' = ductility coefficient

ΔD = the cyclic total strain energy

C = Fatigue ductility exponent, resulting from:

$$C = -0.442 - 6 \times 10^{-4}\,\overline{T}_{SJ} + 1.74 \times 10^{-2} \ln(1 + \frac{360}{t_D}) \qquad (11)$$

T_{SJ} = mean cyclic solder joint temperature

t_D = Half cycle dwell time in minutes (relates to the cyclic frequency and the shape of the cycles and represents the time available for the stress relaxation/ creep to take place.

Other fatigue life models:

Wong [77] has also introduced another life prediction model (equation (12)).

$$N_f = (\Delta W)^c (A_i / A_D) \qquad (12)$$

In this relation, N_f is the fatigue cycles, C=-1.51, A_D=5.9E-3 mm^2 and A_i is solder crack surface in mm^2.

The effect of the frequency on the fatigue life was also reported by Solomon & Tolksdorf through a frequency modified Coffin-Manson [52], [70].

According to the Fig. 19 & 20, as a result of the area confined inside the stress strain curve, the fatigue life has decreased with decreasing the frequency. Increasing the temperature on the other hand has also decreased the thermal fatigue life of the Sn37Pb solders (as a result of the area inside the hysteresis loop) [52].

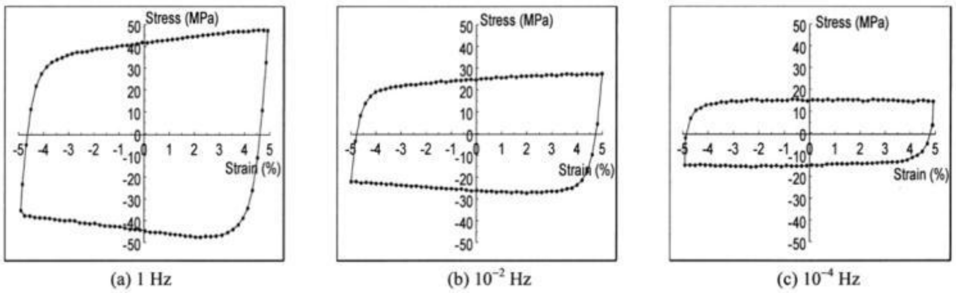

(a) 1 Hz (b) 10^{-2} Hz (c) 10^{-4} Hz

Fig. 19 The effect of the frequency on the hysteresis loop of the Sn37Pb solders (T=25˚C and strain rate of 10%) [27][52]

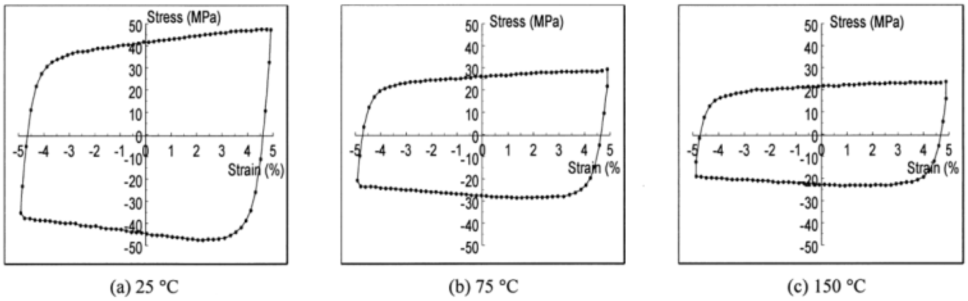

(a) 25 °C (b) 75 °C (c) 150 °C

Fig. 20 The effect of the temperature on the hysteresis loop of the Sn37Pb solders (f=1HZ and strain rate of 10%) [52]

2.3.3.1.2 Key parameters influencing fatigue life

Reviewing various empirical fatigue life prediction models discussed in previous section indicated general agreement in using the induced inelastic strain and strain energy density (caused by the thermal mismatch in the package elements) as the key parameter or descriptor for fatigue life prediction in microelectronics packaging. Reducing the thermal strain by controlling the temperature range (difference in upper and lower temperature values), and minimizing the thermal expansion mismatch of the materials used in package, especially that of the epoxy materials (e.g. epoxy molding compound, underfill, die attach, board and substrate material, etc.) could improve the fatigue life of the microelectronic packages.

Package assembly has a crucial role on the BGA reliability regardless of the solder material [75]. A compliant package-Board assembly will have a better reliability in comparison with the package with high level of thermal mismatch [79]

In addition to the effect of the temperature range on the fatigue life of the BGA solders (T_{high}-T_{low}), the value of the upper and lower temperatures play a significant role on the BGA life. Increasing the upper and lower temperatures, will reduce the thermal fatigue life of the package. Fig. 21 demonstrates this effect for the Sn37Pb and SAC405 solders. Change in BGA geometry which impacts the stress state, influences the solder joint reliability. FEM studies presented in [78] showed a significant impact due a minor change in BGA geometry.

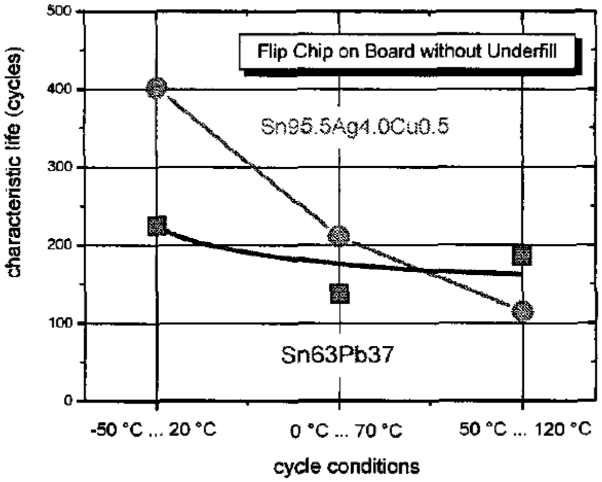

Fig. 21 Effect of temperature values on the BGA characteristic life (cycles) [79]

2.3.3.2 Creep

Creep is defined as a time dependent deformation in the materials and it is generally active at elevated temperatures. Creep models and constitutive equations used in predicting creep deformation and materials response in high temperature are discussed in the following section.

2.3.3.3 Constitutive creep models

There are various constitutive modes which are generally used in determining the temperature dependent strain rate and inelastic creep deformation in materials. In this section some these models used in microelectronics industry will be presented.

Anand constitutive model:

Anand constitutive model is one of the most advanced models used in calculating the inelastic strain rates of the materials [35], [80-83]. The most important feature of the Anand model is its state dependency (strain depends on temperature, stress and loading rate) and the fact that there is no specific yield condition. This means that yield could occur at any non-zero state of stress.

Anand constitutive model is a combination of flow equation with three other equations (equation (13)) which are defining the strain hardening or strain softening of the material [35], [80].

$$\frac{d\dot{a}_P}{dt} = A[Sinh\left(\hat{1}\frac{\sigma}{s}\right)]^{\frac{1}{m}} \exp(\frac{-Q}{KT})$$

$$\frac{ds}{dt} = [h_0|B|]^a \frac{B}{|B|}\frac{d\dot{a}_P}{dt} \qquad (13)$$

$$S^* = \hat{S}\ \{\frac{d\dot{a}_P/dt}{A}\exp(\frac{-Q}{KT})\}^n \quad B = 1-\frac{S}{S^*}$$

In these equations the parameters are as follows:

$\frac{da^{\circ}_p}{dt}$ = effective inelastic deformation rate

σ = effective Cauchy stress

$h_\circ$=hardening constant

s=deformation resistance

s^*=saturation value of s

$\hat{s}$=time derivative of s

T=absolute temperature

m=strain rate sensitivity to stress

a=strain rate sensitivity to hardening

Table (4) lists the constants of the Anand model reported for Sn37Pb and SAC405 BGA solder alloys [35] and [81]. The models are incorporated in finite elements model such as ANSYS.

Table. 4 Constants of the Anand model for the Sn37Pb and SAC405 solders

Parameter	**Sn37Pb**	**SAC405**
$\boldsymbol{s}$	1800 Psi	22.64 Mpa
$\boldsymbol{Q/K}$ **(1/K)**	9400	7619
$\boldsymbol{A}$ **(1/sec)**	4E+6	107.65
$\boldsymbol{\zeta}$	1.5	59.36
$\boldsymbol{h_\circ}$	2E5 Psi	9002 Mpa
$\boldsymbol{m}$	0.303	4.03
$\boldsymbol{\hat{s}}$	2E3 Psi	86.28 Mpa
$\boldsymbol{n}$	0.07	0.0046
$\boldsymbol{a}$	1.3	1.3

Double power law creep model:

The double power law creep model has two terms for low and high strain regimes. Equation (14) shows the typical relation for the Double power law creep.

$$\dot{\varepsilon}_{cr} = A_1 \exp(\frac{-H_1}{KT})(\frac{\sigma}{\sigma_n})^{n_1} + A_2 \exp(\frac{-H_2}{KT})(\frac{\sigma}{\sigma_n})^{n_2} \quad (14)$$

Constants of the double power law creep are reported in the [47], [84], [86-88], and are listed in Table (5)

Table. 5 Constants of the double power law creep model for Sn37Pb and SAC405 materials [84]

Material\Parameter	A1 (1/sec)	H1/K (Kelvin)	n_1	A2 (1/sec)	H2/K (Kelvin)	n_2	σ_n (MPa)
Sn37Pb	1.7E12	5413	3	8.9E24	5413	7	1
SAC405	4E-7	3223	3	1E-12	7348	12	1

Hyperbolic sine creep model:

Hyperbolic sine is the other type of the creep model in which the temperature, and stress dependencies are established via the Arrhenius relation and sinh function, respectively [71], [85]. Equation (15) demonstrates the hyperbolic sine constitutive model commonly used to account for power-law-breakdown occurring at high stress regime. Constants of the hyperbolic sine constitutive model for SAC405 and Sn37Pb solder materials are listed in Table (6) [89] and [90] respectively.

$$\dot{\varepsilon}_{cr} = A[Sinh(\alpha\sigma)]^n \exp(\frac{-H}{KT}) \qquad (15)$$

Table. 6 Constants of the hyperbolic sine constitutive model for the Sn37Pb and SAC405 solder materials

Material\Parameter	A	α (MPa^{-1})	n	H/K (J/mol)
Sn37Pb	10	0.1	2	44900
SAC405	441000	0.005	4.2	45000

2.3.3.4 Key parameters influencing creep

As discussed earlier, time dependent inelastic strain, or creep deformation, has a strong dependency on temperature and stress. Dwell/hold times and temperature are therefore key influencing parameters impacting creep related deformation and failure of the BGAs. As expected, longer hold time at elevated temperature will result in a larger creep effect. Values of the activation energy for creep (Q) and stress exponent (n) (Equation 14) play a significant role in the level of creep occurring in the material.

2.4 Finite Element Method

As a part of the life prediction effort, it is required that we calculate the state of stress and/or energy in particular points of the system. Considering the complexity of microelectronics packaging system, material properties, loading and boundary conditions, determining the system response (e.g. energy, stress, strain, etc.) would become a challenging task. A solution for these challenges would be utilizing the numerical techniques (e.g. ABAQUS, ANSYS) in finding the system response [23]. In these methods the response of the system will be determined based on the given test condition. The principals of the FEM analysis are based on the approximation of the geometry, displacements, material properties and loading and boundary conditions. It has been reported that these parameters could cause inaccuracy in determining the life of the package. Therefore using the proper material properties and geometry data in FEM modes is crucial [69].

2.4.1 How and why to use the FEM for reliability analysis

Commercial FEM codes (e.g. ABAQUS, ANSYS, etc.) are widely used to calculate the response of the complex systems during the fatigue failure analysis. Global (board level) and local (BGA level) FEM solutions are widely utilized for deterministic analysis in conjunction with one of the life prediction models (e.g. Darveaux, etc.) [3]. Global FEM model will provide the displacement of the system which will be used as boundary condition in determining the stress and energy levels of the BGAs (local model).

2.4.2 Key FEM parameters and their significance

Defining the correct geometry, material properties and boundary conditions in the FEM model is critical. Considering the fact that these parameters are the only inputs used by FEM code to determine the system response, it highlights the importance of entering the correct input data in FEM code. Coefficient of thermal expansion (CTE) is one of the material properties which play a significant role in package reliability. Using inaccurate values of the CTE in analysis could result in getting wrong response from the FEM code.

One needs to be cognizant of the fact that the temperature dependency of CTE is defined in two different ways, and inappropriate utilization of it can result in great errors! (Fig. 22)

(i) Tangent CTE which is defined as instantaneous rate of change of the thermal strain with respect to temperature [91]. Equation (16) shows the relation to find the tangent CTE.

$$\alpha_t(T) = \frac{d\varepsilon^{th}(T)}{dT} \qquad (16)$$

(ii) Secant (mean) CTE which is defined relative to T° (reference temperature) [91-92]. Equation (17) demonstrates the secant CTE. T° is the reference temperature in which the strain is equal to zero.

$$\alpha_s(T) = \frac{\varepsilon^{th}(T)}{T - T^{\circ}} \qquad (17)$$

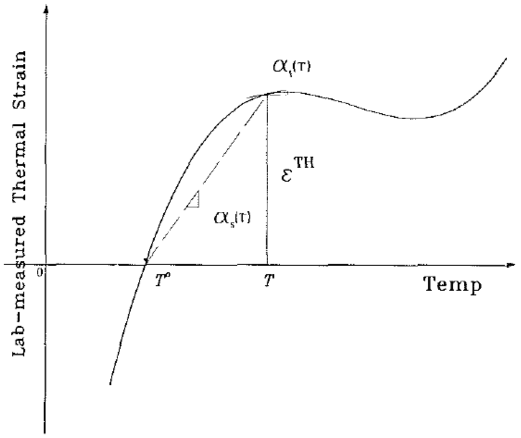

Fig. 22 Comparison between the tangent and secant CTE [91]

It should be noted that ABAQUS uses the secant CTE and entering the tangent CTE instead of secant CTE could result in error.

2.5 Probabilistic methodologies

Natural variabilities are introduced in microelectronic packaging systems during the manufacturing and assembly process, and are present in material properties, component geometry, etc., [12]. It is crucial and an efficient element to include all of these system variabilities into the design of the microelectronic packages to avoid the system failure during the normal operation condition. Even though the optimum values for deterministic analysis is a proper start point for the design process but it is not always reliable. Deviation from the input mean values (nominal values) could result in a substantial impact on the system output (Fig.

23). This fact implies the importance of the probabilistic analysis in manufacturing process of the microelectronic packages. In order to have a reliable and efficient system, the ideal deterministic point must be transferred to the ideal reliable point.

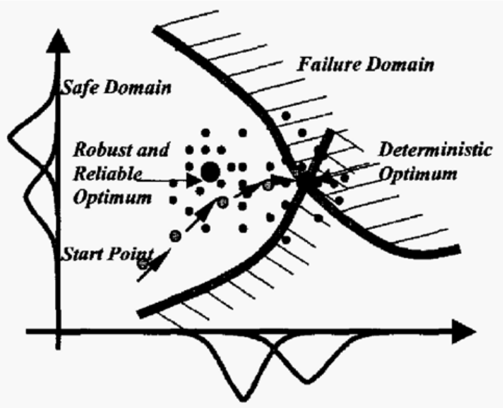

Fig. 23 Comparison between the deterministic and reliable optimum [8]

The probabilistic analysis will insure the safe operation of the microelectronic devices by increasing their reliability. Besides the improvement of the system reliability by incorporating the uncertainties in the design, the level of sensitivity/importance of each variable on the system output could also be determined.

2.5.1 Probabilistic models

Depending on the complexity of the systems and desired confidence level, one of the available probabilistic models could be employed. Direct Monte Carlo model is one of the most recognized and simple models which is widely used for probabilistic analysis. It works based on repeated sampling of the random variables and finding the results of the system for these samples using deterministic analysis. Monte Carlo method requires a large number of samples to be processed in order to get the lower and upper probabilities [94-95].

For the complex and nonlinear systems with multiple physics and complicated geometry, it is required to use the numeric codes (e.g. ABAQUS and ANSYS) in order to predict the behavior and response of the system. In these cases using the Monte Carlo method, which requires hundreds to thousands of random samples, will not be efficient and the theoretical methods (e.g. First Order Reliability Method, Second Order Reliability Method, Mean Value, Advanced Mean Value and Advanced Mean Value Plus) needs to be utilized [95].

Details of these methods are discussed in chapter 6.

2.5.2 SwRI NESSUS and DARWIN

Numerical Evaluation of Stochastic Structures Under Stress (NESSUS) is a modular computer program for performing the probabilistic analysis and it uses one of the many probabilistic methods for structural and mechanical systems analysis [96]. This software has been developed initially by the Southwest Research Institute (SwRI) for NASA in order to perform the probabilistic analysis of the space shuttle main engine components. The capabilities of NESSUS in performing the reliability analysis with different system uncertainties, and probabilistic methods, as well as, its capacity in utilizing the commercially available numeric codes have made it a great tool for reliability analyses [93].

Design Assessment of Reliability With Inspection (DARWIN) is another product from SwRI. DARWIN is a probabilistically-based damage tolerance design code [97] which is originally designed to determine the risk of fracture of the turbine engine.

In this study the NESSUS was used as main tool in predicting the reliability of the microelectronic packages.

Chapter 3

IMPRPK (INTEGRATED METHODOLOGY FOR PREDICTING RELIABILITY OF PACKAGING SYSTEMS)

3.1 Integrated probabilistic approach

It has been decades that the reliability analysis has been implemented in engineering design and manufacturing applications. The principals of the reliability analysis are based on the sampling of the target population and identifying the ratio of the failed samples over the total number of analyzed samples from target population.

$$Reliability = (1 - Probability\ of\ failure) = \frac{Number\ of\ the\ failed\ samples}{Total\ number\ of\ the\ samples}$$

Complexity of the majority of the systems as well as the contribution of different variables on overall system performance necessitates the need for developing a robust and integrated methodology to be used in evaluating the reliability of such systems.

Reliability of any system depends on the performance of the weakest design point of the system. In microelectronics industry first and second level solder interconnects, e.g. C4 Bumps and BGAs, which are commonly used to connect the silicon die to the substrate (first level interconnects, FLI) and as a surface mount technology to connect substrate to PWB printed wiring board (second level interconnect, SLI) [98] are critical reliability concerns. Fig. 24 shows a schematic representation of a FCBGA (Flip Chip Ball Grid Array) microelectronic system with FLI and SLI interconnects. These solders provide mechanical, electrical and thermal support in the electronic packages [40] and are known to commonly fail under the thermal and mechanical loads (e.g. mechanical shocks, thermal cycling, etc.).

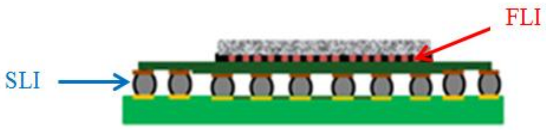

Fig. 24 FCBGA with first and second level interconnects

As it was mentioned previously, the variabilities in any complex system will have direct impact on reliability of that system. This impact could be due to the effect of a single variable (e.g. Substrate thickness, temperature limits or material properties) or a combination of multiple variables.

In the past, and for the most part, the reliability and sensitivity analysis of the microelectronic packages were mainly limited to studying the effect of one or two package variables such as geometry or thermal cycling condition (e.g. Dwell time and temperature range). Example of such approach reported by various investigators is presented in [99].

In order to efficiently study the effect of multiple system parameters (variables) on the overall system reliability, a robust and integrated methodology must be developed. The main goal of this dissertation is to address this need by developing such an Integrated Methodology for Predicting the Reliability of the microelectronics Packaging system (IMPRPK). The IMPRPK methodology also has the capability in incorporating the interaction between many system variables and determining the key parameters influencing the BGA reliability by performing the sensitivity analysis.

The second level BGA interconnects were specifically focused in development and validating the IMPRPK.

The approach which was used in developing IMPRPK consists of three major tasks of (i) Characterization to determine the variabilities and loading condition of the system , (ii) Finite Elements Modeling to calculate the system response to these variables , and (iii) probabilistic and reliability analysis to predict the life and sensitivity of the system.

The details of each task are provided in next section and the dedicated chapters.

3.2 Elements of IMPRPK

This section summarizes the key elements that are used in development and validation of IMPRPK, detailed discussions are provided in next chapters. The three major tasks involved in IMPRPK are:

i. Characterization
ii. Finite Element Method (FEM)
iii. Probabilistic and sensitivity analysis

IMPRPK approach and its key elements are demonstrated in Fig. 25 below.

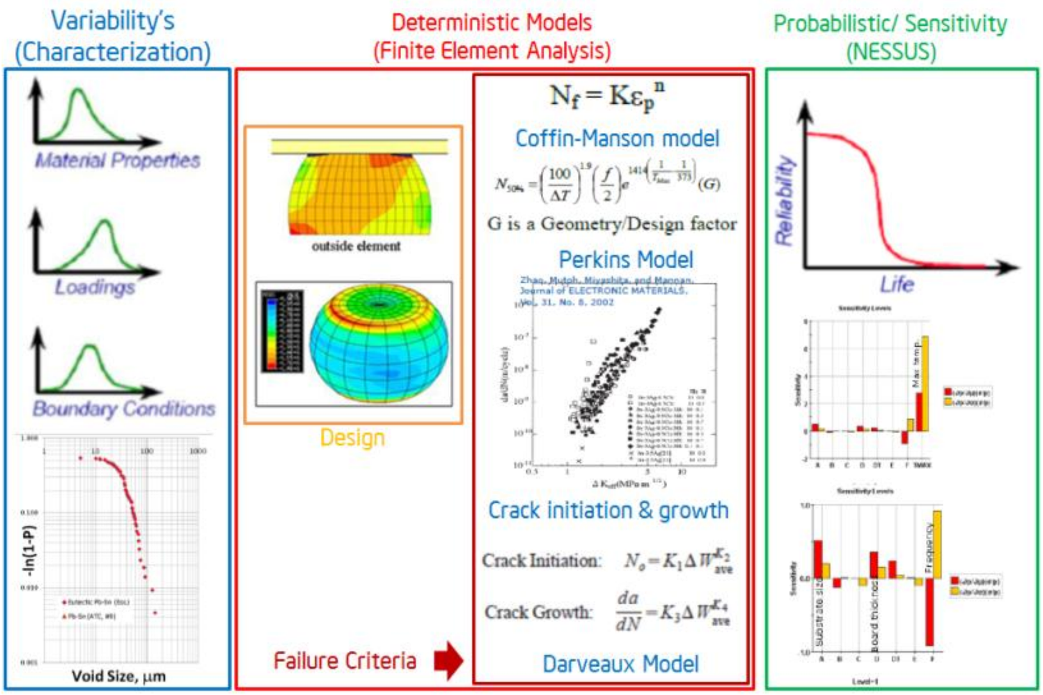

Fig. 25 Overall representation of the Integrated Methodology for Predicting the Reliability of microelectronic Packages (IMPRPK).

Even though IMPRPK is developed using BGA data and analysis, this integrated methodology can be generalized and used for any other system. The key elements involved in extending this methodology to other systems include;

I. identification of the relevant variabilities present in system,

II. development of statistical distributions associated with these variabilities,

III. Identification and selection of appropriate deterministic models for predicting system performance at a specific condition, independent of system variabilities

IV. Incorporating/integrating probabilistic methodology by employing one of the available analysis methods, depending on the complexity of the system and desired confidence level.

Following sections provide a summary of the principles of the three IMPRPK tasks. Detailed discussions are provided in the following chapters.

I. Characterization Task: Characterization is one of the most important elements of any efficient reliability analysis. The information from the characterization task plays a significant role in predicting the reliability of the system. Our effort on this task was focused in collecting various statistical and experimental data in following areas.

- Statistical variabities in geometry and size (e.g. thickness of elements, solder joint stress concentration and radius of curvature)
- material properties (e.g. coefficient of thermal expansion, fracture and failure mechanisms, information on crack initiation and crack growth)
- Defect and microstructural constituents and their size distribution (e.g., post-process/pre-test and post-test porosity size distribution, post-test crack size distribution, inter-metallic components IMC and size distribution)

The statistical data obtained from characterization task I is used in defining the random variable distribution required in the probabilistic analysis section.

Post-test metallography and fractography (Fracture morphology, striation spacing, crack length) data from characterization task is also used to validate the finite element analysis results in task II.

II. Finite Element Method (FEM) Task: FEM method is widely used in determining the response of the system to external loading, including mechanical and/or thermal, providing valuable information on deformation and local stress, strain, displacement, energy density in complex components/systems. In this study FEM models for two complex microelectronics packaging (MEP) systems consisting of (i) molded wire-bond FLI and BGA SLI (ICH form factor), and (ii) flip chip FLI and BGA SLI (MCH form factor) were created. FEM numerical analyses were conducted for these two MEP designs, generating global and local response data on various components, including BGA solders which are the focus of this study. FEM results were generated on both lead-rich and lead-free solder materials.

Solder displacement developed as a result of applied thermal loadings and the thermal mismatch between the components of the package are determined by the “global” coarse mesh density FEM model. The displacement predictions from the global model are then used as the boundary-conditions in fine mesh density “local” model to accurately determine the detailed information on various system responses. The key responses we have used in life prediction models are creep strain and dissipated energy density.

Even though FEM technique is a powerful tool in determining the response of the system, one needs to be careful in ensuring the accuracy and validity of the results obtained from analysis. Chapter 5 discusses potential errors and presents misleading information that may be obtained if a user is not familiar with the FEM and constructs an erroneous model and input data.

There are different numeric codes (e.g. ABAQUS, ANSYS, etc) which are commonly used to calculate the system response. ABAQUS code was used in this study due to its ability in solving the complex solid mechanics problems and the existence of a wide variety of embedded creep models. Details of the Finite Element Model construction and analysis results are discussed in Chapter 5.
The outcomes of the FEM analysis in combination with the statistical data from the characterization section are used in the probabilistic analysis task, and in determining the reliability and sensitivity of complex MEP system to various variabilities.

III. Probabilistic and sensitivity analysis Task: In this task, a probabilistic model such as Monte Carlo, Mean Value, Advanced Mean Value or Advanced Mean Value +is used in determining the reliability of the system experiencing potential variabilities. The variability data are used as different random variables in this approach. The probabilistic approach uses the following steps in determining the nominal probability of the system, as well as, predicting its sensitivity to various parameter. The nominal probability of a system with multiple variabilities is determined by using the mean values of the variables ;

1. Mean and standard deviation values of the random variables are used to construct the appropriate random variable distribution.
2. The deterministic system response for the selected random variables are obtained using the deterministic model
3. A Probabilistic approach, e.g. Monte Carlo, Mean Value, Advanced Mean Value or Advanced Mean Value +, is used in determining the probability of system failure by constructing the nominal probability of the failure (cumulative density function (CDF)) using the mean values of the random variables.
4. The important/critical factors of the system and the sensitivity of the system to various factors are determined by calculating the derivatives of the nominal probability with respect to the mean and standard deviation for each of the probability levels. A plot of the probability derivatives vs. the applied changes to any of the system variables are then constructed for graphical representation of sensitivity analysis. The random variable associated with higher sensitivity values is then considered to have the bigger impact on the reliability of the system compared to the other random variables.

Details of the probabilistic analysis including the random variable selection is discussed in Chapter 6.

In summary, IMPRPK highlights the importance of the parameters which have the largest impact on overall system reliability. Application of this robust and integrated methodology in microelectronics industry will result in considerable time and cost reduction during design and development cycle of future products, as one substitutes IMPRPK simulation for costly and long-cycle reliability tests.

Chapter 4

CHARACTERIZATION

4.1 Introduction

The reliability of the BGA solders as second level interconnects is of significant importance to the performance of microelectronics components and systems. Product design/form-factor, solder alloys, and the inherent variability in materials and/or geometry greatly influence product reliability. Characterization effort is the initial step of three fundamental tasks to develop the Integrated Methodology for Predicting Reliability of microelectronic Package system (IMPRPK). Various characterization techniques (e.g. electrical continuity test, serial sectioning, dye and pry and optical/scanning electron microscopy (SEM) imaging techniques) were employed to process the ICH and MCH packages. The outcomes of the characterization effort are utilized in construction and validation of the Finite Element models (FEM).

Statistical data on crack and defect distribution from the un-tested and tested BGA solders was collected through the characterization activity in order to determine and define the system variability distribution. These random variable distributions will be used in combination with the probabilistic analysis to predict the reliability of the system.

4.1.1 Processing the ICH and MCH packages

Two package form factors were analyzed in this study. Details of these packages which are used to package the I/O control Hub (ICH) and Memory Controller Hub (MCH), are presented in Fig. 26

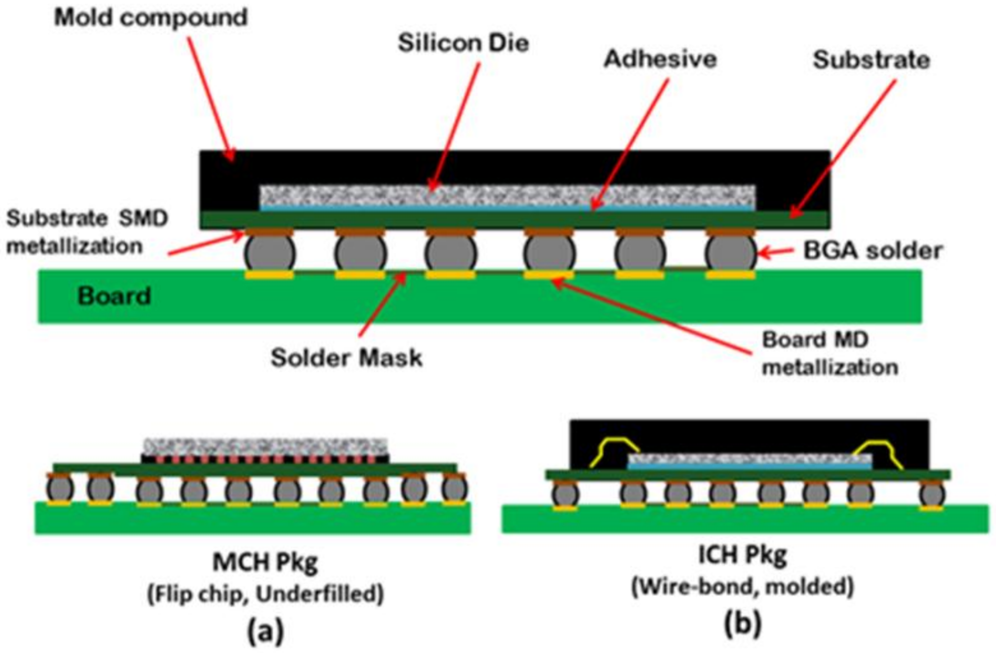

Fig. 26 Details of the ICH and MCH packages.

As it is shown in Fig. 26, the MCH package contains the under filled Flip Chip (FC) First Level Interconnect (FLI) with a full array of Second Level Interconnects (SLI), hence a “FCBGA” design while the ICH package is an over-molded package with wire connections as first level interconnects. The ICH package uses a partial BGA array as second level interconnects (Fig. 27).

MCH and ICH BGA layouts are presented in Fig. 27 (A) and (B), respectively. The nomenclature we use in identifying the physical position of each individual

BGA solder in MCH and ICH packages are also provided in Fig. 27. For example, solder H10 represents a horizontal position of “H”, and the vertical position 10. This solder designation is used throughout our study, including in discussion of the FEM results.

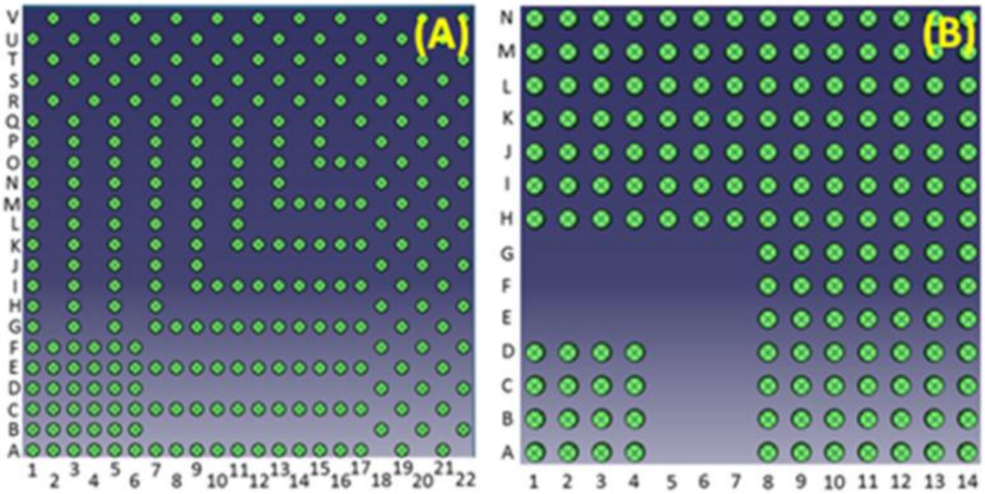

Fig. 27 BGA solder layout in (A) MCH package and (B) ICH package

After the attachment of the ICH and MCH packages to the mother board, these packages were thermally cycled (ATC test) and the extent of the BGA damage in these packages were evaluated utilizing the different characterization techniques.

Fig. 28 shows the simplified typical thermal cycle process which was utilized in processing of the ICH and MCH packages.

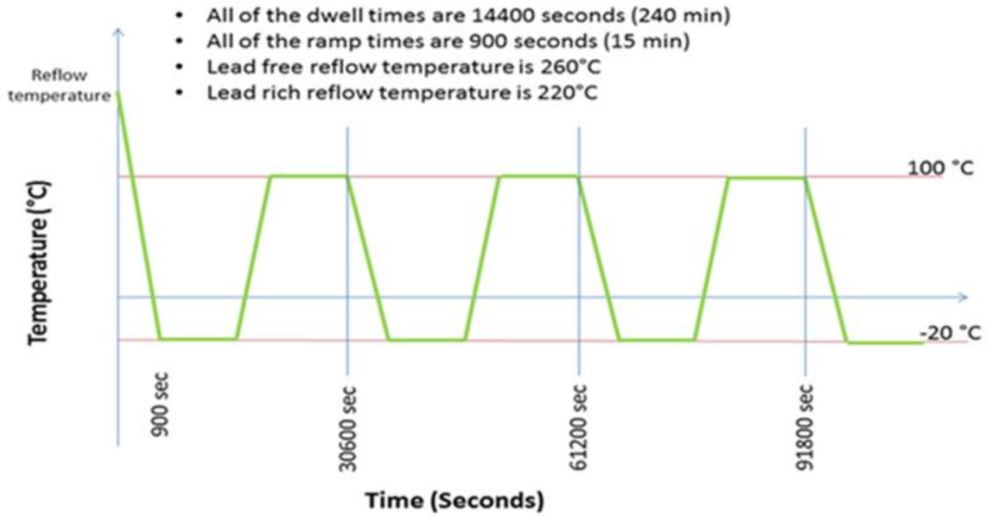

Fig. 28 Temperature cycle profile used in accelerated thermal cycled (ATC)

In each cycle, the ICH and MCH packages were cooled down from the high temperature source to the low temperature source and were heated up to complete the thermal cycle loop. Each of these thermal cycling loops were formed by combination of two ramp steps (ramp down and ramp up) and two dwell or hold steps at upper and lower temperature sources. The actual ramp (temperature-time) profile used in the ATC test of the ICH and MCH packages is shown in Fig. 29.

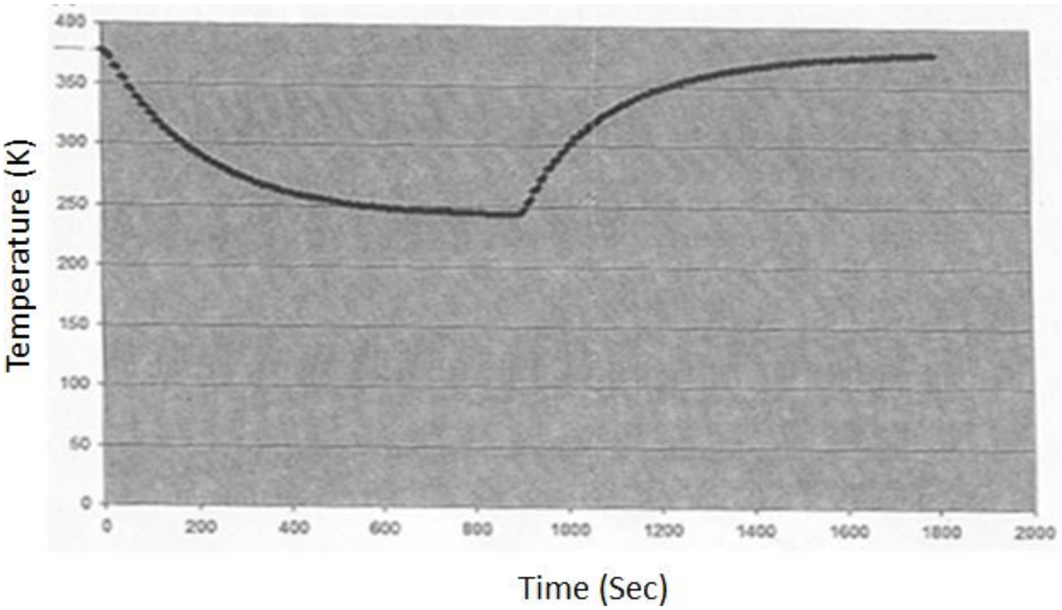

Fig. 29 Temperature-time profile for the ramp steps during the thermal cycling process.

4.2 Characterization Task

In this study, the characterization task was initiated by conducting the electrical continuity test on all of the 47 received boards (Fig. 30). Table. 7 demonstrates the details of the received mother boards with respect to the BGA material properties.

The total of 30 boards were subjected to accelerated thermal cycling test and the details of the ATC test conditions are presented in Table. 8. Details of the received mother boards from Intel Corporation are presented in Appendix B.

Table. 7 Configuration of the Boards evaluated during the IMPRPK project.

Solder material	Number of ATC boards	Number of EOL boards
Sn37Pb	17	7
SAC405	13	10

Table. 8 Details of the ATC test and reflow process

parameter	value
Different dwell times	60 min, 240 min, 480 min
Upper temperature limit	100 ºC
Lower temperature limit	-20 ºC
Reflow temperature	220ºC (Sn37Pb) and 260ºC (SAC405)
Ramp time	900 Sec

The IMPRPK characterization process consists of two major tasks:

1. Non-destructive tests (e.g. X-ray, electrical daisy chain continuity test)
2. Destructive tests (e.g. Dye and Pry, serial sectioning, fractography analysis)

4.2.1 Non-Destructive tests

4.2.1.1 Electric daisy chain continuity test

The first characterization task we performed on the ATC and EOL boards was the electrical continuity test [100].

The principles of the electrical connectivity test is based on the variation in measured resistance of the daisy chained loops (Fig. 31) in the ATC packages and compare them to the resistance of the reference (un-tested time zero) packages.

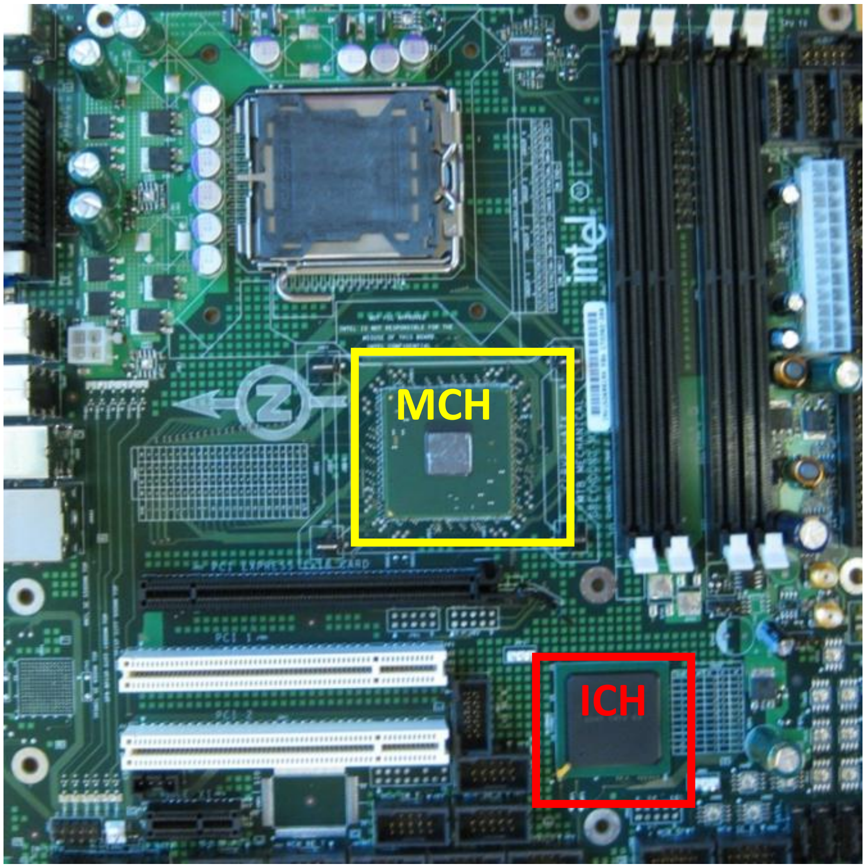

Fig. 30 Overall view of the mother board with the MCH and ICH packages

In these test boards, the BGA solders within the ICH and MCH packages were connected to each other through a daisy chain setup forming an electrically closed loop. Number of the daisy chain rings in any of these ICH and MCH test packages (Also known as test vehicles (TVs)) depends on the areal density of the BGA solders in any of these packages.

The resistance measurements of the ICH and MCH test packages were conducted in two levels using a standard volt meter:

a) Package level measurement

b) Board level measurement

Fig. 31 demonstrates the simple setup which was used to measure the resistivity of the loops (package level resistivity) and the resistivity of the individual lines within the loops. As it was mentioned before, the resistances of the ICH and MCH loops in the EOL (un-tested) packages were used as reference to measure the variation of the resistance in ATC packages. The End of Line (EOL) package level resistances of the ICH and MCH packages (reference resistances) were measured to be 3Ω and 11Ω respectively. In Fig. 31, NW, NE, SE and SW represent the corners of each loop with in the ICH and MCH packages.

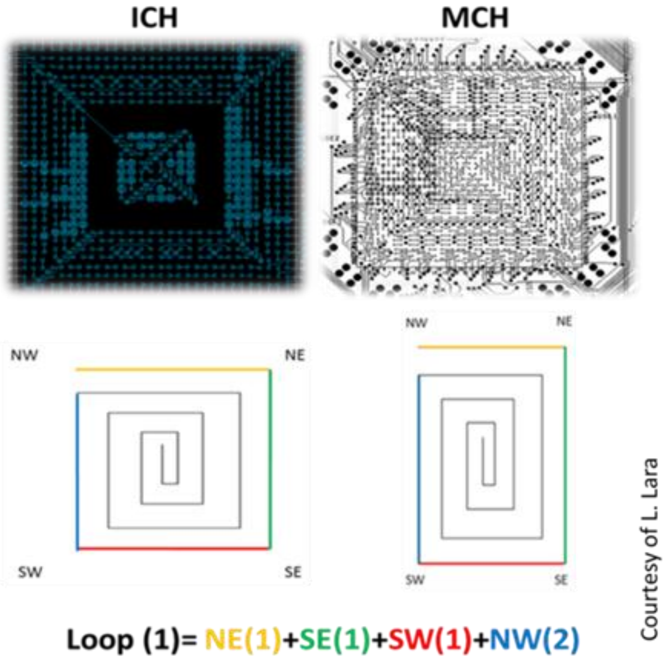

Courtesy of L. Lara

Fig. 31 Setup to measure the electrical continuity of each loop (and individual lines) in the ICH and MCH packages.

Fig. 32 shows the board level (total resistance) resistance measurement setup for the ICH and MCH packages. The board level resistance includes the resistance of the embedded metallization lines inside the board plus the resistance of each loop. The total resistances for the EOL ICH and MCH packages (reference resistances) were 5Ω and 13Ω respectively.

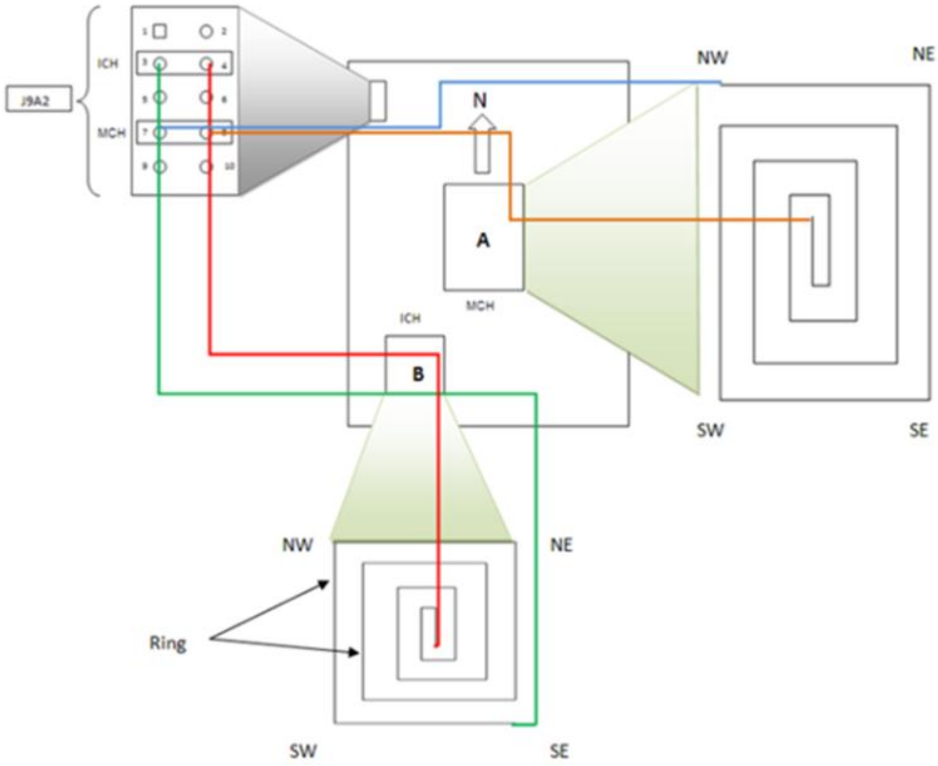

Fig. 32 Setup used to measure the total resistance of the ICH and MCH loops including the resistance of the metallization lines across the mother board. [100]

A color code classification method was constructed based on the measured resistance values along the each line of the loops in daisy chain setup (Fig. 33). It has been reported that the variation in measured resistance of the loops could be used to develop the relation between the inelastic strain (or dissipated energy density) and package life (number of cycles to failure) during the accelerated thermal cycling process [10]. According to this classification, the dashed green line is the indication of having the intact BGA solders while the yellow and red colored lines represent the partial and full electric discontinuity of the BGAs respectively. Increasing the failure percentage of the BGA solders (higher measured resistivity values) will shift the color of the lines from green to yellow, orange and red. Fig. 33 shows the electrical test result for the ICH and MCH packages. The electrical continuity test was performed on 100% of the received mother boards.

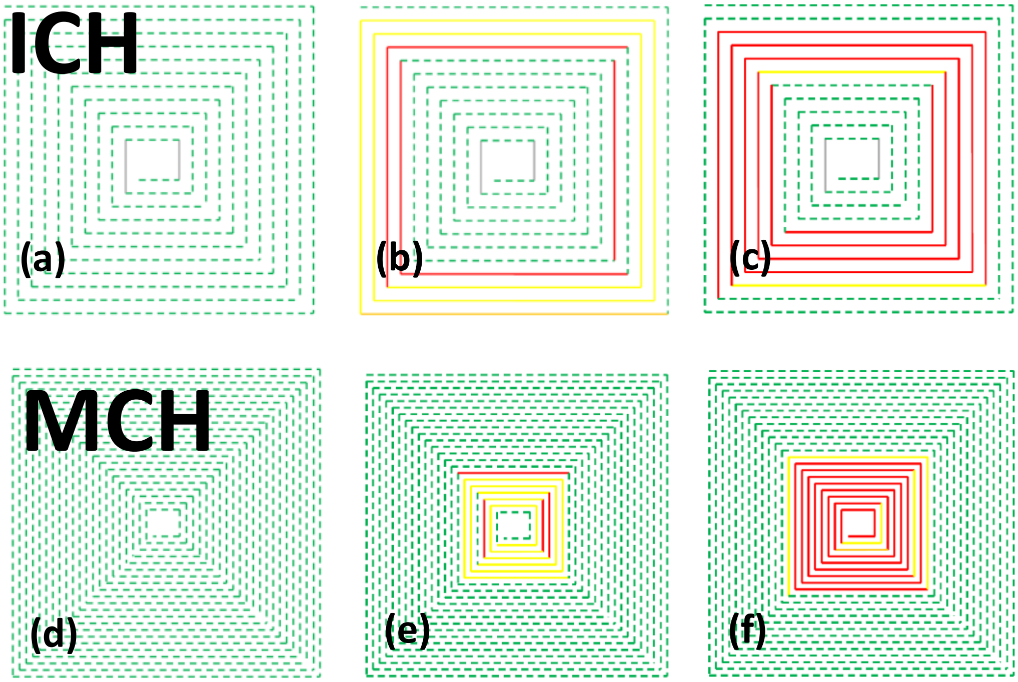

Fig. 33 Typical electrical continuity test results from the ICH and MCH packages [100] Details of the test conditions are (all Sn37Pb BGA solders):

(a) Board-7	(b) Board-5	(c) Board-9	(d) Board-7	(e) Board-9	(f) Board-8
EOL	(-20°C to +100°C)	(-20°C to +100°C)	EOL	(-20°C to +100°C)	(-20°C to +100°C)
	Dwell:480 min	Dwell:240 min		Dwell:240 min	Dwell:240 min
	2338 cycles	3075 cycles		3075 cycles	3526 cycles

The main outcome from this characterization technique was identifying the failure pattern of the ICH and MCH packages. This analysis revealed that the ICH packages have failed outside of the die shadow and under the molding compound area while the MCH packages showed failure pattern under the die shadow region. CTE mismatch between the silicon die, molding compound, and substrate is believed to be responsible for this behavior. FEM analysis in chapter 5 discusses this effect in detail.

Electrical continuity measurements not only defined the failure pattern of the ICH and MCH packages but also provided some valuable information regarding the relation between the dwell time and the number of thermal fatigue cycles (Predicting the dominant failure mechanism for the ICH and MCH packages containing the Sn37Pb and SAC405 solder materials). The electrical test results indicated that in MCH design the number of cycles is more damaging than the dwell time. ICH and MCH packages with about 4400 cycles and 60 minute dwell time demonstrate more damage compared to the similar packages with about 2300 cycles and 480 minute dwell time (Fig. 34). Therefore by reviewing the electrical test results one could conclude that the thermal fatigue failure is more damaging than the creep failure as a result of ATC process.

According to Fig. 34, the intermediate number of cycles and dwell times would result in the highest number of BGA failure

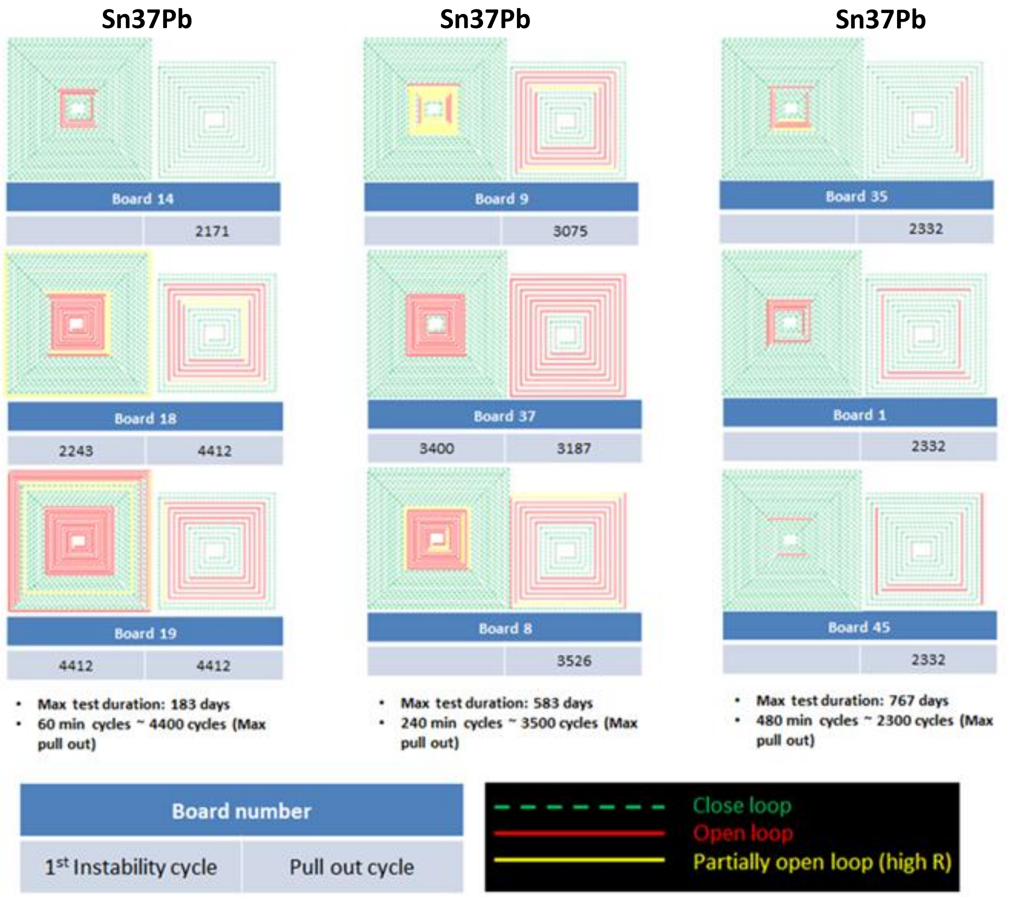

Fig. 34 the electrical test results on Sn37Pb solders proved that the number of cycles are more damaging than the dwell time (Fatigue failure is dominant) [100]

4.2.2 Destructive tests

4.2.2.1 Dye and pry test

After conducting the electrical continuity test and in order to identify the extent of the failure (crack penetration in the BGA solders), a couple of the ICH and MCH packages were selected for the dye and pry experiments (Fig. 35).

Dye and pry is one of the commonly used techniques in microelectronic industry to study the extent of the crack in the solders [27]. Basically in this method the ICH and MCH packages were separated from the mother board (using the water jet cutting unit) and then were placed in the dye solution inside the vacuum chamber for about five minutes. The vacuum level used in this experiment to remove the trapped air from the inside of the package was about 250 torr. This process was repeated for a couple of times and after each run the chamber pressure was increased to atmospheric pressure.

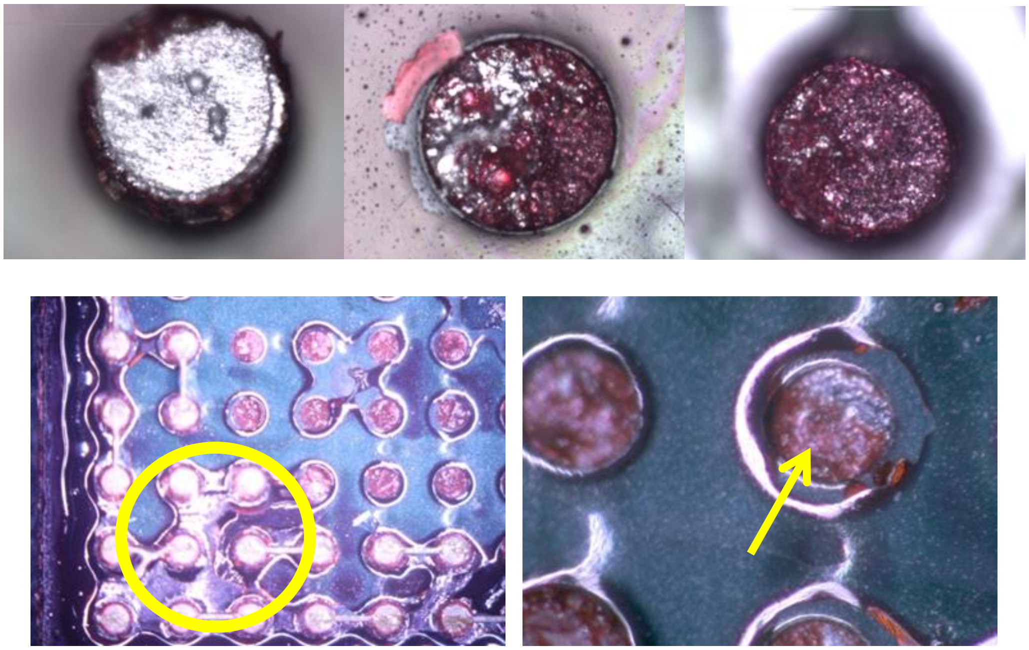

Fig. 35 Dye and pry experiment to determine the extent of the crack in the solders. (Overloaded solder in pry (top-left), partial open solder (top-center), completely open solder evident by full dye coverage (top-right)) & Partial crack growth in the solder (bottom).

The “Dykem” dye solution was used for the dye process. After this step, the dyed packages were let to cure at room temperature overnight. A couple of these dyed and cured packages were pried later (Fig. 35) and the rest were mounted in the clear epoxy resin for future processes steps (polishing and serial sectioning). During the dye and pry process, by removing the trapped air from the interior parts of the package (using the vacuum chamber), the dye solution penetrated inside the crack sites facilitating the precise measurement of the crack penetration in the solder.

Dye and pry is the best way to identify the extend of the crack in the BGA solders since it provides the areal coverage of the failure. These data could be used in detailed life prediction of the BGA solders.

There are two techniques to pry the packages.

1) Twisting the package until the BGAs failure resulting in separation of substrate from the printed circuit board (PCB)
2) Separate the substrate from the PCB by pulling the substrate while the boardside is fixed (Fig. 37).

The second method is recommended since the solders don't get extra damage during the prying process (twisting could add un-wanted damages to the BGAs).

Prying test results of the ATC samples revealed that almost 75% of the BGA solders had failed from the solder neck region in the substrate side of the package and very low percentage of the BGA solders had resin failure (were detached from the epoxy in the board side) (Fig. 36).

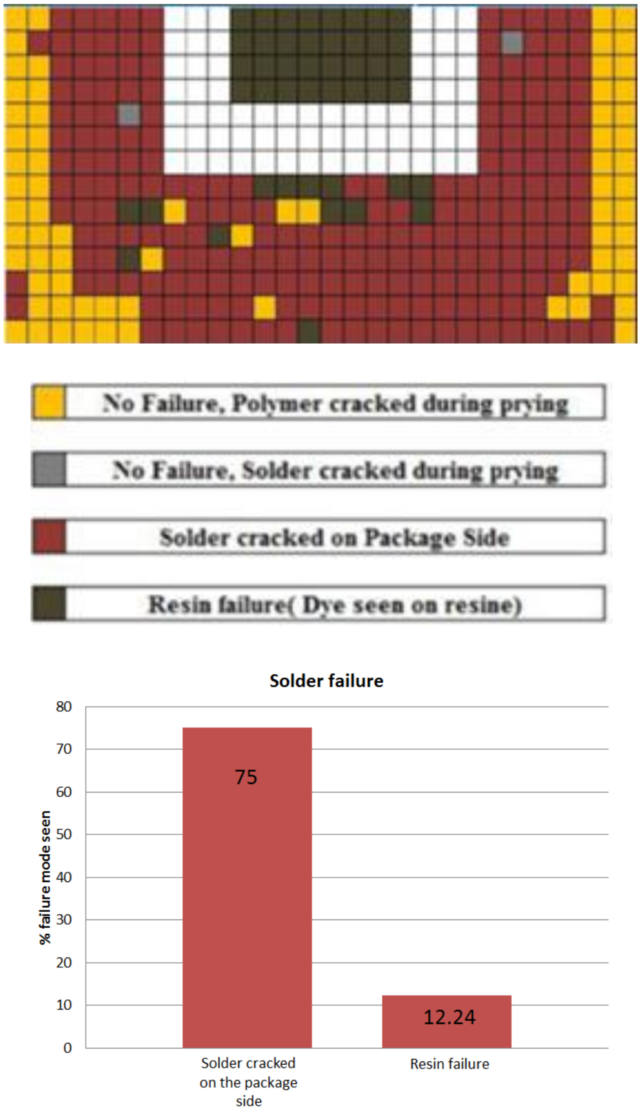

Fig. 36 Solder failure pattern including the position of failure in ICH packages captured from dye and pry experiment. [101]

In Fig. 36, the yellow dots represent the resin failure during the pry test (no failure) while the maroon region represents the BGA failure due to the existence of the cracks

Some of the ICH and MCH packages were only pried (without dyeing). These samples were later used to conduct the fractography analysis on the fracture surfaces in effort to identify the failure mode.

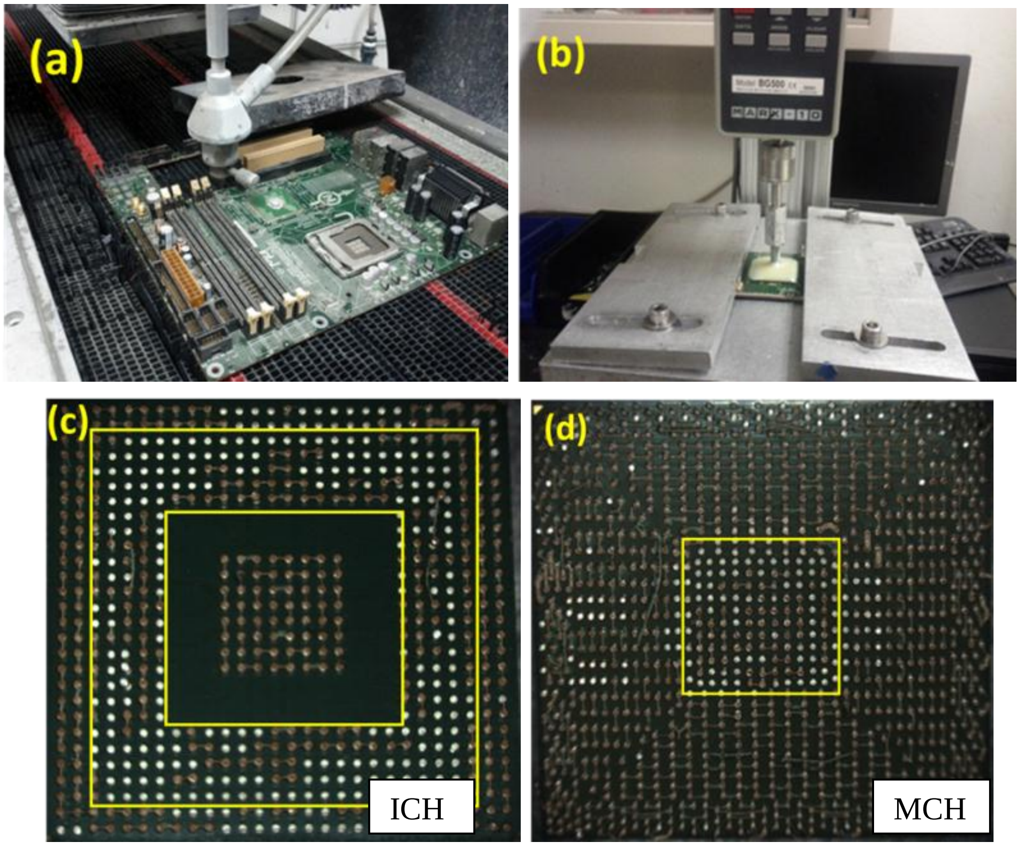

Fig. 37 Cut and pry setup (a & b) [102] and substrate-side solder cracking (bright points) on ICH (c) & MCH (d) packages (Board #8) (Board #8 is tested for 3526 cycles with 240 min dwell times and -20˚C to 100˚C temperature range).

Fig. 37 (a) & (b) shows the sample preparation steps for prying of the ICH and MCH packages. The failure patterns captured from the pry test of the ICH and MCH packages agreed with the failure patterns obtained from the electrical continuity test. Where, in the molded wire bond ICH package shows majority of BGA failure/damage outside of the die shadow region (Fig. 37 c), while the unmolded flip chip MCH package demonstrates the damage under the die region (Fig. 37 d). In this figure the brighter spots represent the BGA solder crack failure while the darker points are the intact BGA solders.

4.2.2.2 Serial sectioning

ICH and MCH packages were mounted in the clear epoxy solution for the accurate serial sectioning Fig. 38. The “EpoFix” resin and hardener solution mixture was utilized to mount these packages. A vacuum chamber with the vacuum level in the range of 250 torr was used to remove the air bobbles from the epoxy solution prior to curing the resin. The curing process took 12 hours to complete.

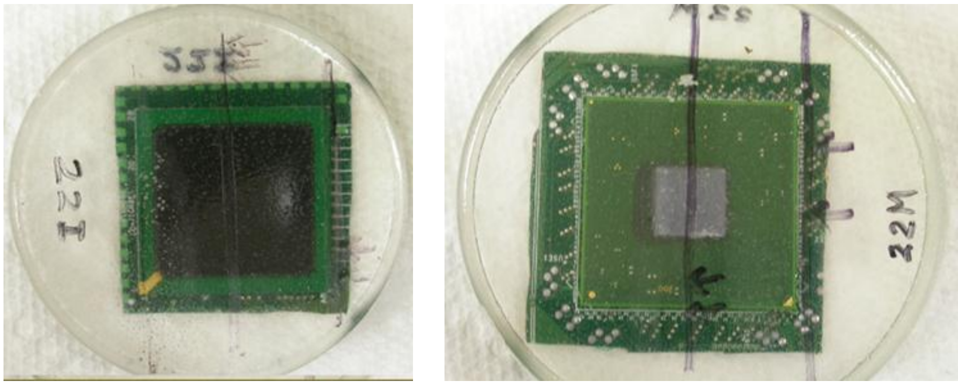

Fig. 38 Epoxy mounted ICH (left) and MCH (right) packages.

These mounted packages were then sliced (using diamond saw) and polished through the center and edge of the packages (Row A and N or V (for ICH and MCH packages respectively)). [For the position please refer to Fig. 27]. The cut position was set based on the dimensions of the package and using the installed micrometer on the diamond saw. A micrometer was also installed on the precision polishing tool as well to insure the proper material removal from the surface of the package.

The Allied high tech diamond saw and precession polishing units were utilized in the sample preparation process of this study.

Precession and hand polishing units with different grit polishing papers (600 & 800 grit for surface removal and 2000 grit for minor surface removal and surface finish) and polishing cloth in combination with polishing solutions (e.g., 1µm Alumina suspension and 0.04 µm colloidal silica suspension) were used as final step for surface finish. In this process the rough polishing papers (600 & 800 grit) were used to remove the material to reach a desire level and then the fine grit polishing pads (2000 grit) were used to smooth out the package surface (5-10 min / 70-100 RPM). The polishing process was completed by using the cloth polishing pads to reach a clean and shiny surface. Polished samples were then analyzed using the different imaging techniques.

4.2.2.3 Optical imaging

Optical microscopes are widely used for characterizing the electronic components (e.g. BGA level solders in microelectronic packages). Optical imaging techniques are accurate and affordable metrology methods providing the detail geometry and defect (e.g. voids and cracks) size and distribution data required for the statistical analysis. Fig. 39 and 40 demonstrate the typical cross section images of the polished surfaces of the Sn37Pb and SAC405 BGA solders.

Fig. 39 represents the End of Line (EOL) Sn37Pb BGA solder. The EOL is a term which is used for the BGA solders after the reflow process and before conducting any ATC tests on them. The End of Line (EOL) SAC405 solders microstructures (Fig. 40) reveals the presence of the needle and round shaped dendrites. The morphology/size of these dendrites is influenced by the cooling rate of the BGAs. The effect of the cooling rate on the shape of these dendrites are presented in [46], [103].

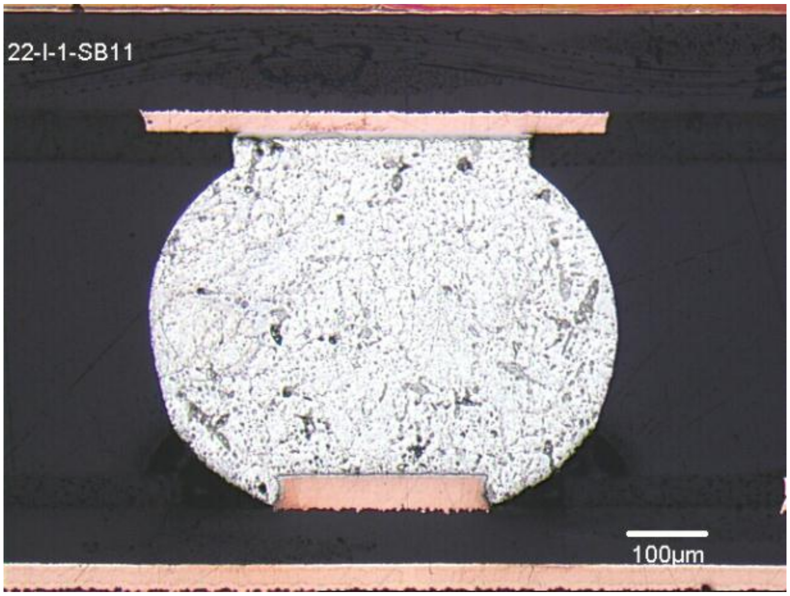

Fig. 39 Typical optical image from the MCH Sn37Pb BGA solders

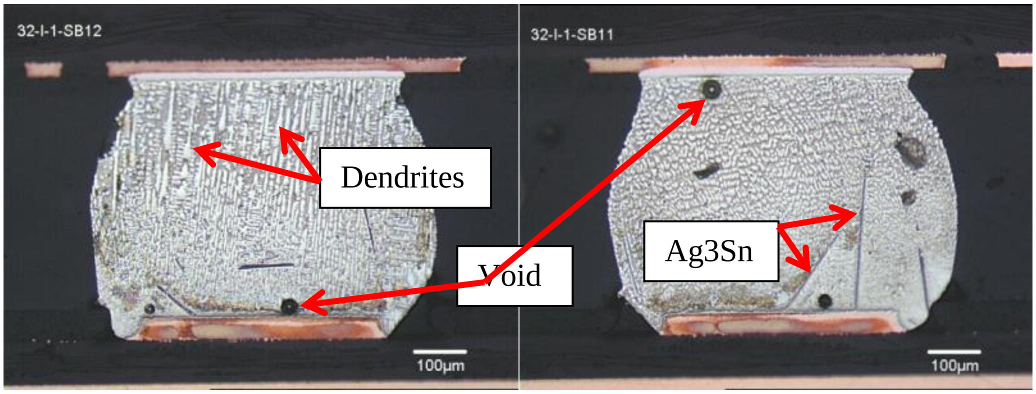

Fig. 40 Typical optical image from the MCH SAC405 BGA solders

4.2.2.3.1 Defect (void) distribution

The location and size of the internal voids and defects in the EOL and ATC samples were investigated and their distributions were populated using the Weibull distribution for the SAC405 and Sn37Pb BGA solders. Since the size of the defects varies between the zero and the size of the component which contains the defect, therefore the Weibull distribution will be appropriate distributions to use for defect distribution. Porosity size distribution observed on BGA solders in this study are presented in Figures 41and 42. Following is some observations based on these data:

- End-Of-Line (EOL) Sn37Pb BGA solders have larger void sizes compared to the SAC405 BGA solders. The largest observed void size (associated with the probability level of 0.5%) for the Sn37Pb solders was about 150 µm while this value was around 80 µm for the SAC405 solders (Fig. 41). Increased defect size could be a contributing factor in increased failure rate of Sn37Pb solders compared to SAC405 BGAs, observed in this study.
- Void sizes are larger in the ATC tested samples, diffusion and consolidation of the smaller voids during thermal cycling could be responsible for this effect. Fig. 42 demonstrates the increase in void sizes after the ATC process. The largest void size associated with ATC Sn37Pn solders are about 230 µ.

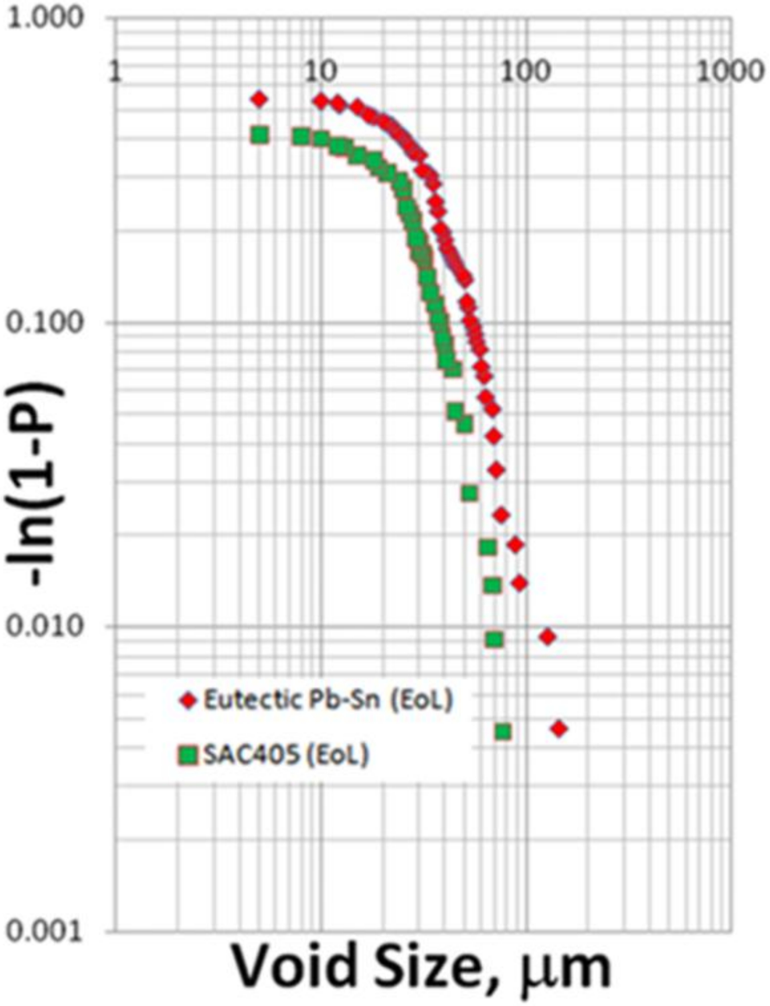

Fig. 41 Void distribution comparison in EOL SAC405 and Sn37Pb solders.

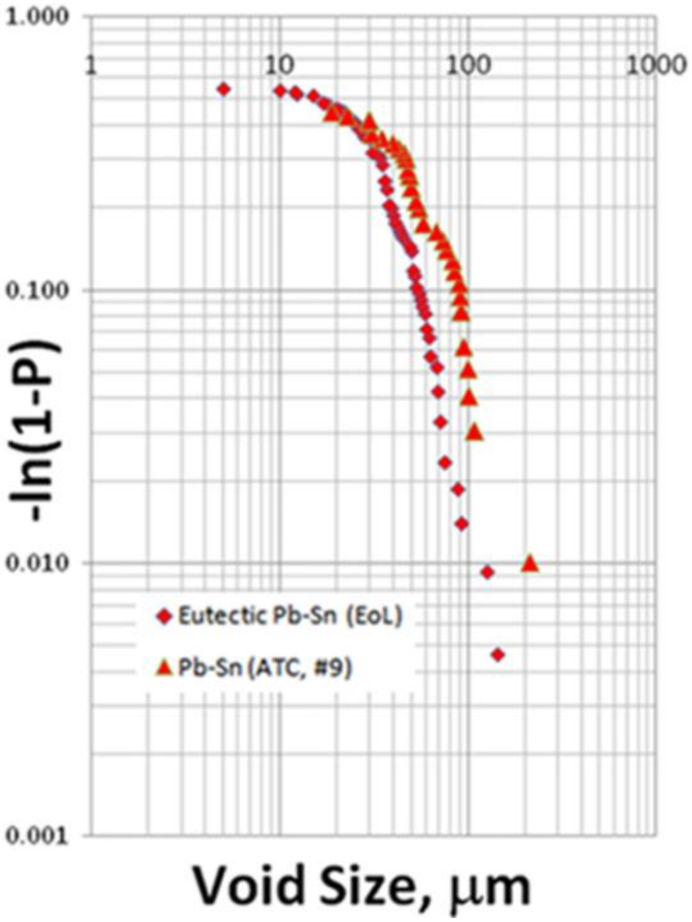

Fig. 42 Increase in void size after ATC test could be due to diffusion and consolidation of smaller voids and forming larger voids.

4.2.2.3.2 Post ATC tested BGA Failure & Cracking

BGA solder crack morphology, location, and size were studied using the optical imaging tools. Fig. 43 and 44 demonstrate the distribution of the cracked BGA array solders in ICH and MCH packages respectively. In the ICH and MCH packages the cracks were populated in different locations with respect to the position of the silicon die and mold compound. In the flip chip MCH package, the cracked BGA joints are mostly located under the silicon die, while the BGA solder joints in the ICH packages with molding compound cracked solders were mostly outside of the silicon die shadow region and under the molding compound. This behavior is mainly associated with the thermal mismatch between the silicon, substrate, molding compound, and the board.

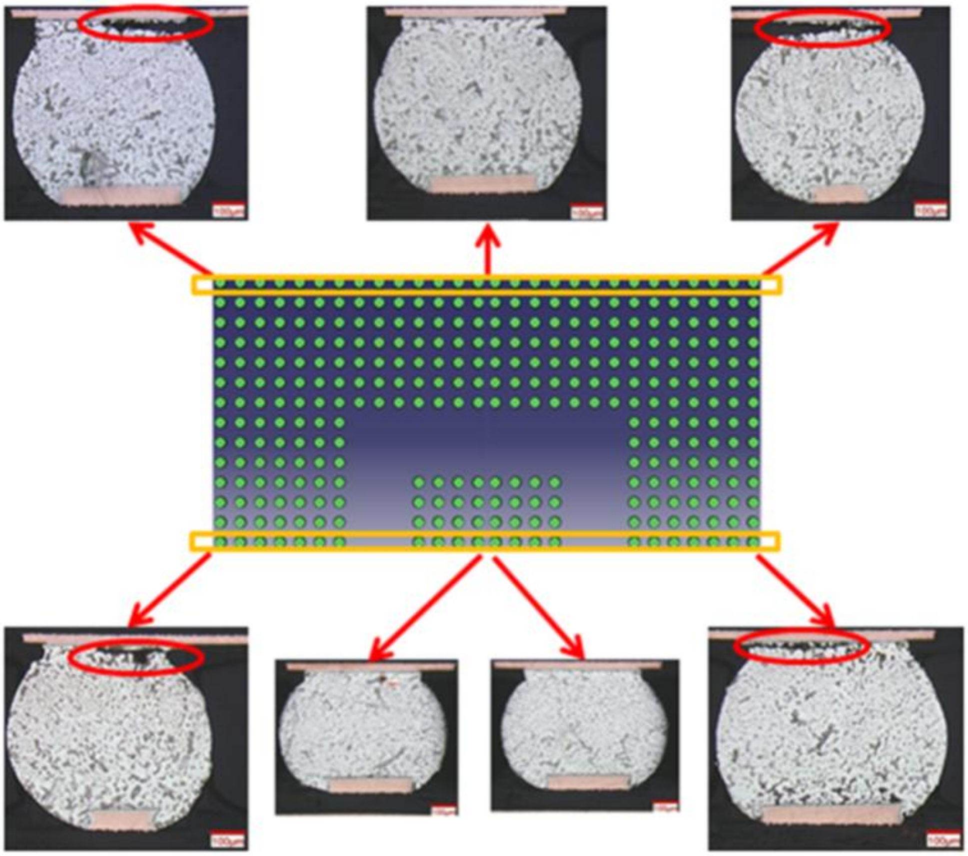

Fig. 43 Crack distribution in the ICH package

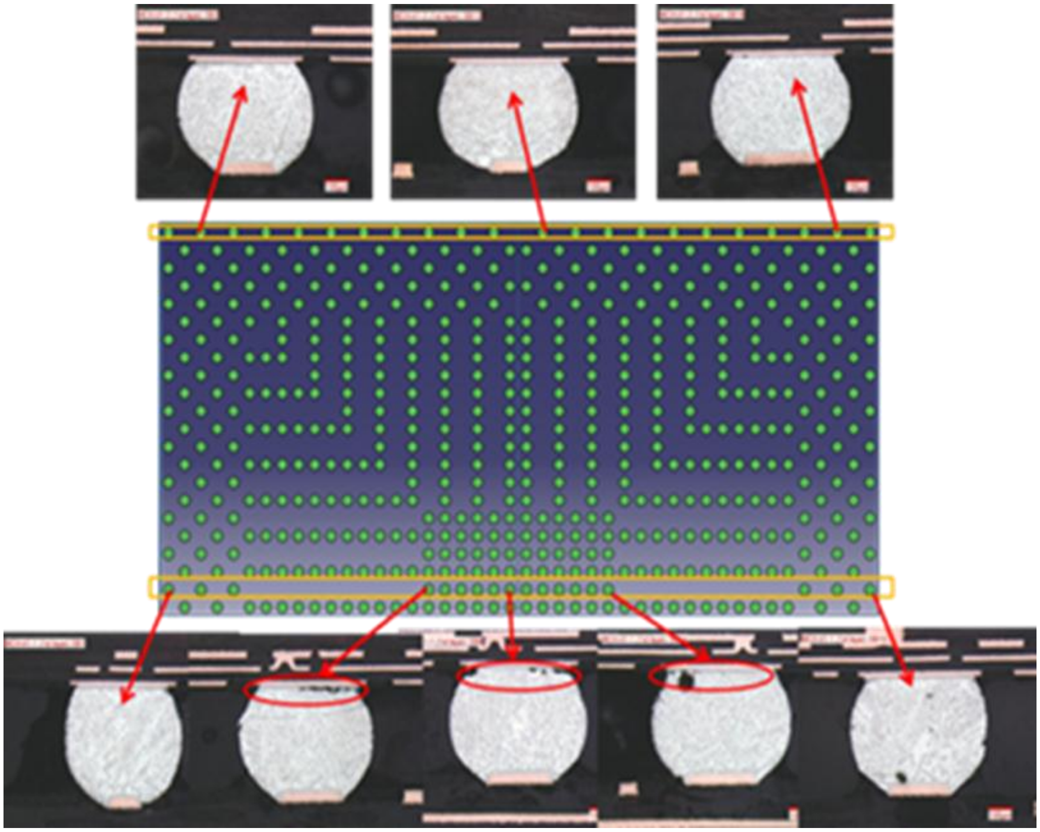

Fig. 44 Crack distribution in the MCH package

The failure patterns observed through metallographic analysis presented here are similar to that observed in the electrical continuity and dye and pry tests. The measured crack length data versus the distance from neutral point (DNP) obtained from cross sectioned ICH and MCH packages are presented in Fig. 45. Each data point in the consolidated graphs in Figure 45 represents the crack length in single solder from the array.

These failure patterns are used in validating the FEM analysis. Chapter 5, discusses the approach and the integrity of the FEM models through independent comparison of model prediction with these characterization data.

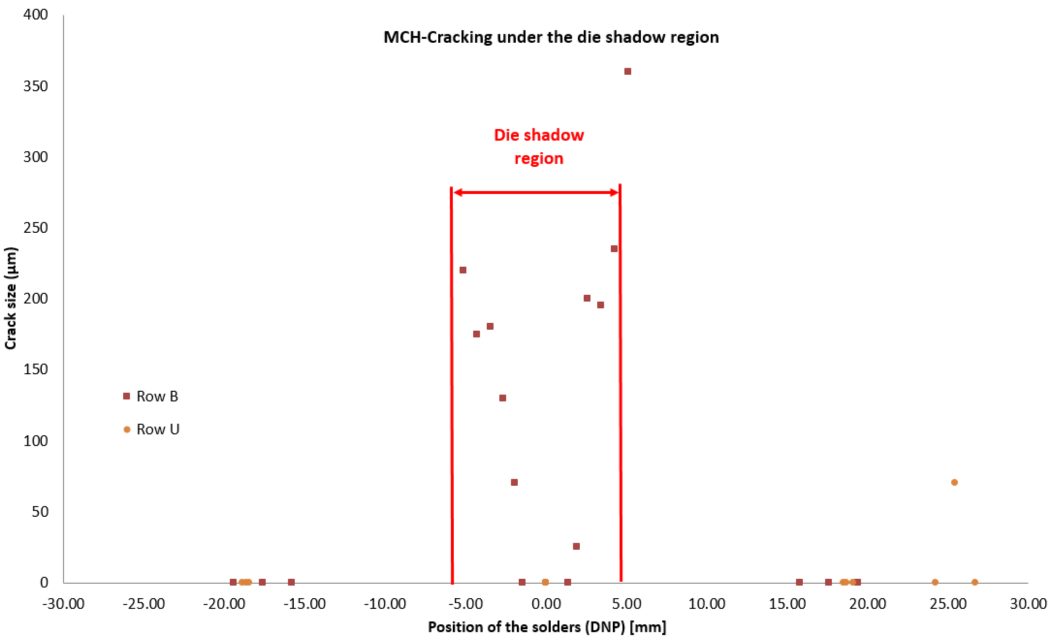

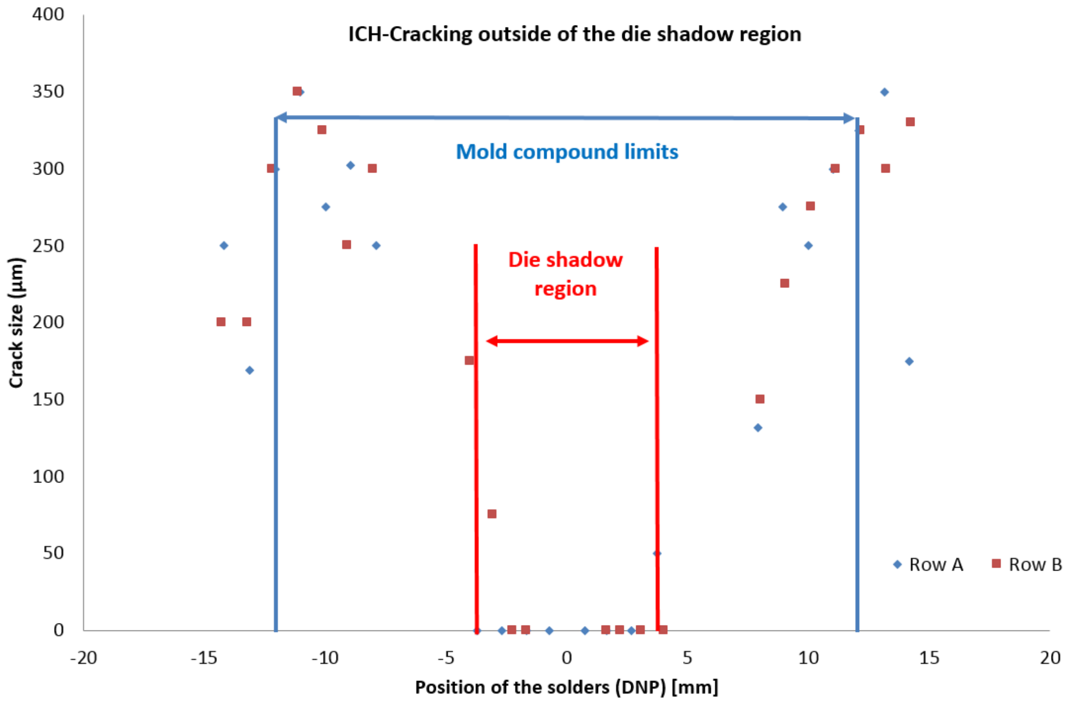

Fig. 45 Crack distribution vs. Solder position (DNP) in the MCH (top) and ICH (bottom) packages. (Data are from board#9 (Sn37Pb))

4.2.2.3.3 BGA Solder crack Morphology

Solder crack morphology was evaluated by optical microscopy of the sectioned and polished samples. Cracks are commonly initiated from the interior side of the BGAs (facing to the neutral point). Intergranular cracking (crack growth along the grain boundaries), as well as transgranular cracks (passing through the grains) are observed in these solder joints. Intergranular cracking is indicative of brittle failure due to weak grain boundaries and/or due to creep failure, while transgranular failure could be associated with fatigue failure. Fig. 46 shows a view of the intergranular cracks. The intergranular failure in creep dominated failure mode is associated with nucleation, growth and coalescence of the cavities on grains or interphase boundaries [37].

Fig. 47 shows the transgranular crack observed in cross sectioned ICH package from board number 9 (Sn37Pb solder). This sample was exposed to dye prior to cross sectioning of the sample. In this figure the penetrated dye in the crack site is also visible.

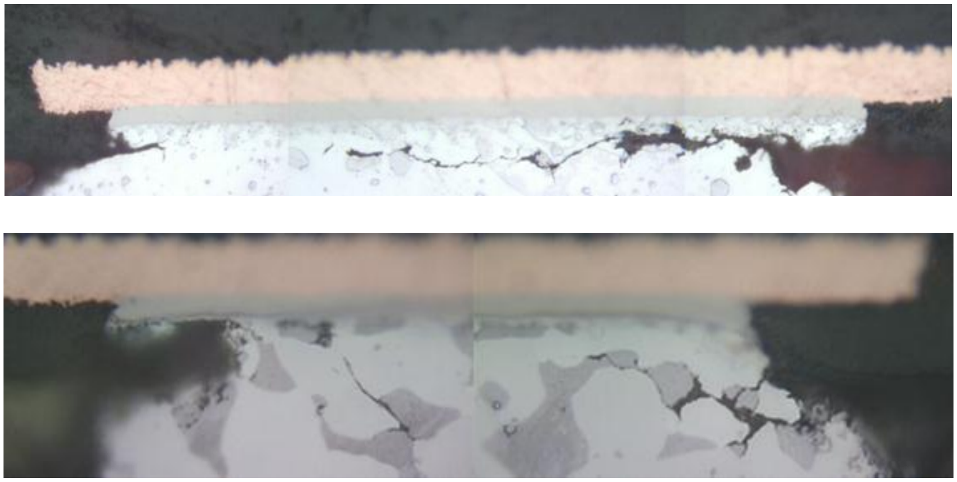

Fig. 46 Intergranular cracking in SAC405 (Board # 41) (top) and Sn37Pb (Board # 9) (bottom) solders.

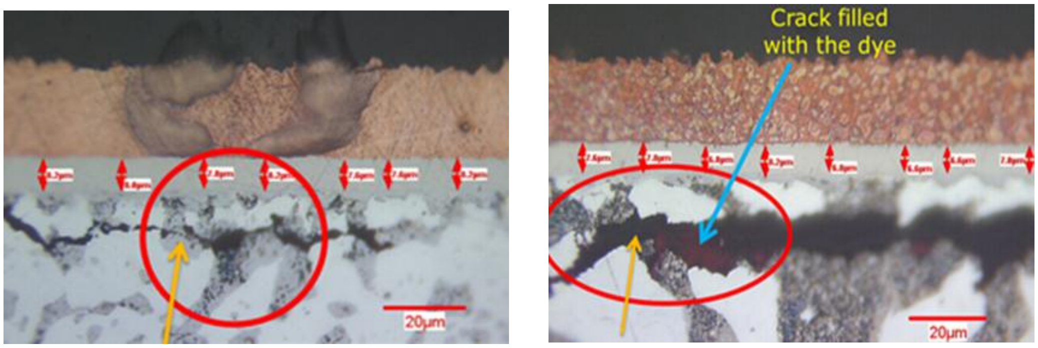

Fig. 47 Transgranular crack in the package side (Sn37Pb (Board #9))

Based on these observations, the contribution from both fatigue and creep failure mechanisms in overall BGA failure is speculated.

4.2.2.3.4 Inter Metallic Compound (IMC)

The Inter Metallic Compound (IMC) layers are one of the co-products of the BGA formation process (Fig. 48). Formation of these IMC layers is mainly due to the diffusion of the Copper and Tin atoms in each other’s sites and creating the Cu_5Sn_6 composition (Fig. 53).

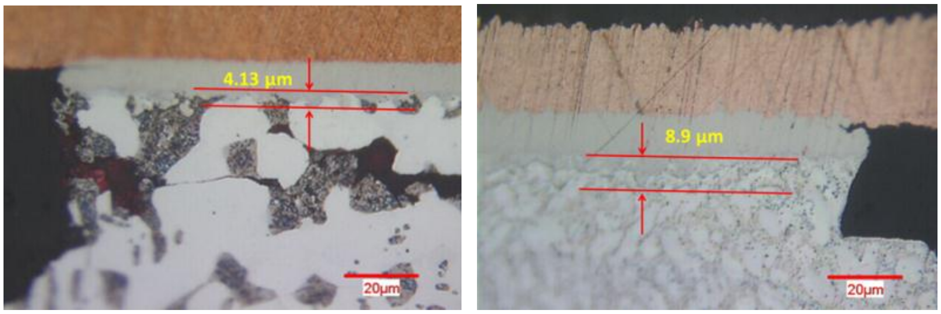

Fig. 48 Intermetallic compound layer thickness (Sn37Pb (left) and SAC405 (right))

These IMC layers are located at the interface of the solder and copper layers. Because of the brittle nature of these IMC layers they play a significant role in BGA failure by providing the crack initiation sites at the solder-copper interface. In some cases the solders would fail through the IMC layer (Fig. 49)

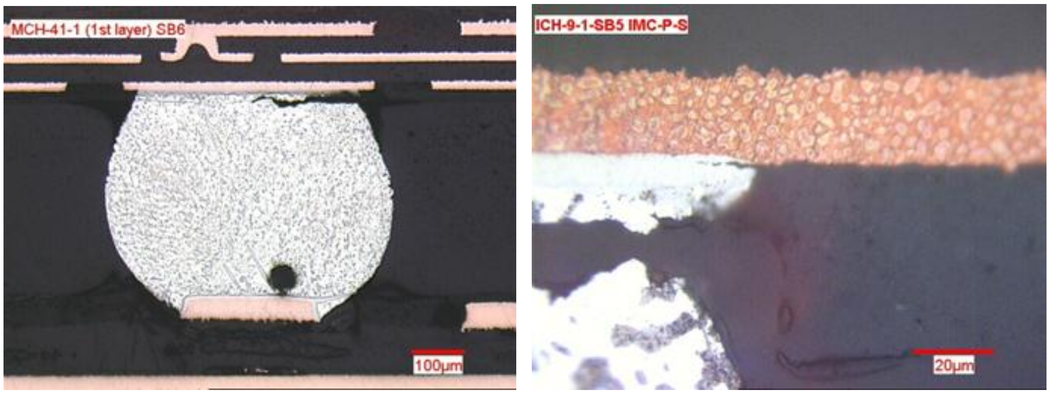

Fig. 49 Initiation and penetration of the cracks through the IMC layer or along the solder-IMC interface (SAC405-MCH (left) and Sn37Pb-ICH (right)).

Substrate side of the packages will undergo multiple thermal exposures and therefore the thickness of the IMC layers in the substrate side of the BGAs is slightly larger than the board side. Thicknesses of the IMC layers were also sensitive to the solder material composition and processing condition. Comparison between the SAC405 and Sn37Pb solders indicated a thicker IMC layers in SAC405 solders over the Sn37Pb solders. This is due to the higher reflow temperature in soldering process of SAC405 BGAs (260˚C and 220˚C for SAC405 and Sn37Pb solders respectively). Fig. 48 demonstrates the higher IMC thickness in SAC405 solder compared to Sn37Pb solder.

4.2.2.3.5 Inter Dendritic Cracks (IDC)

The Inter Dendritic Cracks (IDC) was observed in the lead free BGAs in metallographically prepared samples and optical imaging. Even though the SAC405 solder is a ternary eutectic alloy it solidifies to off-eutectic microstructure due to non-equilibrium solidification [104]. Weibull distribution of the IDC sizes is shown in Fig. 50. IDC size as large as 100μm was observed on the BGA's evaluated. It was also noticed that the majority of these IDCs are oriented along the 45 degree angle. These IDCs can act as potential fatigue crack initiation site in SAC405 solders.

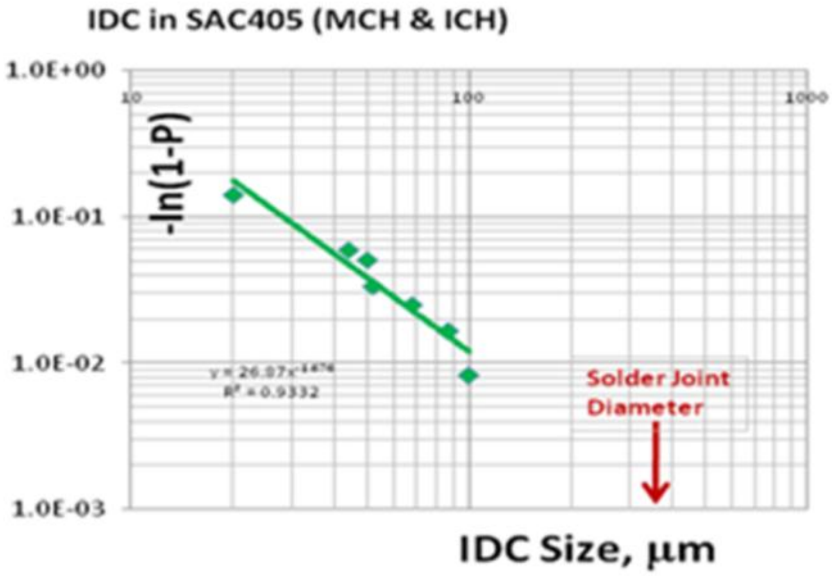

Fig. 50 IDC distribution in the SAC405 BGA solders.

Typical position of the voids and IDCs in the EOL SAC405 solders is presented in Fig. 51.

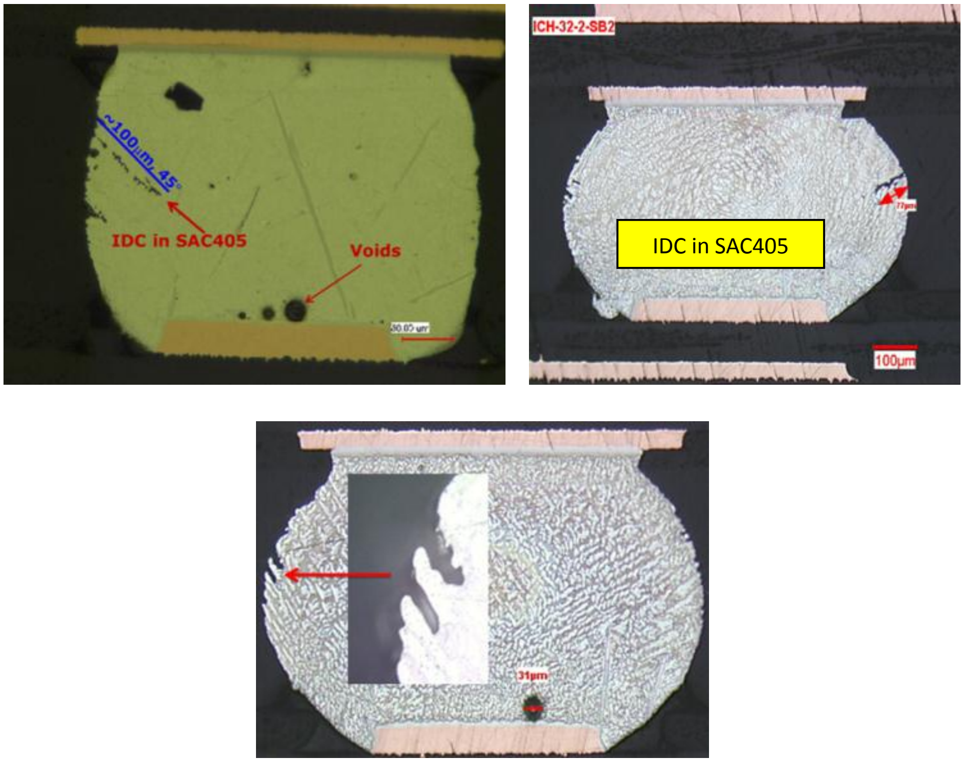

Fig. 51 The typical position of the voids and IDCs in the EOL ICH SAC405 solders.

4.2.2.4 SEM imaging & EDX (Energy dispersive X-Ray spectroscopy)

The Cross sectioned surfaces of the polished ICH and MCH packages were analyzed using the Scanning Electron Microscopy (SEM). The surfaces were coated with a thin layer of gold to prevent the charging effect during the SEM imaging. The charging effect is a result of electrons accumulation on non-conductive material and creation of an electric shock. In addition to information on the position of the cracks and IMC thickness (Fig. 52), the compositions of these intermetallic compounds were also identified using the energy dispersive x-ray spectroscopy (EDX) (Fig. 53). Energy Dispersive X-ray Spectroscopy (EDX) also provided valuable information about the composition of the components in the solder. Composition of the IMC layer in the SAC405 solder is shown in Fig. 53.

Fractographic analysis of fracture surfaces by SEM provided valuable information on failure modes. Presence of the striation on the fracture surface (Fig. 54) is an indication of fatigue failure in the ICH packages. The striation spacing data could be used in validating fatigue crack growth rate.

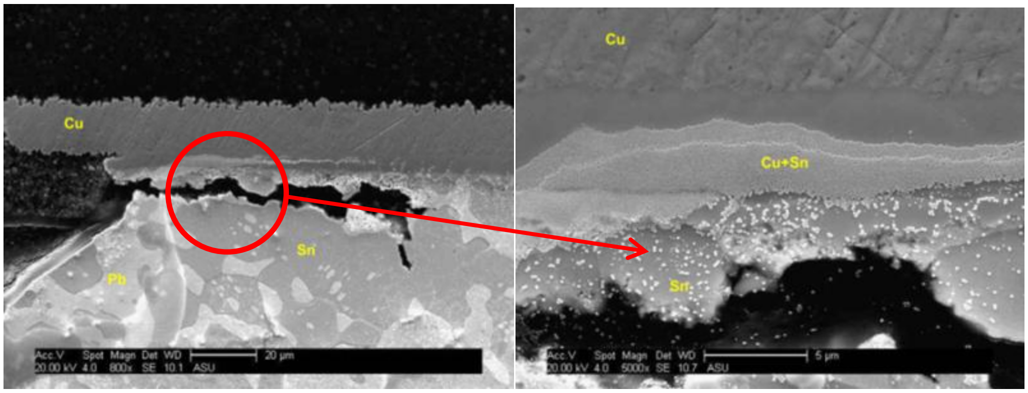

Fig. 52 SEM image shows the position of the cracks in the solder neck region (Substrate side) ICH Sn37Pb

Fig. 52 reveals the crack initiating in the solder-IMC interface and then penetrating in the body of the BGA (intergranular failure).

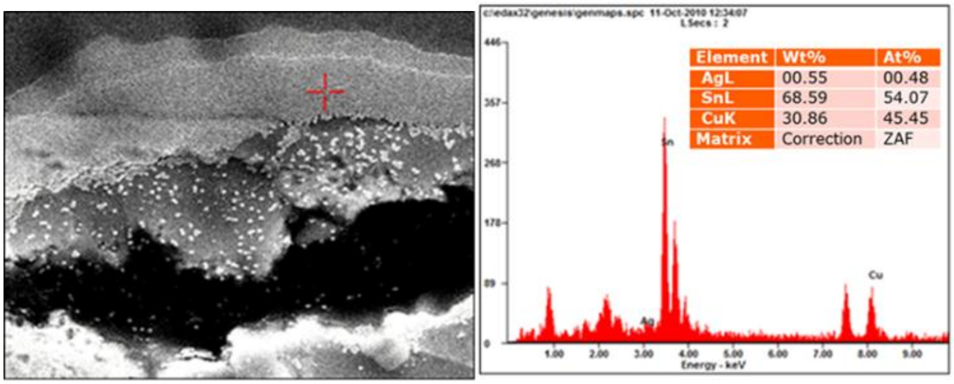

Element	Wt%	At%
AgL	00.55	00.48
SnL	68.59	54.07
CuK	30.86	45.45
Matrix	Correction	ZAF

Fig. 53 EDX data obtained from the cross section of the ICH SAC405 (Board # 41) solder shows the composition of the IMC (Cu_5Sn_6) layer in solder neck region.

4.2.2.5 Fractography analysis

The fracture surfaces of the pried packages were analyzed using the Scanning Electron Microscope (SEM) to evaluate the fracture surface and identify the potential failure mode. Captured SEM images from the fracture surface revealed the existence of the striation rings on the fracture surface which was an indication of the fatigue failure mode. The recent observation supports the fatigue failure mode in the Sn37Pb solders and is in agreement with the electrical test results. Fig. 54 displays these striations on the fracture surface of the ICH-Sn37Pb solders.

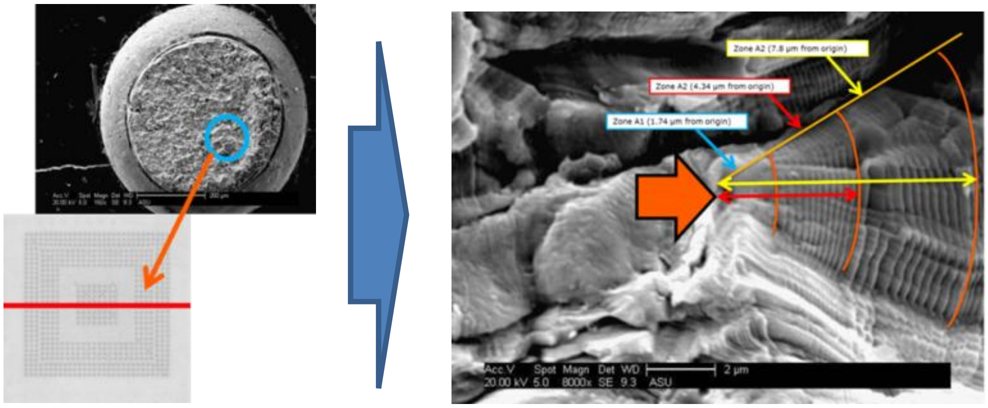
Zone A2 (7.8 µm from origin)
Zone A2 (4.34 µm from origin)
Zone A1 (1.74 µm from origin)
Acc.V Spot Magn Det WD 2 µm
20.00 kV 5.0 8000x SE 9.3 ASU

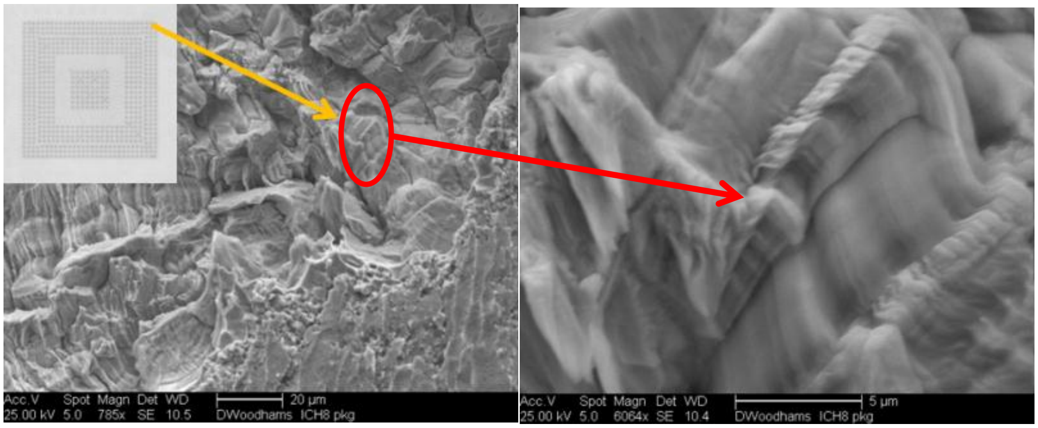
Acc.V Spot Magn Det WD 20 µm
25.00 kV 5.0 785x SE 10.5 DWoodhams ICH8 pkg
Acc.V Spot Magn Det WD 5 µm
25.00 kV 5.0 6064x SE 10.4 DWoodhams ICH8 pkg

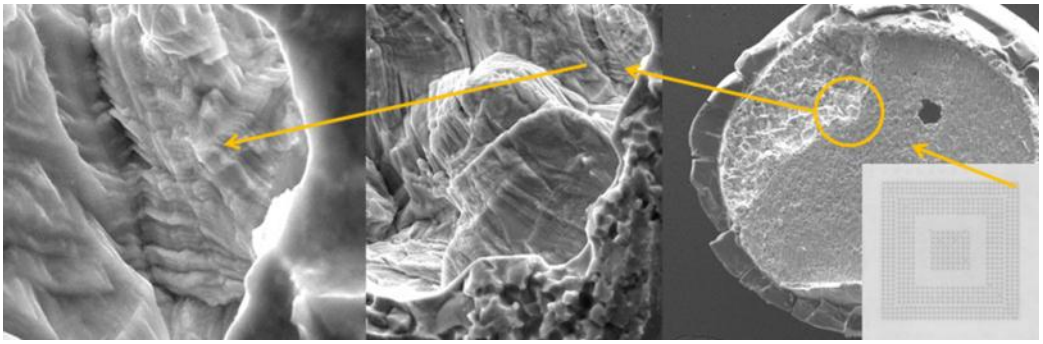

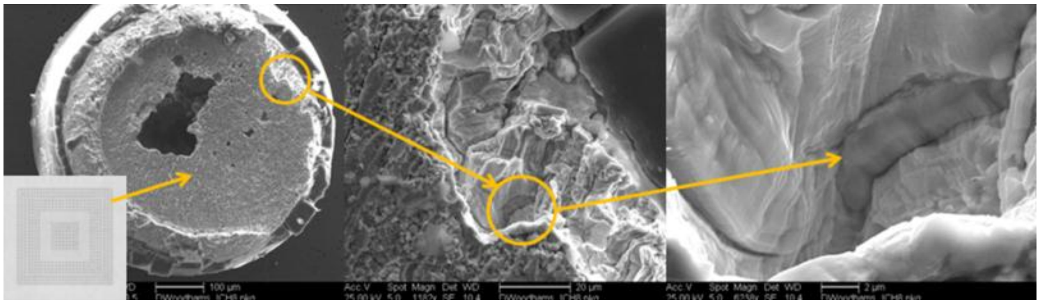

Fig. 54 SEM images from the fracture surface of the ICH Sn37Pb BGA, demonstrating the Fatigue Failure mode (ICH-Sn37Pb).

Limited SEM images from the fracture surface of the SAC405 solders did not show such clear striation rings, as those seen in the Sn37Pb solders.

Striation spacing data can be used in estimating crack growth rate and hence, the constants of Darveaux's model. The presence of voids and cavities in the fracture surface of the BGAs (package side) were also noted in SEM analysis, as shown in Fig. 54. These voids and surface defects could be potential sites for the crack initiation and growth.

In addition to the striations, failure along grain boundaries were also observed on the fracture surface. Fig. 55 shows such intergranular separation (this mode of fracture is reference as a "rock candy" fracture by some investigators).

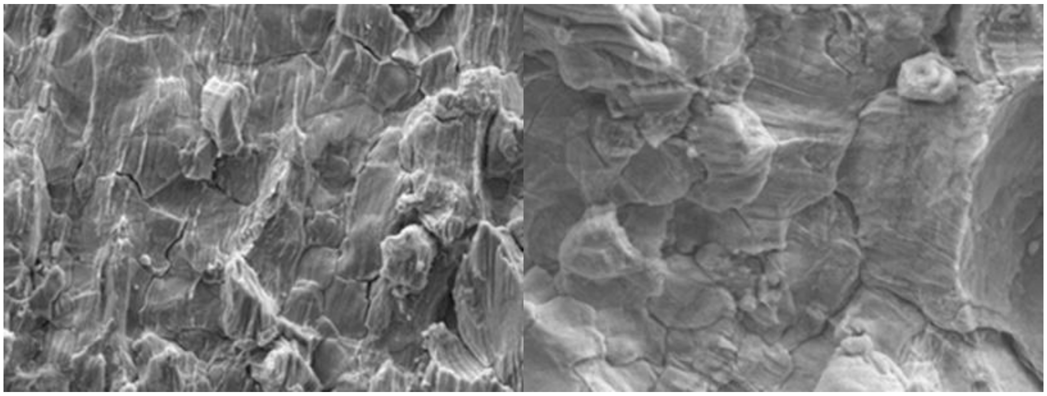

Fig. 55 Intergranular features on the fracture surface (ICH-Sn37Pb)

The recent observation is the evidence supporting the fatigue failure in the Sn37Pb solders.

4.3 Summary

For the most part, captured data from the characterization segment of the IMPRPK has provided valuable statistical data required in probabilistic analysis. The results of the electrical continuity, dye and pry and crack distribution patters have shown similar trend. Striation spacing, as well as, the extent of cracking from metallographic analysis in combination with dissipated energy values in the solder neck region (From FEM analysis) could be used in developing the crack growth model and/or calculating the constants of such crack growth based life prediction model (e.g. Darveaux's model). It was also noticed that the failure mode in the ICH and MCH packages is a combination of the fatigue and creep mechanisms. Statistical data on void size were used in the probabilistic analysis task as one of the variability present in MEP systems.

Chapter 5

FEM ANALYSIS

5.1 Introduction

Finite Element Method (FEM), also known as Finite Element Analysis is a numerical technique which is used to find the approximate solutions for Partial Differential Equations (PDE) and integrals. Essentially, the main concept of the FEM analysis is reducing the complications of the complex systems by dividing the system into small elements and solving them with respect to the rest of the elements. Using this technique, to solve the complicated systems is more efficient and effective. The FEM analysis in the form that we use today was first introduced by R.L. Courant in 1942 [105]. With developments in computing systems, the FEM approach has entered in a new phase with improved mathematical and numeric techniques [106-107].

The unique capability of the finite element analysis in solving complex problems makes it an extremely powerful tool for design engineers in different industries (e.g., Aerospace, Automobile, defense and electronics).

In general, the principles of the engineering computational techniques, like FEM, are based on obtaining the response of the systems to external loading and boundary conditions. Local force, weight and pressure are some of the common types of the external loads.

The results of the FEM analysis are used in making and/or justifying the engineering decisions and improving their performance [108]

5.2 Applicability of the FEM in IMPRPK

Finite Element Methods were employed to determine the response of the mechanical and thermal systems particularly with complex geometry and material properties as a result of the applied loading. Airplanes, cars, electronic packages are some examples of such complex systems.

Considering the different commercially available finite element solutions (e.g. ABAQUS, ANSYS, etc.), ABAQUS, because of its capabilities in solving complex thermal and mechanical problems and its capability in communicating with NESSUS was selected to be incorporated in IMPRPK. The combination of ICH and MCH geometries, material properties and boundary and loading conditions used in IMPRPK create the thermally induced stresses and strains in the BGA solders. These induced stresses and strains can induce failure in in BGA solders in the microelectronic packages [23].

Utilizing FEM to analyze the ICH and MCH packages is necessary due to the following facts:

- Complexity of the microelectronic packages (geometry, material and boundary condition)
- Complexity of the interaction between the package components through the thermal cycling test
- Non-linearity of the system
- Lack of access to measure the induced stresses and strains in the BGAs

Because of the mentioned complications above, the Finite Element Method (FEM) will facilitate finding the system response in ICH and MCH packages quickly and efficiently. Determining the response of these ICH and MCH packages to external loading without Finite Element techniques would be almost impossible.

5.3 Global and local FEM models

5.3.1 Geometry details

The FEM models for two package form factors were developed during the course of this study. The FEM models of these two package configurations (so-called ICH or I/O Controller Hub, and MCH or Memory Controller Hub), were constructed using the geometry (e.g. dimensions and thickness) and material information, as well as the data from the characterization task. In both of these ICH (Wire bonded with molding compound) and MCH (Flipchip with underfill) packages, the second level interconnects (BGAs) provide the mechanical, electrical and thermal connection between the substrate and printed circuit board (PCB) [17]. Details of the ICH and MCH packages including their components are presented in Fig. 56.

The details of the geometry information for these two ICH and MCH packages are presented in Table 9.

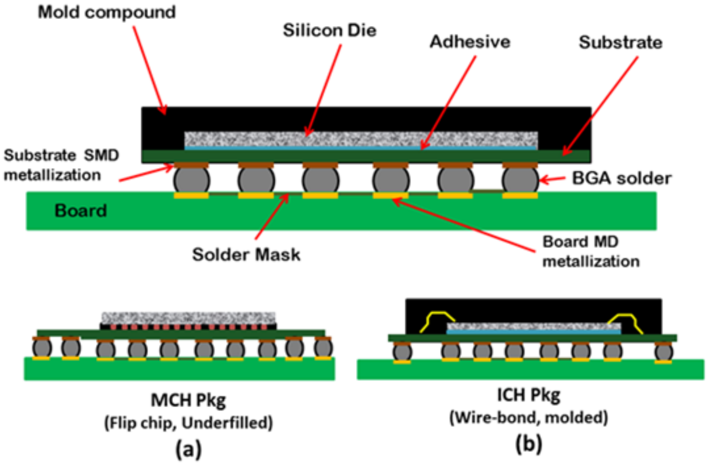

MCH Pkg
(Flip chip, Underfilled)
(a)

ICH Pkg
(Wire-bond, molded)
(b)

Fig.56 Graphical demonstration of (a) MCH and (b) ICH packages

Table. 9 Detailed geometry information for the ICH and MCH packages.

Component	Thickness (mm)	Dimension (mm)
Mold compound	1.18 (ICH)	13.2 x 13.2 (ICH)
Silicon Die	0.43 (ICH) & 0.556 (MCH)	4.4 x 4.4 (ICH) & 5.4 x 5.4 (MCH)
Die attach	0.067 (ICH)	4.4 x 4.4 (ICH)
Underfill	0.137 (MCH)	5.4 x 5.4 (MCH)
Copper pad (Board and substrate side)	0.021 (ICH) & 0.017 (MCH)	N/A
Substrate thickness	0.54 (ICH) & 0.96 (MCH)	15.4 x 15.4 (ICH) & 19.8 x 19.8 (MCH)
Board thickness	1.25 (ICH) & (MCH)	45 x 45 (ICH) & (MCH)
Solder standoff	0.464 (ICH) & 0.378 (MCH)	N/A
Solder Diameter	0.67 (ICH) & 0.494 (MCH)	N/A

The first step in creating the global FEM models were patterning the individual BGA units (Fig. 57) and forming the ICH and MCH BGA layouts. Among these two packages, the ICH uses the partial BGA pattern while the MCH has a full array of BGAs connecting the substrate to the printed circuit board. The position of the BGAs in these layouts were obtained from the X-Ray imaging of the ICH and MCH packages. Fig. 58 shows the BGA arrays for the ICH and MCH packages.

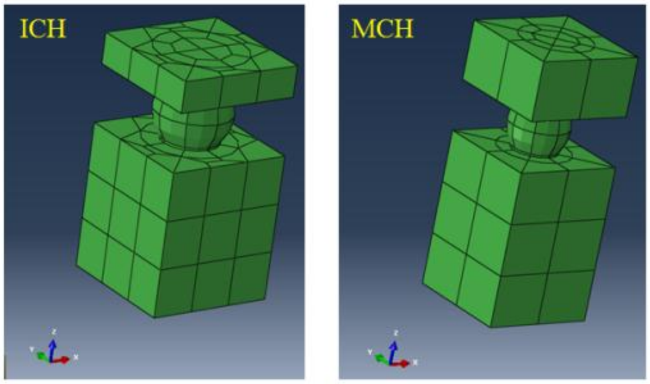

Fig. 57 Individual units with coarse mesh in the BGA area used to build the global ICH and MCH models

These patterned BGA arrays were merged to form the center part of the global model. Due to the existence of four fold symmetry in ICH and MCH global packages, only quarter sections of these packages were modeled. Analyzing the quarter section of these packages significantly reduces the simulation time.

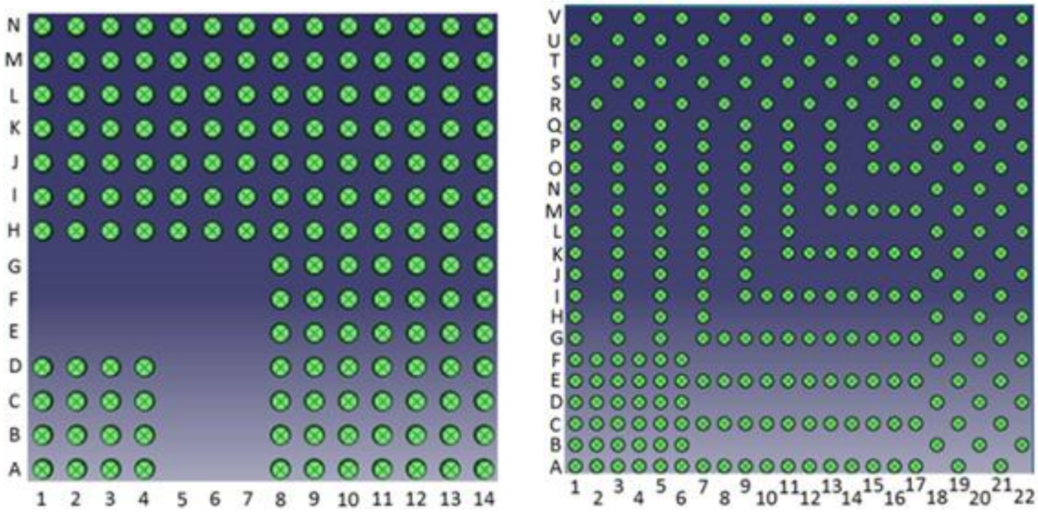

Fig. 58 BGA solder pattern for the ICH (left) and MCH (right) packages

Different parts of the global ICH and MCH packages (e.g. top, center and board extension parts) were assembled together using the tie constraint (Fig. 59).

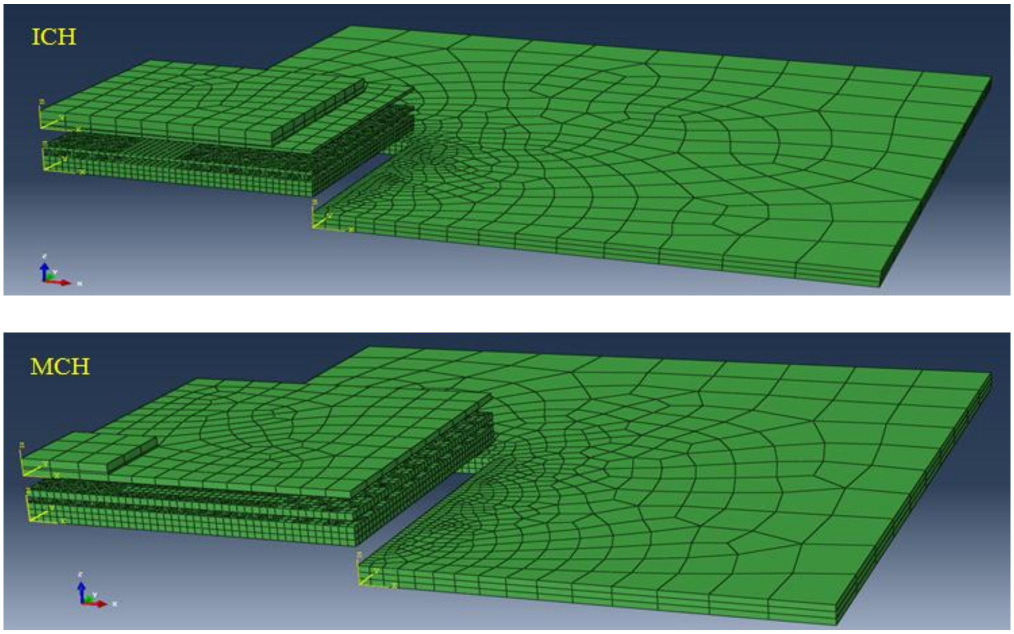

Fig. 59 Combination of three major parts (top, center and board extension) forming the global ICH and MCH FEM models

Fig. 60, shows the assembled global models for the ICH and MCH packages used in IMPRPK.

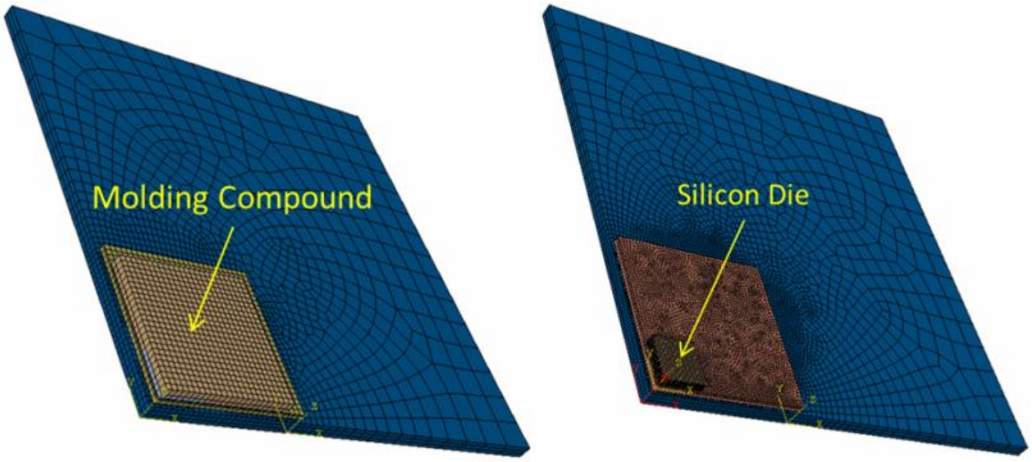

Fig. 60 The global ICH (left) and MCH (right) packages

The advantage of using the tie constraint is its capability in attaching the different parts of the package with dissimilar element shape and mesh density. Using the tie constraint will make it possible to replace different parts of the model without the need to re-design the entire model.

The local FEM models are the refined versions of the global BGAs with higher mesh density and detail geometry (Fig. 61). There are two copper pads located on the substrate and board sides of the local BGAs, which are called SMD (Solder Mask Defined) and MD (Metal defined) respectively. The board side copper pad is at times called NSMD (Non-Solder Mask Defined) as well. Fig. 62 shows the details of the single solder with its copper pads.

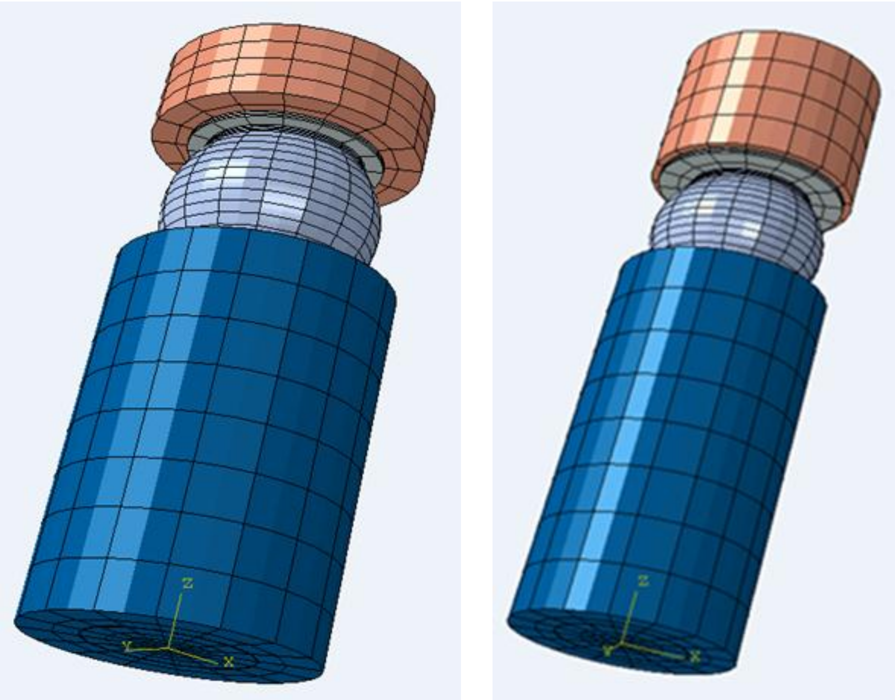

Fig. 61 Local ICH (left) and MCH (right) models

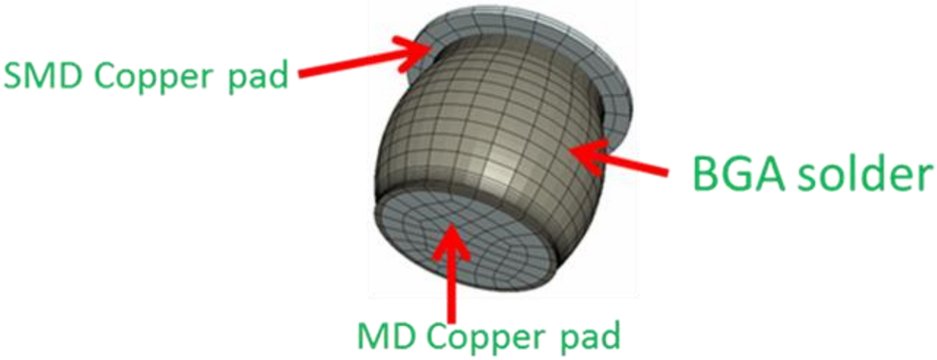

Fig. 62 The details of the single BGA solder

A Non-linear finite element analysis with quadratic element type (C3D20R) was utilized in construction of the ICH and MCH global and local FEM models.

The advantages and disadvantages of utilizing the non-linear FEM analysis in analyzing the ICH and MCH models are:

- It will improve the accuracy of analysis
- It will increase the chance of singularity (primarily in smaller elements)
- It will require a longer simulation time.

Table. 10 shows the total number of the elements used in the formation of the ICH and MCH global and local models.

Table. 10 Total number of elements used in ICH and MCH models

Package type	ICH	MCH
Local FEM Model	3456	2912
Global FEM Model	39468	38522

5.3.2 Material properties and constitutive creep models

Material properties, as well as the boundary condition and geometry, are key elements in the construction of efficient FEM models. Using the correct material properties in creating any FEM model is crucial in predicting the accurate system response. The material properties of the ICH and MCH packages used in IMPRPK were collected from different sources. The majority of the material properties were supplied by Intel Corp., some were measured during the course of this study (e.g., CTE and Tg of the molding compound), and the rest were obtained from published data in literature [17], [84], [87], [109]. Table. 11 shows the detailed material properties used in ICH and MCH package components.

Two types of solder materials were used in modeling the ICH and MCH packages.

1. Lead free solder material (Sn-4Ag-0.5Cu) which also referred to as (SAC405).
2. Lead rich solder material, which also referred to as (Sn37Pb).

These two solder alloys will behave differently during the ATC test due to their differences in microstructure, active elements in their composition and melting temperature. Plasticity was included in analyzing both SAC405 and Sn37Pb BGA solders.

Considering the melting temperature of the Sn37Pb and SAC405 solders and since the ratio of the absolute operating temperature to the absolute melting temperature (Homologous temperature) of these solders is larger than 0.5, even at room temperature, the creep effect would be active in both of these BGA solders, therefore the creep deformation models needs to be incorporated in the FEM models [86].

Among the different constitutive creep models which are used in analyzing solder deformation in MEP, there are mostly simple constitutive models (e.g., Double power law creep model [86-87], and hyperbolic sine creep models [80],[89-90]). Complex models (e.g., Anand Model) [81-82], [110] are used in limited cases by some investigators. Considering the limitations in computation time, the hyperbolic sine constitutive model was used for the creep effect in analyzing the BGA solders. Equation (18) demonstrates the hyperbolic sine constitutive model with its constants for SAC405 and Sn37Pb solder materials [89-90].

$$\dot{\varepsilon} = A[Sinh(\alpha\sigma)]^n e^{(\frac{-Q}{RT})} \qquad (18)$$

$$(SAC405)\quad A = 441000, \alpha = 0.005(MPa^{-1}), n = 4.2, Q = 45000(J/mol)$$
$$(Sn37Pb)\quad A = 10, \alpha = 0.1(MPa^{-1}), n = 2, Q = 44900(J/mol)$$

In this relation (A) is the pre-exponential factor, (n) is the stress order, and (Q) is the activation energy of self-diffusion.

The creep strain rates of the SAC405 and Sn37Pb solders (Fig. 63) show higher creep strain rates for the Sn37Pb solders compared to the SAC405.

Table. 11 Material properties of the ICH and MCH package components.

Material	Temperature (K)	E (MPa)	Poisson's Raatio	CTE (PPM/°C)	Plasticity
Die Attach	248	13000	0.36	1.70E-05	N/A
	298	12000	0.36	1.70E-05	N/A
	373	11000	0.36	1.70E-05	N/A
	473	10000	0.36	1.70E-05	N/A
Board (Orthtropic)	Not temperature dependent	E1=24000 E2=24000 E3=16000	Nu12= 0.2 Nu13= 0.143 Nu23= 0.143	Alpha11=1.96E-5 Alpha22=1.96E-5 Alpha33=5E-5	N/A
Underfill	Not temperature dependent	9900	0.23	2.40E-05	N/A
Copper	Not temperature dependent	128700	0.3435	1.70E-05	N/A
Mold Compound	318	23000	0.36	8.08E-06	N/A
	473	23000	0.36	3.57E-05	N/A
Silicon Die	Not temperature dependent	131000	0.3	2.60E-06	N/A
Substrate (Anisotropic)	Not temperature dependent	E1=31000 E2=31000 E3=4580	Nu12= 0.24 Nu13= 0.24 Nu23= 0.24	Alpha11=1.79E-5 Alpha22=1.79E-5 Alpha33=4E-5	N/A
Solder (Sn37Pb)	273	32000	0.4	2.16E-05	Yield stress=45.03 at 297K (plastic strain=0 - 0.1) Yield stress=42.44 at 333K (plastic strain=0 - 0.1) Yield stress=35.51 at 368K (plastic strain=0 and 0.1) Yield stress=21.65 at 403K (plastic strain=0 and 0.1)
	298	29800	0.4	2.22E-05	
	323	27600	0.4	2.28E-05	
	348	25400	0.4	2.30E-05	
	373	23200	0.4	2.30E-05	
Solder (SAC405)	248	54386.5	0.3	2.13E-05	
	273	52780	0.3	2.19E-05	
	298	51029.5	0.3	2.24E-05	
	348	47672.5	0.3	2.34E-05	
	398	44315.5	0.3	2.44E-05	
	473	39280	0.3	2.60E-05	

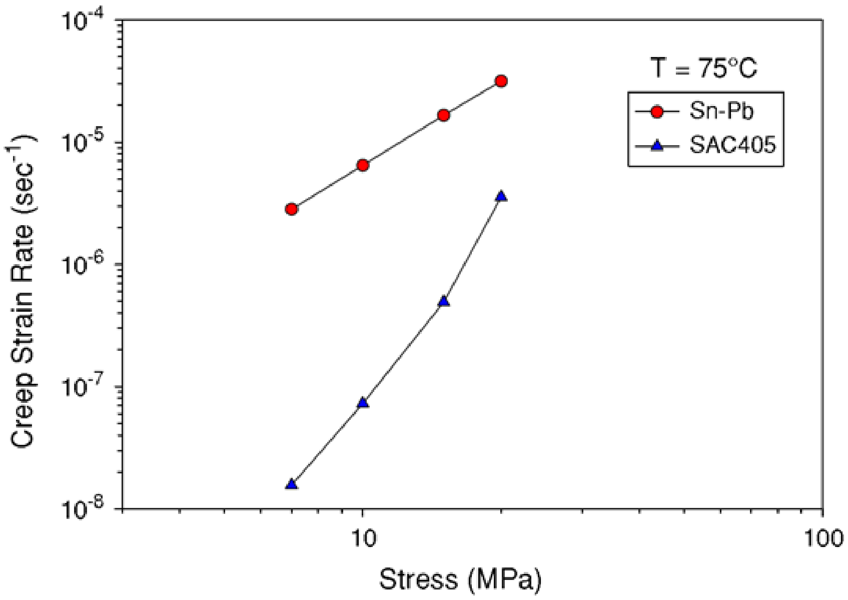

Fig. 63 Creep strain rate for the SAC405 and Sn37Pb solders at 75˚C [89].

5.3.3 Boundary Condition and Accelerated Thermal Cycle (ATC) test requirements

Due to the existence of the four fold symmetry in the ICH and MCH global packages, the symmetric boundary conditions were applied to the symmetric surfaces (X=0 & Y=0) of the packages (Fig. 64). The center point of the packages was also fixed in three degrees of freedom (X=Y=Z=0) [80]. Fig. 64 shows the boundary condition used in modeling the ICH package. The red dots represent the nodes with limited degree of freedom in the boundary surface. A similar boundary condition was applied to the MCH package as well.

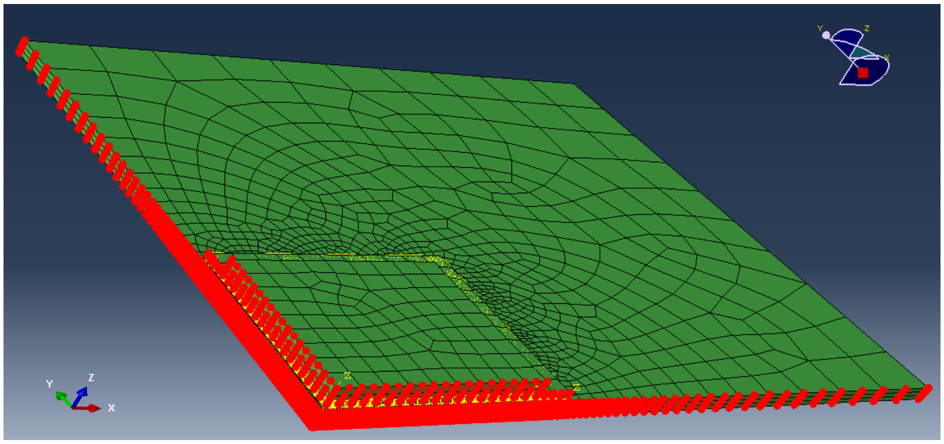

Fig. 64 Boundary condition of the ICH package

5.3.4 Incorporating CTE Temperature Dependency and Glass-Transition Temperature in ABAQUS

Selecting the correct material properties and appropriate representation in FEM will have a significant impact on predicted dissipated energy density and stress/strain levels.

A simple experiment was conducted in order to demonstrate ABAQUS’ s response to various ways that one may input the CTE temperature dependency and the glass transition temperature of the molding compound in the model. This validation was conducted utilizing a simple cube which was fixed in the XY plane. Values of the E33 were predicted for different scenarios. Table. 12, shows the details of these scenarios.

Table 12. Example of CTE input in ABAQUS, various way to input CTE temperature dependency

Scenario - 1	Scenario - 2	Scenario - 3	Scenario - 4	Scenario - 5
Tg= 391 K T=223 K CTE=8.928E-6 T=390 K CTE=8.928E-6 T=392 K CTE=3.7187E-5 T=523 K CTE=3.7187E-5	Tg= 391 K T=273 K CTE=8.928E-6 T=390 K CTE=8.928E-6 T=392 K CTE=3.7187E-5 T=423 K CTE=3.7187E-5	Tg= 273 K T=223 K CTE=8.928E-6 T=390 K CTE=8.928E-6 T=392 K CTE=3.7187E-5 T=523 K CTE=3.7187E-5	Tg= 391 K T=223 K CTE=8.928E-6 T=523 K CTE=3.7187E-5	Tg= 273 K T=223 K CTE=8.928E-6 T=390 K CTE=8.928E-6 T=523 K CTE=3.7187E-5

The comparison between ABAQUS predictions using different scenarios and the experimental data for molding compound Tg is shown in Fig. 65.

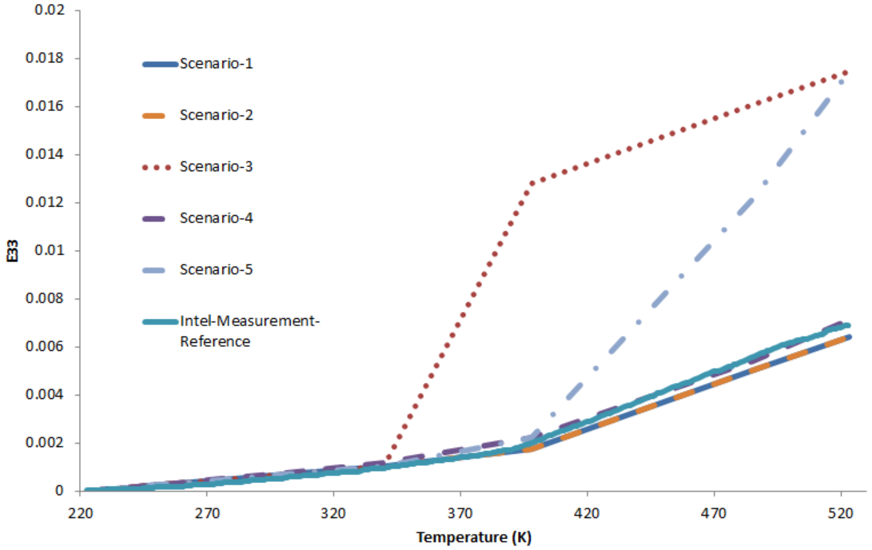

Fig. 65 Effect of the molding compound material selection on the strain.

Reviewing these results indicate that scenario 4 is the closest case to the real CTE measurements done on the molding compound which is used in our ICH packages. In the actual CTE measurement of the Molding Compound, the initial length of the sample (L0=1.111974 mm) was measured at 223K. This temperature was used as reference temperature in ABAQUS. The value of strain will equal to zero at reference temperature. Fig. 66 shows the experimental strain data obtained for the molding compound material using the Thermo Mechanical Analysis (TMA) tool, and its comparison with the secant CTE values used in ABAQUS. It is important to mention that ABAQUS uses the Secant CTE values (CTE value with respect to the reference temperature). A reference to this issue was also provided in chapter 2.

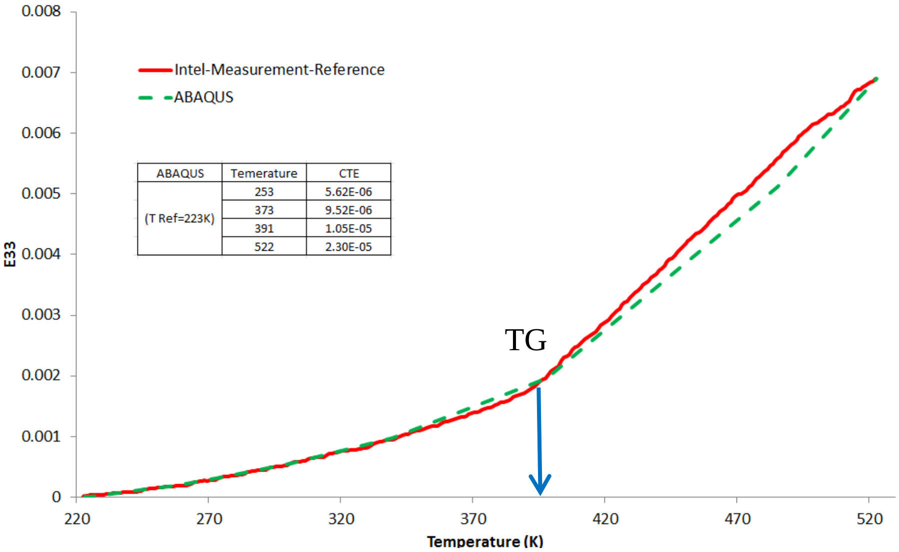

ABAQUS	Temerature	CTE
(T Ref=223K)	253	5.62E-06
	373	9.52E-06
	391	1.05E-05
	522	2.30E-05

Fig. 66 Strain measurements of the molding compound material using the TMA [Courtesy of Intel].

Other investigators have reported that after the first two to three thermal cycles the dissipated energy density (ECDDEN) and accumulative creep strain (CEEQ) will be stabilized with minor fluctuations [87]. Considering the fact that the majority of the 30 accelerated thermally cycled mother boards which were used in our experiment, had dwell times equal to 240 minutes with the temperature ranging between -20˚C and 100˚C, the FEM simulations in this task were developed and validated using the 240 minutes dwell (hold) times. The effect of different dwell times on system response was evaluated as a part of the probabilistic and sensitivity analysis presented in chapter (6)). It is also assumed that the dwell temperatures are constant and there is no temperature fluctuations or "mini cycles" due to the workloads (e.g. running different programs) during the hold steps at high and low temperatures. It has been reported [87] that the existence of these mini cycles (small thermal fluctuation during the hold times) do not have a significant impact on the SAC405 solders while according to the same study this effect is significant for Sn37Pb solders causing them to fail faster than SAC405 BGAs. This could be due to the lower creep rates of the SAC405 solders in comparison to the Sn37Pb BGAs [3], [89]. Fig. 67 shows the effect of the mini cycles on thermal fatigue life of Sn37Pb BGA solders.

The temperature-time profile of the ICH and MCH FEM models is presented in Fig. 68.

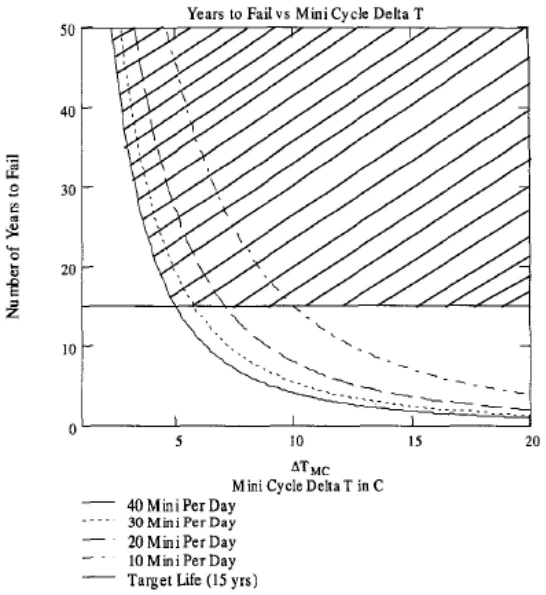

Fig. 67 Effect of the mini cycles in the thermal fatigue life of the solder joints [3]

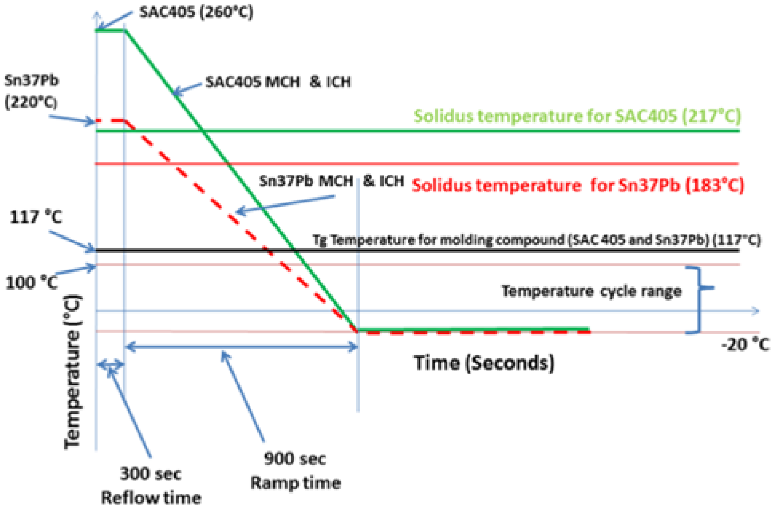

(a)

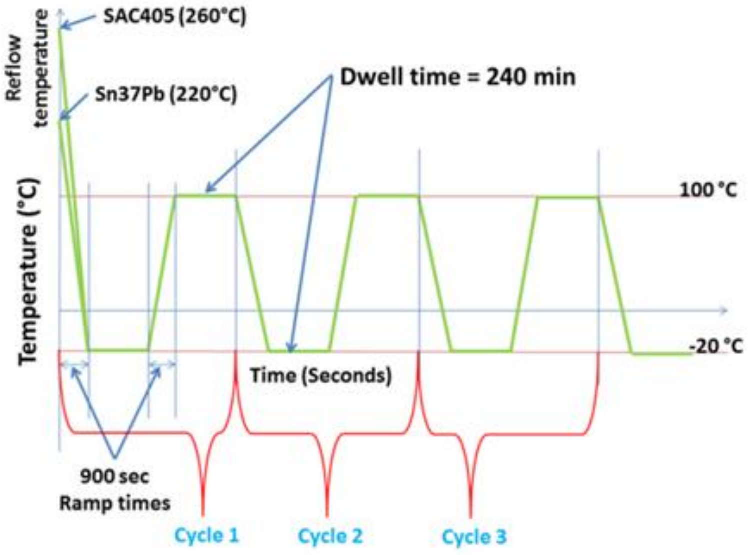

(b)

Fig. 68 Temperature profile (a) and Thermal cycle profile (b) used in the FEM simulation

5.4 ICH and MCH (SAC405 and Sn37Pb) packages

5.4.1 ICH validation

After conducting the accelerated thermal cycling test using the global ICH finite element models, the obtained results were validated by comparing the characterization outcomes. The global FEM results revealed strain energy density pattern in line with the failure pattern observed in electrical continuity test, as well as, dye and pry and serial sectioning tests. Note that the strain energy density represent the area confined inside the stress and strain curve represents the average of the volumetric dissipated energy in the solder neck region. The FEM results showed higher dissipation energy density per unit volume (ECDDEN) in the solder neck region outside of the die shadow. As a post process, volumetric average energy (ECDDEN) was used in the local ICH model to avoid the effect of local high stresses and prevent a stress singularity in the solder neck region [86-87],[111]. The volume used in determining the average energy density in ICH solder neck region in this simulation consisted of a disc shaped section of 336 μm diameter and 25 μm height. Effect of volume selection on cumulative and 3rd cycle ECDDEN predictions are discussed in section 5.4.2, below.

The thermal mismatch between the silicon die, substrate and molding compound is primarily responsible for these stresses and strains. Fig. 69 shows the variation in accumulated strain energy density values (ECDDEN) after 3 accelerated thermal cycles (a) and in the third thermal cycle (b) along row A in the ICH package (see Fig. 58 for the position reference). The strain energy density results for the third cycle shown in Fig 69b is questionable and should be further investigated.

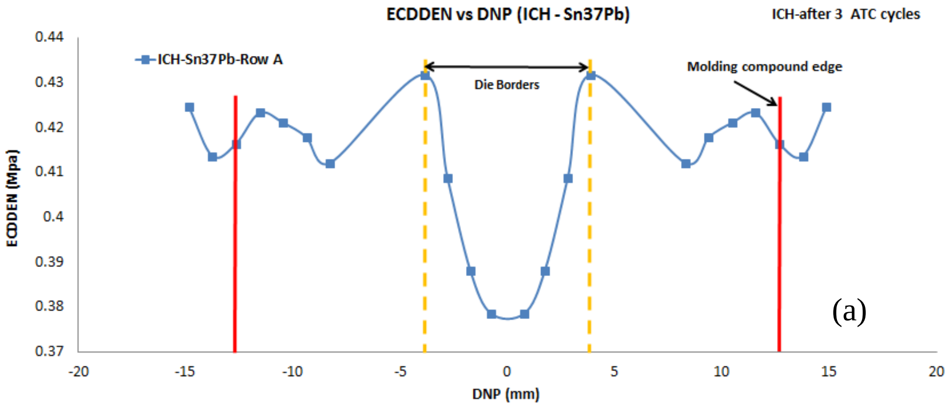

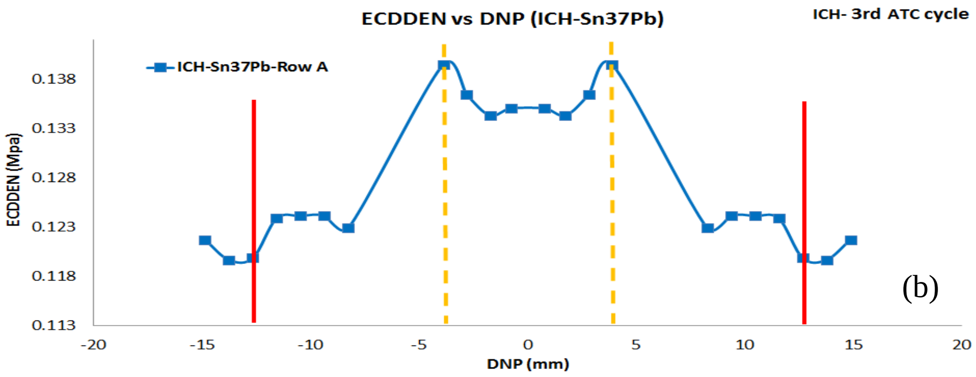

Fig. 69 Averaged dissipated energy density (ECDDEN) in the solder neck region vs. the distance from neutral point (DNP) for Sn37Pb solders (along row A in Fig. 58). (a) After 3 ATC cycles (b) 3rd ATC cycle (The results are based on “local” FEM analysis).

In Fig. 69 the region confined between the two dashed orange lines represents the die shadow region and the solid red lines represent the border of the molding compound. The energy values (ECDDEN) are volumetrically averaged in the solder neck region

In the ICH packages, the majority of failure occurs outside of the die shadow region and under the molding compound. In the FEM results section of Fig. 70,

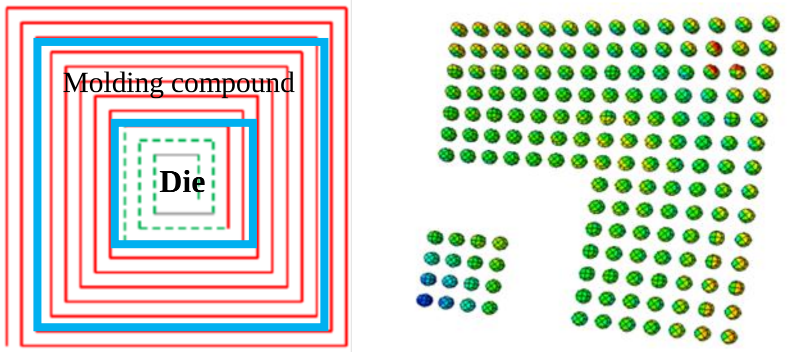

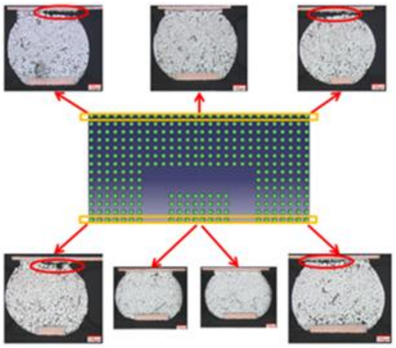

Fig. 70 Validation of the extent of failure in ICH package through electrical testing results (top left), dissipated energy density from FEM analysis (top right) and serial sectioning (bottom) for Sn37Pb.

The blue color represents the lower energy and the red color shows the maximum energy in the BGA solders.

5.4.2 ICH results and discussion

Effect of different package parameters on dissipated energy density of the BGA solders was studied. The preliminary results are presented in this section. The effect of some system variables on dissipated energy density are listed here:

- *Effect of solder material on dissipated energy density:*

  Changing the solder material from SAC405 to Sn37Pb showed a decrease in dissipated energy density values. Fig. 71 shows the effect of different solder material on cumulative dissipated energy density (ECDDEN) for 3 thermal cycles, in the solder neck region along row A (for positions please refer to the Fig. 58).

Increase in dissipated energy density value is expected to reduce the thermal fatigue life of the BGA solders.

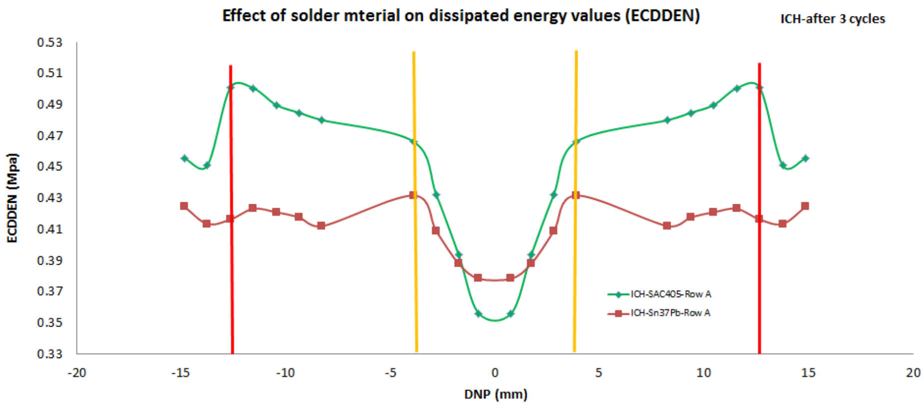

Fig. 71 Effect of the solder material on cumulative dissipated energy density (ECDDEN) vs. the distance from neutral point (DNP) after 3 ATC cycles (The results are based on "local" FEM analysis)

- *<u>Effect of dwell time on dissipation energy density:</u>*

Increasing the dwell times in ICH SAC405 and Sn37Pb packages increased the dissipated energy density in these BGAs. Fig. 72 demonstrates the effect of the dwell time on the cumulative dissipated energy density (ECDDEN) for SAC405 and Sn37Pb solders.

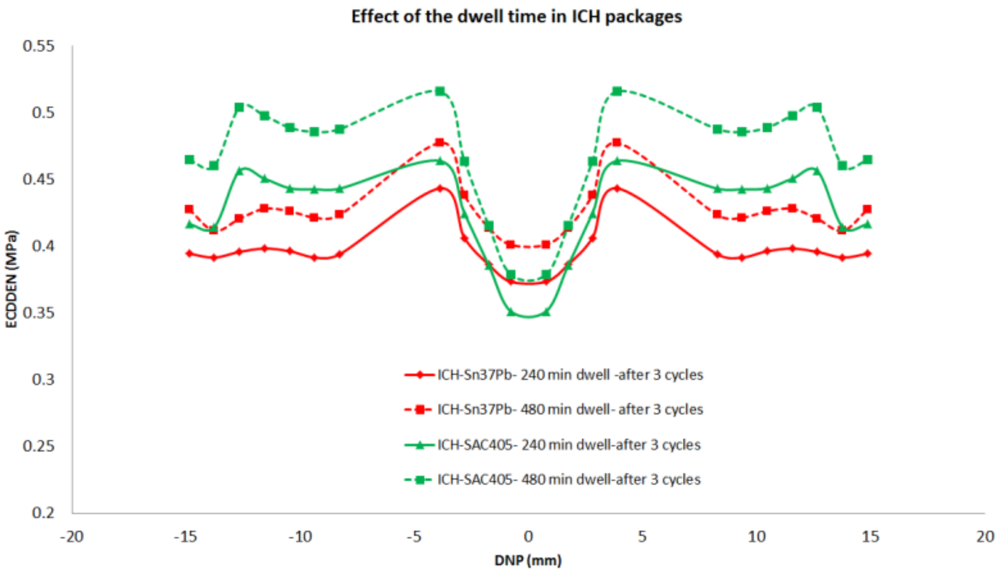

Fig. 72 Effect of the dwell time after 3 ATC cycles of the ICH packages (SAC405 and Sn37Pb) along row A (for the position of the row A please refer to Fig. 58) The results are based on “local” FEM analysis.

Additional FEM analysis showed minor increase in dissipated energy density values by doubling the dwell time in both SAC405 and Sn37Pb BGA solders. (10% increase in ECDDEN for the hold time of 480 minutes compared to hold-time of 240 minutes).

- *Effect of volume selection in the BGA neck region on dissipation energy density:*

Selection of an appropriate volume to calculate the volumetric average of dissipated energy density is very important. Fig. 73 shows the impact of the selected BGA neck region volume (i. disc volume of 0.00221 mm^3, and ii. ring volume of 0.000123 mm^3) on the average cumulative energy density after 3 thermal cycles (a), and the third cycle ECDDEN (b) .

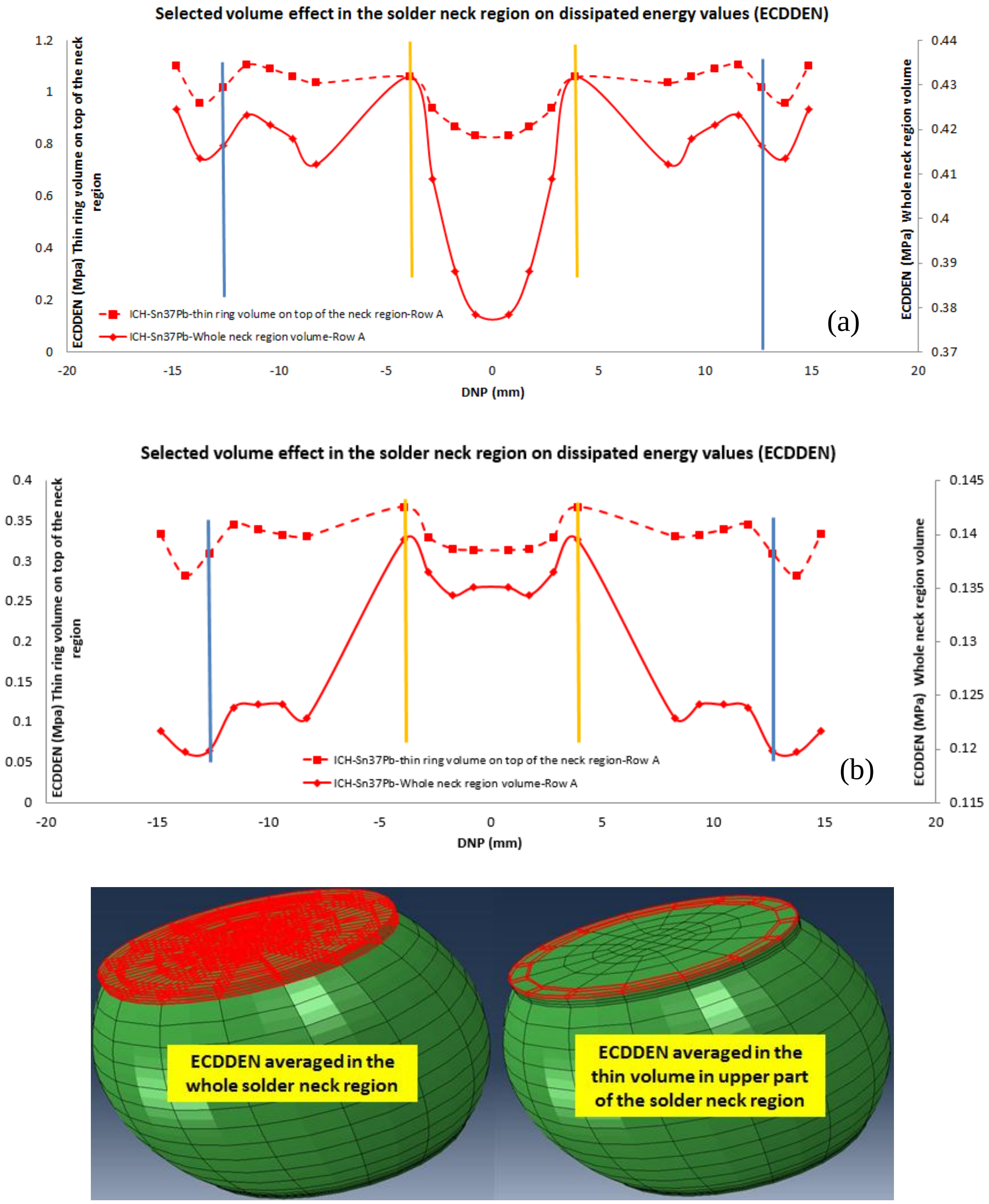

Fig. 73 Effect of the volume selection on the averaged cumulative dissipated energy density (a) after 3 ATC cycles in the BGA neck region, and (b) 3rd cycle ECDDEN (The results are based on “local” FEM analysis)

The Volume effect and other concerns associated with ICH FEM model will be discussed by other investigators.

- *Effect of internal voids on dissipation energy density:*

The effect of the internal voids in ICH packages on cumulative dissipated energy density was evaluated. Figure 74 shows the results of Local FEM simulation for SAC405 and Sn37Pb solders residing in row "A" of ICH package design. This analysis was conducted by including a large void of 140μm in each individual solder balls, when performing the "local" analysis. Fig. 75 shows a schematic of void location in each solder ball.

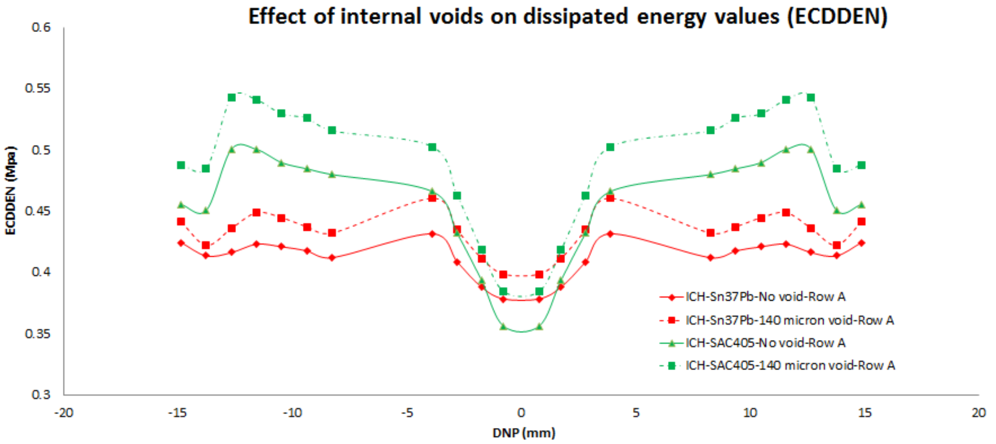

Fig. 74 Effect of the internal voids (140μ) on cumulative dissipated energy density after 3 ATC cycles (The results are based on "local" FEM analysis)

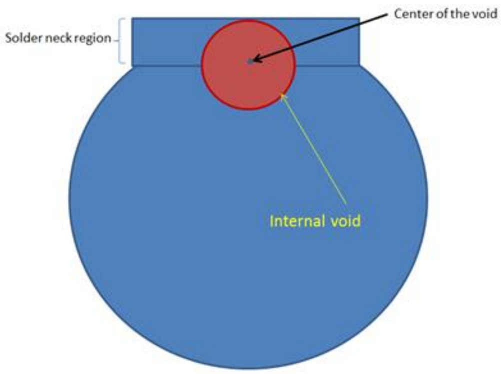

Fig. 75 schematic of void location in each solder ball

Presence of internal voids on each solder ball results in an increase on dissipated energy values (e.g., 10% increase in ECDDEN for 140μ diameter voids in these simulations). It should be noted that the probability of having such large voids in all of the solder balls is extremely low, however, a single solder within the array of BGA's has a finite probability (e.g., 1% per characterization data presented in pervious chapter) of containing such large void size. Overall system related probability, e.g., probability of defect size distribution in conjunction with the probability associated with the void location in the solder, as well as, the solder array location and loading condition, should be further investigated in future programs.

- *Effect of solder material on creep strain:*

Effect of solder material on cumulative equivalent creep strain (CEEQ) was evaluated. Fig. 76 shows the FEM analyses results, where Sn37Pb solder experience higher accumulated creep strain (CEEQ) values compared to the SAC405 solders. Increase in BGA failure rates is expected as a result of a higher creep strain, according to many fatigue models, e.g., Coffin-Manson [9-11] and Syed [86], etc.

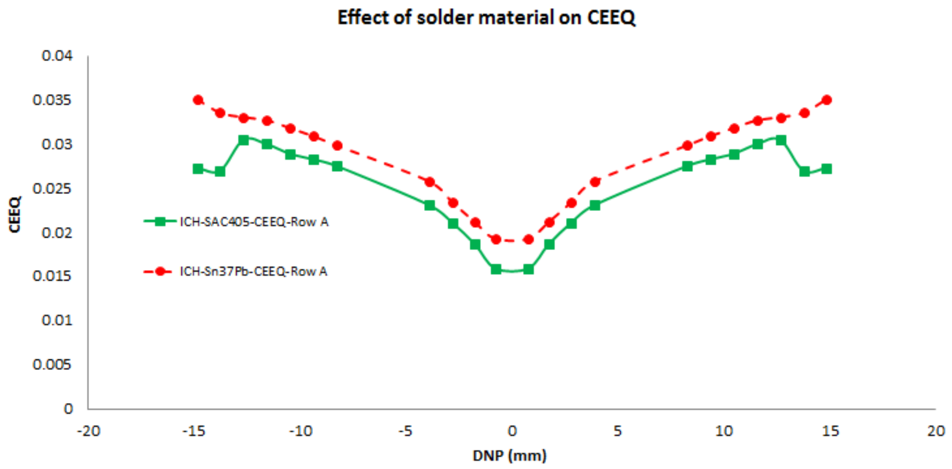

Fig. 76 Accumulated creep strain (CEEQ) values in the solder neck region for the SAC405 and Sn37Pb solders vs the distance from neutral point (DNP) after 3 ATC cycles (The results are based on "local" FEM analysis)

5.4.3 MCH validation

The FEM results for MCH packages were validated using the characterization results. Fig. 77 shows the "local" FEM analysis results for averaged cumulative energy density (ECDDEN) distribution along the MCH row A (see Fig. 58 for position references). The analysis shows a higher dissipation energy density per unit volume in the solder neck region in MCH BGAs under the silicon die region, in agreement with the failure pattern observed in MCH packages. In this figure the area confined between the two dashed orange lines represents the die shadow region.

According to the predicted energy values presented in Figures 77 and 78, and according to strain energy based models, such as Darveaux's model, BGA failure under the die shadow region is expected. The maximum value of dissipated energy was observed in the edge of the silicon die (due to the high thermal mismatch between the silicon die and substrate). Similar result has been reported by other researchers [23].

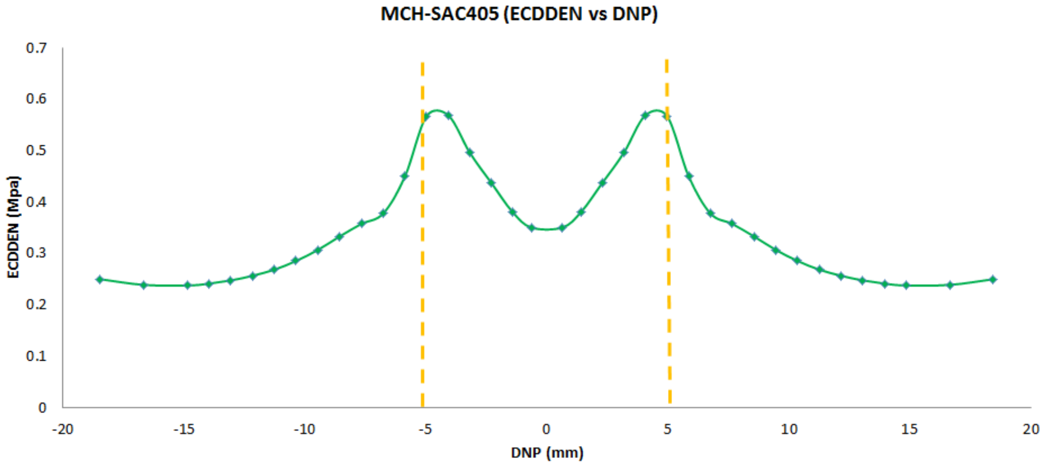

Fig. 77 Cumulative dissipated energy density (ECDDEN) after 3 ATC cycles vs. the distance from neutral point (DNP) (SAC405) along row (A). The results are based on "local" FEM analysis.

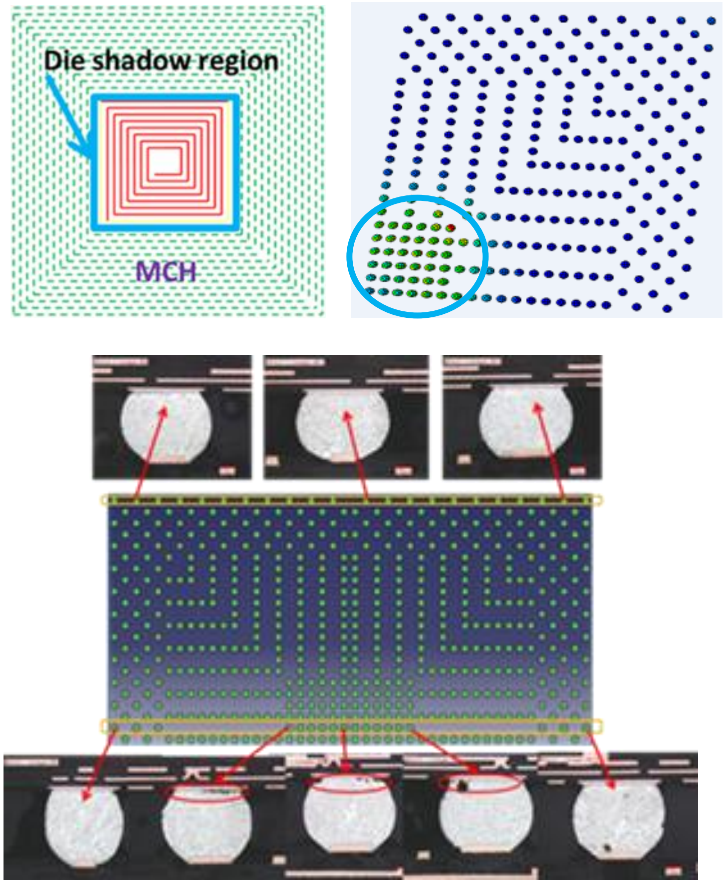

Fig. 78 Validation of the extent of the failure in MCH package by electrical testing results (top left), dissipated energy density from FEM analysis (top right) and serial sectioning (bottom) for SAC405.

5.4.4 MCH results and discussion

Effect of various package parameters on dissipated energy density (ECDDEN) values in MCH packages was investigated. The deterministic analysis results are presented here. A probabilistic approach used in evaluating the impact of these parameters on dissipated energy density (ECDDEN) will be discussed later in chapter 6.

- *Effect of the solder material on dissipated energy density:*

FEM analysis of MCH models, shows higher average cumulative dissipated energy density for Sn37Pb BGA solders compared to the SAC405 BGAs. Fig. 79 shows the effect of the solder material on cumulative dissipated energy density after three ATC cycles in the solder neck region of MCH packages.

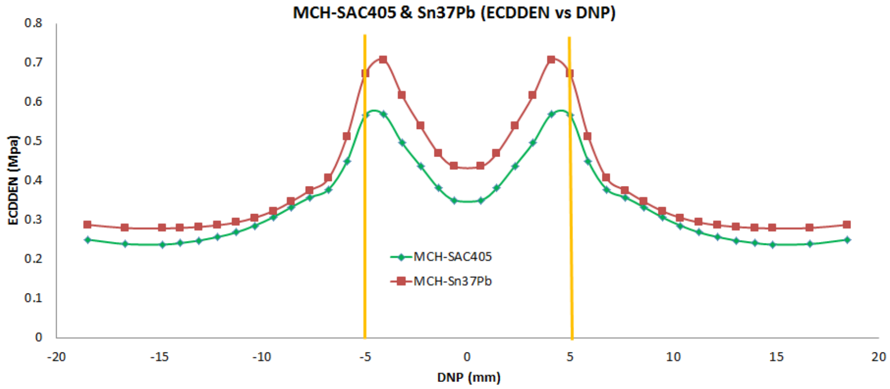

Fig. 79 Effect of the solder material after 3 ATC cycles (ECDDEN) vs. (DNP) along the row A (for the position of the row A please refer to Fig. 58) (The results are based on “local” FEM analysis).

- *Effect of the dwell time on dissipated energy density:*

Similar to ICH packages, increasing the dwell time increases the dissipated energy density values in MCH package. This is mostly due to the effect of the creep in the BGA solders (Fig. 80).

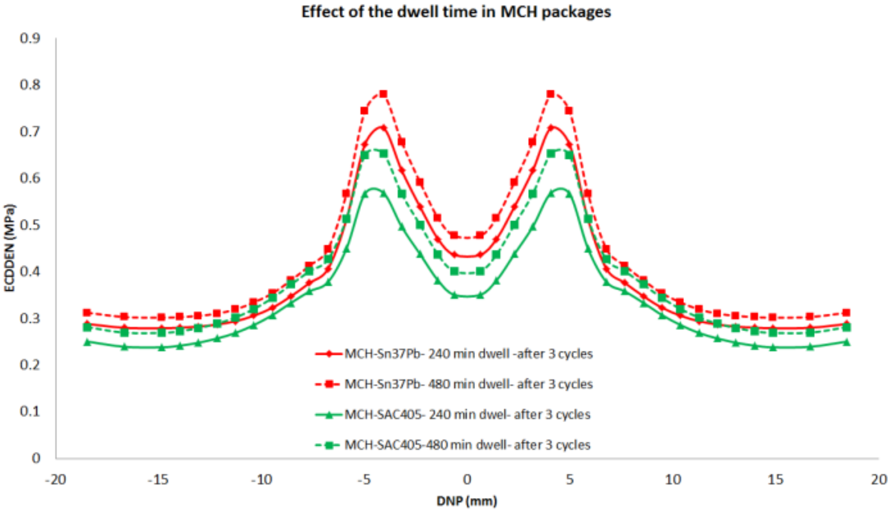

Fig. 80 Effect of the dwell time after 3 ATC cycles (ECDDEN) vs. (DNP) along the row A (for the position of the row A please refer to Fig. 58) The results are based on “local” FEM analysis.

- *Effect of voids in BGA solders:*

The effect of internal voids (150µm) on dissipated energy density was evaluated in MCH packages (Fig. 81)

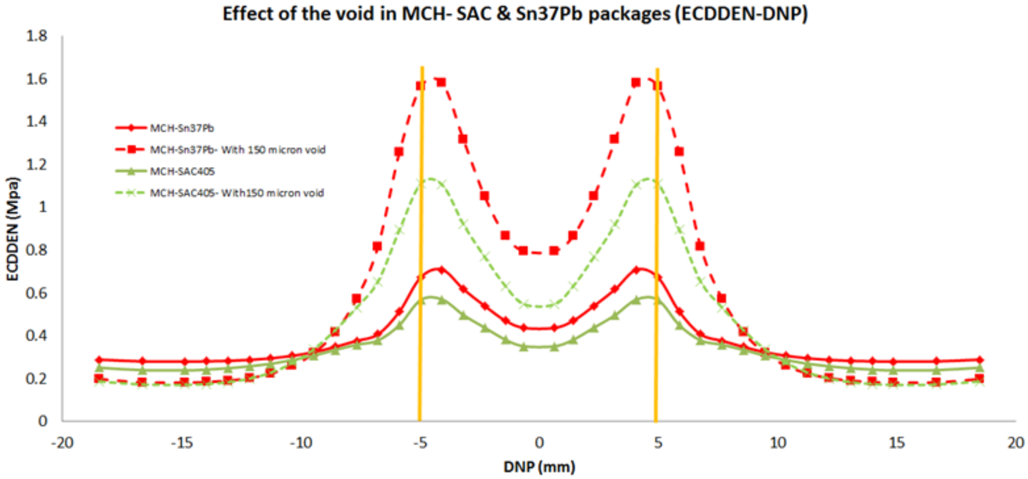

Fig. 81 Effect of the internal voids (150µ) on dissipated energy density in MCH SAC 405 and Sn37Pb package along the row (A) after 3 ATC cycles (for the position of the row A please refer to Fig. 58) The results are based on “local” FEM analysis.

Presence of the 150µ internal voids in MCH SAC405 and Sn37Pb packages resulted in an increase in dissipated energy density values compared to the case without voids. This increase in energy values was more significant at the edge of the silicon die.

A higher failure rate is expected for solders with void. It should be noted that this FEM analysis represents an unrealistic condition, as the probability of having such large voids in all of the solder balls is extremely low.

The probabilistic analysis on the effect of the internal defects (voids) will be discussed in detail in the probability and sensitivity chapter.

- *Effect of solder material on MCH BGA creep strain:*

Effect of solder material on cumulative equivalent creep strain (CEEQ) was evaluated for MCH package as well. The results are presented in Fig. 82. Higher accumulated equivalent creep strain (CEEQ) values were predicted in the die shadow region of the MCH packages, where a higher BGA failure rate is then expected.

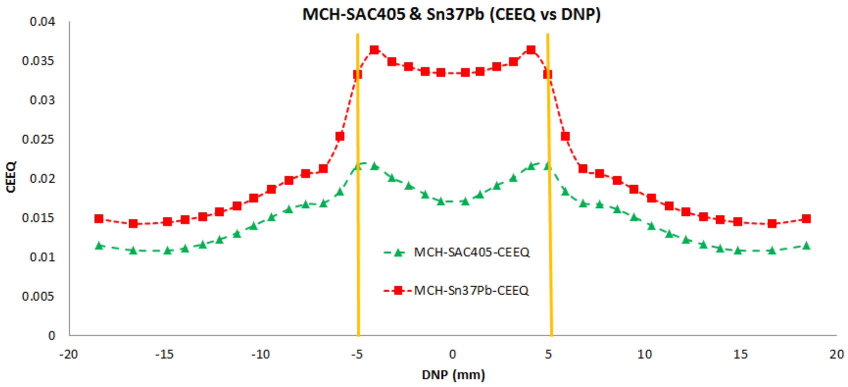

Fig. 82 Accumulated creep strain (CEEQ) values of the SAC405 and Sn37Pb solders vs the distance from neutral point (DNP) after 3 ATC cycles (The results are based on “local” FEM analysis)

5.4.5 Steady State Dissipated Energy Density (Hysteresis Loop) per Cycle

Many life prediction methods such as Darveaux’s crack initiation and growth model use the steady state strain energy density as a descriptor or independent variable for predicting BGA solder life. In this section the ECDDEN values predicted by ABAQUS for the 3rd ATC cycle (assuming that steady state is reached within the initial 2-3 cycles) for ICH and MCH designs, as well as, the SAC405 and Sn37Pb solder materials are presented. Figure 83 shows the local FEM prediction of “3rd cycle” ECDDEN values as a function of distance from Neutral point (DNP). The volume used in determining the average ECDDEN in MCH local models was a disk of 256 μm diameter and 22 μm in height (note the difference in the neck region volume in the ICH and MCH). The pattern of these data for ICH deviates from the expected/observed behavior, further evaluation of the ICH FEM model and validation of its accuracy will be conducted by other investigators.

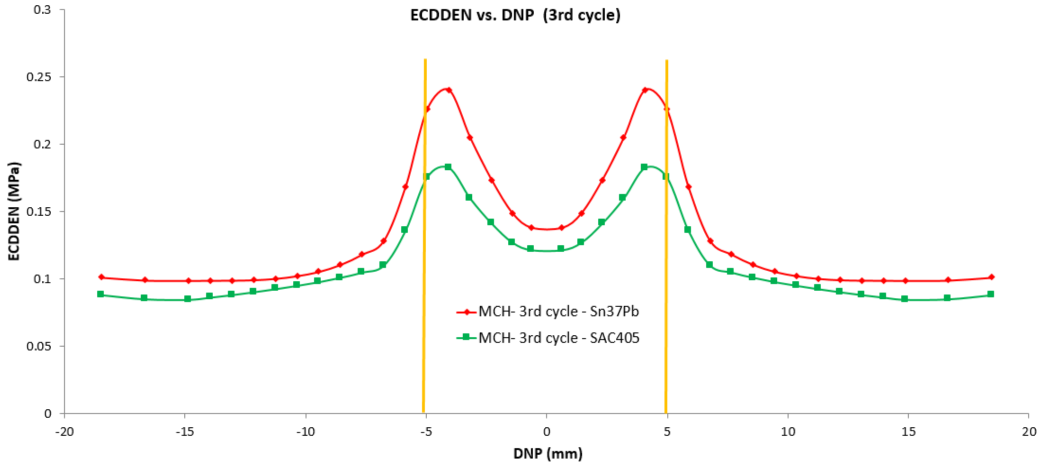

Fig. 83 Effect of the solder material in the MCH 3rd cycle (ECDDEN) vs. (DNP) along the row A (for the position of the row A please refer to Fig. 58) (The results are based on "local" FEM analysis).

5.5 Integrating ABAQUS FEM with NESSUS Probabilistic Method

We have focused on using the dissipated energy density (ECDDEN) from the FEM analysis for life prediction and our probabilistic analysis. We have used an approach similar to that recommended by Darveaux [110] and others [72]. These models are based on crack initiation and growth and follow a power law dependency for crack initiation and crack growth rate. Equation (19) below presents such model:

$$\Delta W_{avg} = \frac{\sum \Delta W \times V}{\sum V} \qquad (19)$$

$$N_0 = K_1 \Delta W_{avg}{}^{K_2} \quad \text{And} \quad \frac{da}{dN} = K_3 \Delta W_{avg}{}^{K_4}$$

A volumetric average of energy value was used in these crack initiation and growth life prediction models to avoid the effect of singularity. The FEM prediction of strain energy density (ΔW) for a given set of design and materials parameters (deterministic levels) is used in these life prediction models to predict the survival life of the solder under such condition. To leverage the NESSUS probabilistic model for sensitivity analysis and determination of the effect of the various system variabilities, the ABAQUS and the lifing model were integrated with NESSUS in this program. Next chapter provide a detailed discussion of this integration.

5.5.1 Validation of the probabilistic analysis software (NESSUS) by performing the deterministic analysis

The probabilistic model in NESSUS was validated by conducting a single deterministic analysis using the mean values of the system variables. Comparison between the results of this deterministic run with the previously conducted FEM analysis (using the same mean values) will confirm the proper probabilistic model setup. For the deterministic analysis, NESSUS will only run the FEM model once.

5.5.2 Parameterizing the ABAQUS input file

The global and local ICH and MCH FEM models were parameterized for use in NESSUS. Parameterizing package parameters, such as thickness, material properties and some process / use conditions, facilitates the process of altering the parameters needed in probabilistic analysis.

5.6 Summary

Preliminary results of the FEM analysis revealed that system variabilities will greatly influence the system response (e.g., dissipated energy density). These effects and the sensitivity of system to these variabilities will be discussed in detail in the probabilistic analysis section of this dissertation. The conclusions attained from FEM analysis presented in this chapter (via deterministic approach) are listed below.

- Distribution of the cumulated strain energy density values predicted by FEM model is in line with the failure patterns observed via the characterization effort of the ICH and MCH packages, Changing the solder material from SAC405 to Sn37Pb caused an increase in MCH dissipated energy density (ECDDEN). This current FEM model of ICH shows an opposite behavior, where the dissipated energy density (ECDDEN) value for Sn37Pb is lower than that for SAC405.This predictions are not validated, as the accuracy of the ICH FEM need to be further validated.
- Increasing the dwell time resulted in larger dissipated energy density values in both ICH and MCH packages (SAC405 and Sn37Pb solder material).

- Presence of the internal voids in solders increases the dissipated energy density in both ICH and MCH packages.
- FEM results revealed higher accumulated creep strain for the Sn37pb solders compared to the SAC405, which can further lead to shorter thermal fatigue life in the Sn37Pb solders, in agreement with the experimental reliability data.

Chapter 6

PROBABILISTIC & RELIABILITY ANALYSIS

6.1 Introduction

Probabilistic methodologies are powerful tools used in analyzing the overall reliability and performance of the systems including the uncertainties by:

(i) identifying the key system parameters that are of significant importance to system reliability

(ii) Determining the sensitivity of the system to the variability and/or applied changes associated with these parameters.

Among the different probabilistic solutions, NESSUS because of its ability and efficiency in solving the complex limit state functions and predicting the reliability of the system with high accuracy was utilized to fulfill the probabilistic analysis requirements of the IMPRPK [112-115]. The Numerical Evaluation of Stochastic Structures Under Stress (NESSUS) is a general-purpose tool for determining the probabilistic response and reliability of engineered systems. NESSUS could be used to determine the uncertainties in load, geometry, material properties, and other user-defined random variables to predict the probabilistic response, reliability and sensitivity of the engineering systems [93], [115].

NESSUS probabilistic method which is integrated into IMPRPK uses “limit state function” in determining system failure. Limit state function “g” is defined as the difference between the material limit for failure “R” (e.g., yield strength S_y, fracture toughness, critical crack length, etc.) and the current state of the materials "S" (e.g., stress σ, stress intensity factor, crack length, etc.). The criterion for failure is therefore based on limit state function and is represented by the range associated with g≤0. This is equivalent to failure occurring when stress exceeds the yield strength of material, in the example mentioned above (Fig. 84).

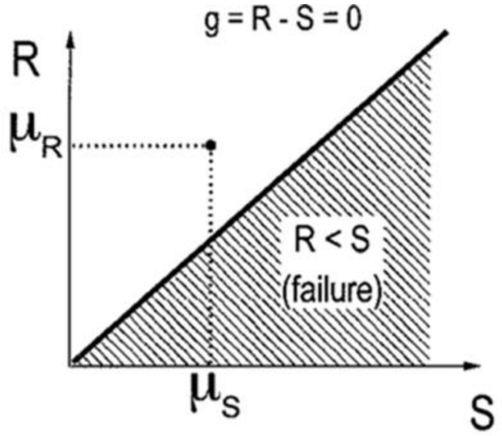

Copyright SwRI ®

$$failure\ if\ R \le S\ or\ g \le 0$$

Fig. 84 Graphical demonstration of the limit state function (R=Strength of the material and S=stress from external loading) [112]

Predicted crack length from the deterministic model, and radius of the solder neck region were used as state of system "S" and failure criteria "R" through the IMPRPK.

In order to determine the state of material/system, NESSUS will use the mean values of each parameter/variable to perform the analysis using the appropriate deterministic model. For example, finite element analysis is used to determine dissipated strain energy density, life prediction model based on crack initiation and growth (Darveaux's model discussed in chapter 5) is then used to determine the crack length.

After determining the response of the system using the mean values of variables (nominal response) it will be compared against the failure criteria to identify if the failure has occurred or not (Fig. 85). As the next step, NESSUS will start selecting random values from each one of the system variable distributions and by performing the deterministic analysis using these values, it will determine if the selected values will result in a system failure or not. The recent process will be repeated multiple times with different random variable combinations until the desired confidence level has been achieved.

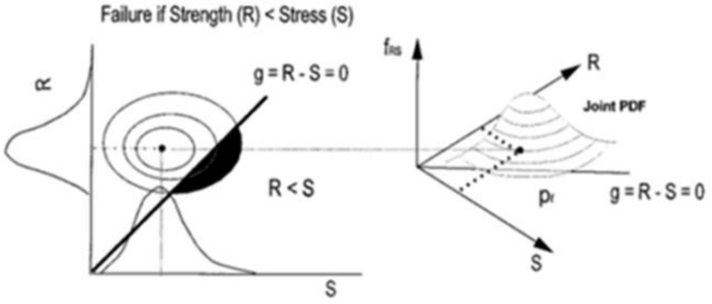

$$p_f = \int \cdots \int_{\Omega} f_{\underline{x}}(\underline{x})\, d\underline{x}$$

$$p_f = \iint_{g \le 0} f_R(R)\, f_S(S)\, dR\, dS$$

- $\underline{x}$ – vector of random design variables
- p_f – the probability of failure
- Ω – the failure region

Fig. 85 Definition of probability of failure (P_f) for joint probability density function [112], [114].

Considering the number of the failed samples out of the total number of evaluated samples, will be used in defining the probability of failure using the equation (20).

$$P_f = \frac{Number\ of\ failed\ samples}{Total\ number\ of\ samples} \quad (20)$$

$$Reliability = (1 - P_f)$$

6.2 Probabilistic approaches used in NESSUS

NESSUS is equipped with different probabilistic methods (e.g. sampling, theoretical and hybrid methods). The principles of these methods are based on satisfying the limit state function with different approach in finding the failed samples and determining the probability of failure (or reliability). Fig. 86 shows the comparison between the accuracy and efficiency tradeoff for different probabilistic methods in NESSUS. This figure shows the high accuracy and low efficiency of the standard Monte Carlo method, and indicates that the AMV+ is the most optimum method satisfying both accuracy and efficiency (high efficiency with low number of iterations).

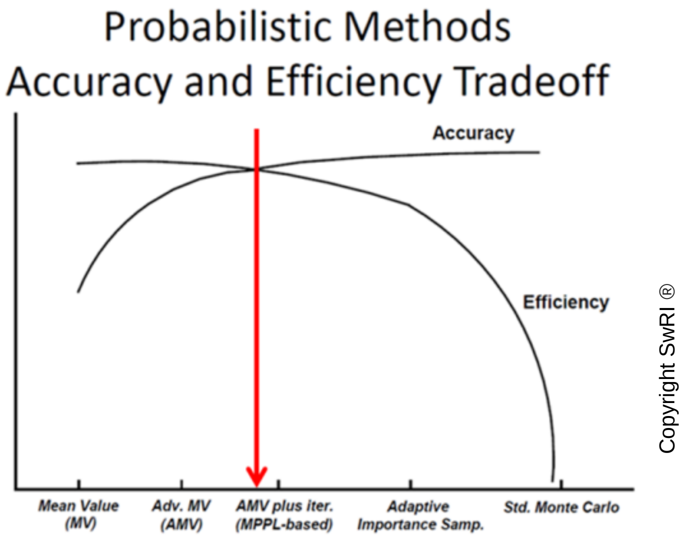

Fig. 86 Probabilistic methods accuracy and efficiency tradeoff [113]

Due to the complexity of the MCH and ICH global and local FEM models, the AMV+ has been selected to be used as probabilistic analysis method in IMPRPK project. AMV+ will predict the reliability of the complex systems with much higher efficiency compared to other theoretical and sampling methods. The details of different probabilistic methods including their advantages and disadvantages will be presented in the following sections of this chapter.

The reliability of the packages used in IMPRPK was predicted using the AMV+ probabilistic method. Table. 13 shows the list of the random variables used in the IMPRPK reliability analysis. Besides the probability analysis, the sensitivity of the system to any of the random variables was also determined by taking the derivatives of the probability function with respect to the mean (μ) and standard deviation (σ) of random variables.

Table. 13 List of the random variables used in IMPRPK-NESSUS analysis.

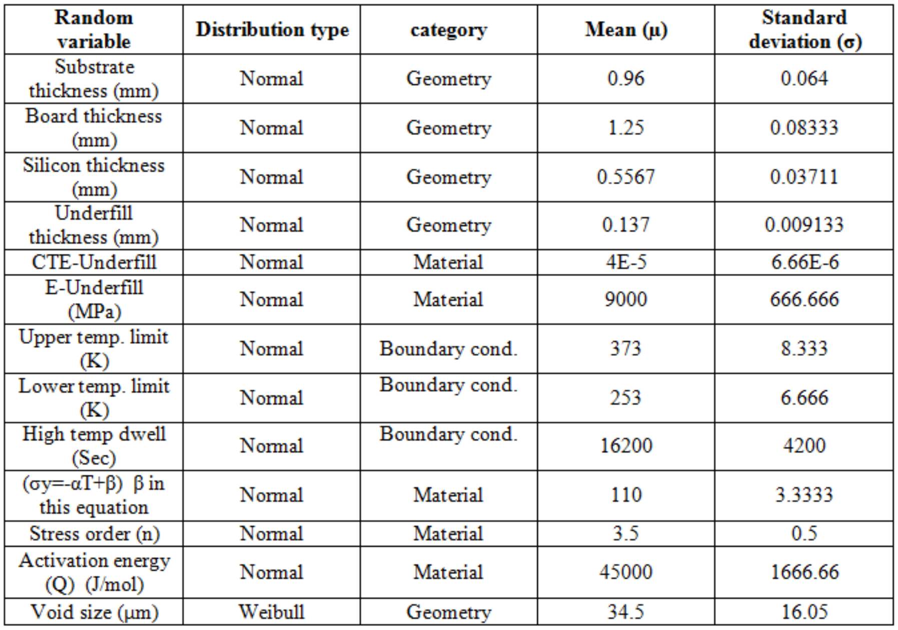

Random variable	Distribution type	category	Mean (μ)	Standard deviation (σ)
Substrate thickness (mm)	Normal	Geometry	0.96	0.064
Board thickness (mm)	Normal	Geometry	1.25	0.08333
Silicon thickness (mm)	Normal	Geometry	0.5567	0.03711
Underfill thickness (mm)	Normal	Geometry	0.137	0.009133
CTE-Underfill	Normal	Material	4E-5	6.66E-6
E-Underfill (MPa)	Normal	Material	9000	666.666
Upper temp. limit (K)	Normal	Boundary cond.	373	8.333
Lower temp. limit (K)	Normal	Boundary cond.	253	6.666
High temp dwell (Sec)	Normal	Boundary cond.	16200	4200
($\sigma y=-\alpha T+\beta$) β in this equation	Normal	Material	110	3.3333
Stress order (n)	Normal	Material	3.5	0.5
Activation energy (Q) (J/mol)	Normal	Material	45000	1666.66
Void size (μm)	Weibull	Geometry	34.5	16.05

The sensitivity analysis will determine how crucial is the impact of one variable on overall reliability of system with respect to the rest of the variables. Performing the sensitivity analysis will become more complicated as the number of variables increases. Dependency and interaction between the random variables are the other contributors involved in complexity of the sensitivity analysis.

6.3 Validation and Results

6.3.1 General approach Used in Determining Efficiency and Accuracy of the NESSUS (SwRI)

Efficiency and accuracy of the NESSUS in performing the probabilistic analysis was validated using the fatigue life prediction scheme for a three point-bend specimen with Paris law cyclic crack growth rate (CCGR) equation.

Equation 21 below represents the fatigue life based on integration of Paris-law CCGR. This is a common exercised proposed by SwRI [112] for the validation of analysis using NESSUS.

$$N_f = \frac{2\times(a_f^{(1-n/2)} - a_i^{(1-n/2)})}{C(2-n)\times(Y\sigma_{\max}\sqrt{\pi})^n} \quad for\ n \neq 2 \qquad (21)$$

$$\sigma_{\max} = \frac{3PS}{2B^2}$$

In this relation, a_f and a_i represent final and initial crack length, P is the point load, S and B are the beam length and width, C and n are the Paris constant and exponent and Y is a dimensionless constant that depends on the geometry.

During this validation, the efficiency of various probabilistic methods were compared. Figs. 87-89 show the number of samples/runs required for accurate prediction using various statistical methods, such as Monte Carlo (MC), Advance Mean Value (AMV), etc.

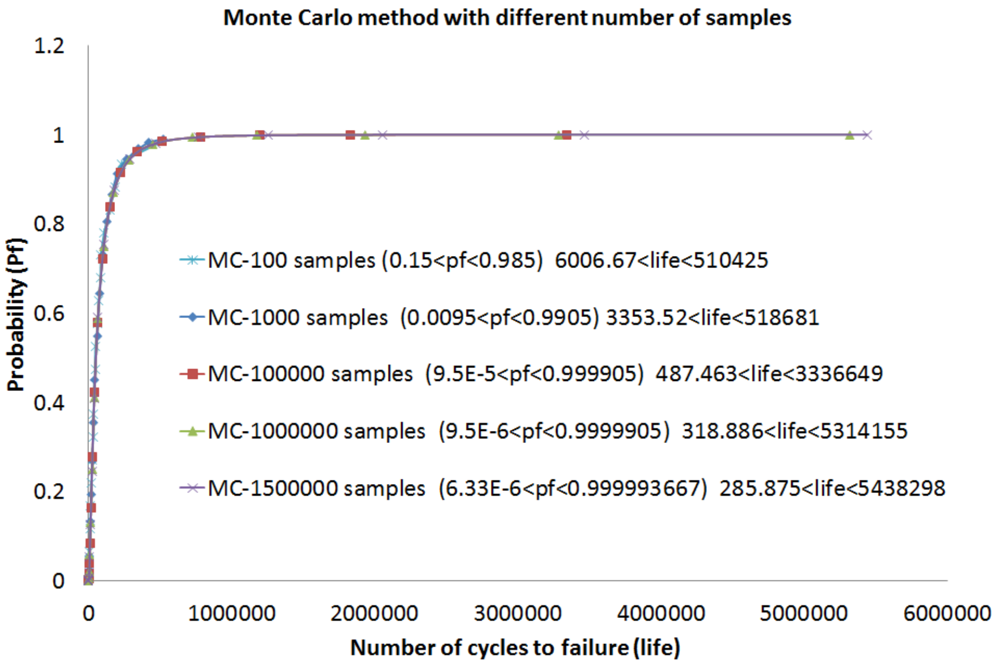

Fig. 87 Monte Carlo (MC) analysis comparison for different number of samples.

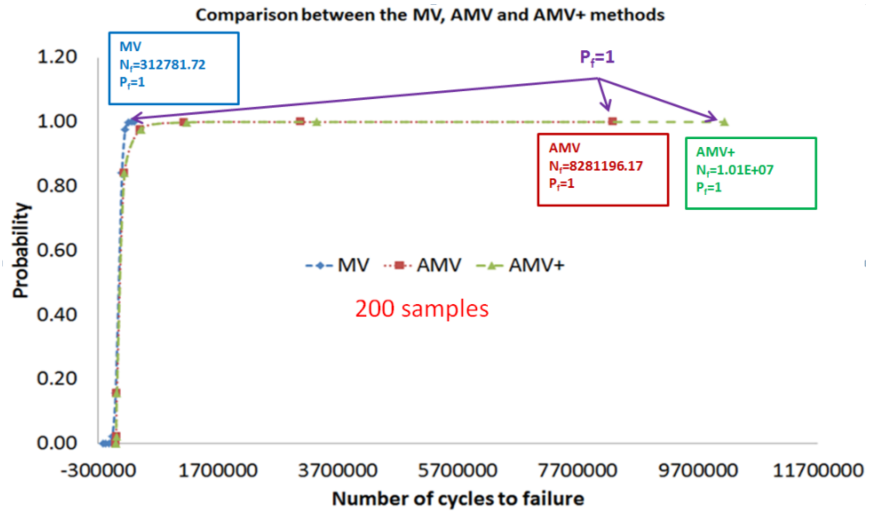

Fig. 88 MV, AMV and AMV+ comparison

According to Fig. 87, increasing the number of processed samples in Monte Carlo model (from 100 samples to 1,500,000 samples) shows a significant improve in probability results in the tail regions (better probability prediction).

This simple example clearly proves that having large number of samples is vital in obtaining the accurate results by using the standard Monte Carlo analysis.

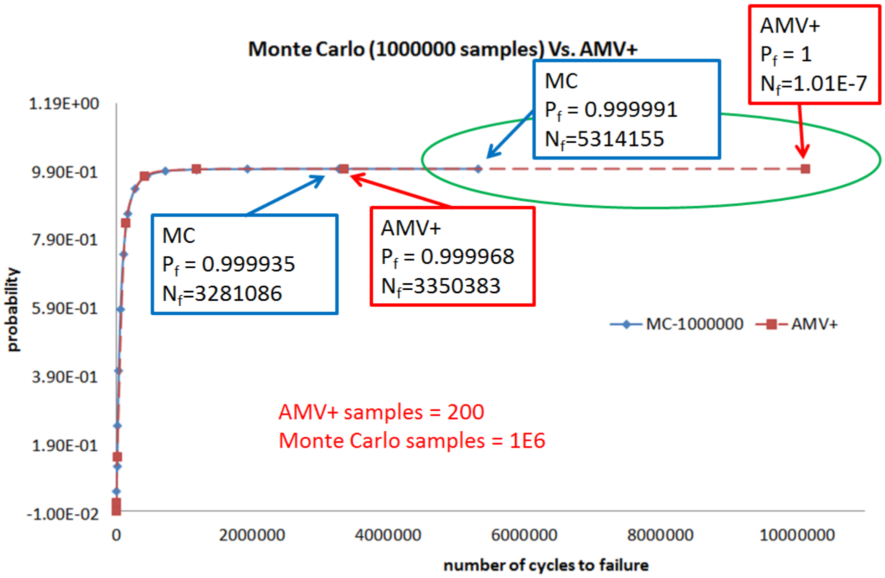

Fig. 89 Monte Carlo (1,000,000 runs) compare to AMV+ (200 runs)

A similar improvement in probability prediction in tail region was observed moving from MV to AMV and AMV+ methods (Fig. 88). According to this figure, AMV+ predicts the probability of failure more accurately in the tail regions of the probability density function compared to the MV and AMV.

In order to verify the efficiency of the AMV+ over the standard Monte Carlo method, the result of 1,000,000 runs (using standard Monte Carlo analysis) was compared to only 200 runs of AMV+ (Fig. 89). The results, proved the efficiency of the AMV+ technique over the standard Monte Carlo with much less required samples and similar probability prediction, especially in the tail regions of the probability function. In this validation the time spent for the Monte Carlo analysis was 85 times more than AMV+.

Sensitivity of the system to each one of the random variables in Paris Law model was also evaluated in Fig. 90. Sensitivity analysis provides valuable information, regarding how crucial the impact of each random variable is on overall system reliability. The result shown in Figure 90 indicates that beam width (parameter (B)) has the most significant impact followed by initial crack length (parameter (AI)). The yellow and red histograms represent the sensitivity of the system probability to the applied changes in the mean and standard deviation of the parameters, respectively.

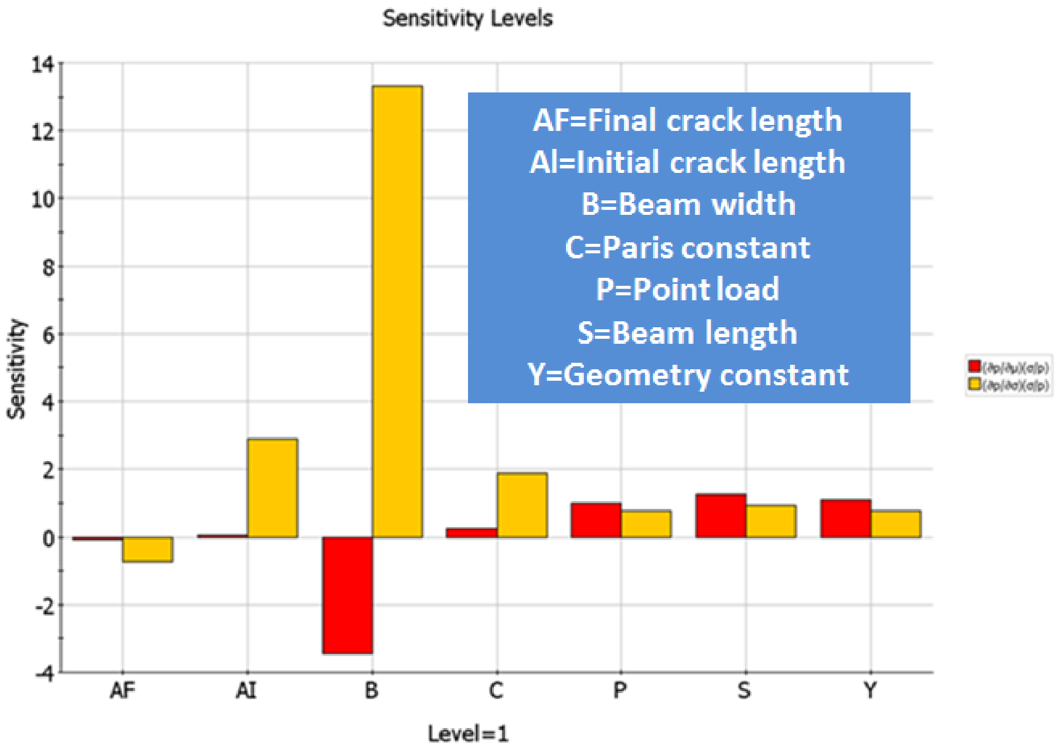

Fig. 90 Sensitivity of the overall system response to each of the random variables in Paris equation.

6.3.2 IMPRPK Results

Probabilistic and sensitivity analyses were conducted through the course of this study and the impact of the random variables on reliability of SAC405 MCH package was evaluated. The main reason for selection of the SAC405 MCH package is the wide range of the lead free flip chip applications in microelectronic industry, and our confidence on the MCH FEM model compared to ICH model. It should be noted the MCH package tested under ATC conditions of -20C to 100C with 240 min dwell time had experienced solder cracking at die shadow region after 4500 ATC cycles (see board number 41 data presented in the characterization chapter).

Due to large result files generated by each analysis when many random variables associated with material, geometry, and used condition are considered, we opted to perform few simulations with smaller number of random variables involved. In all of these analyses, the CTE value of the underfill material was included as the reference parameter. Table. 14 shows the details of these probabilistic and sensitivity runs.

Table. 14 Details of the parameters were analyzed through probabilistic analysis

Parameters		Run detail			
	Run A	Run B	Run C	Run D	Run E
Underfill CTE	✓	✓	✓	✓	✓
Underfill E	✓				✓
High temperature	✓			✓	
Low temperature	✓				
High temperature dwell	✓				
Substrate thickness		✓		✓	✓
Board thickness		✓			
Die thickness		✓			
Underfill thickness		✓			
Activation Energy			✓	✓	
($\sigma y=-\alpha T+\beta$) β in yield equation			✓		
Stress order (n)			✓	✓	
Void size			✓		✓

The results of these runs are presented in Fig. 91-95. These figures demonstrate the probability, sensitivity and importance level of the random variables for each run. The first graph (e.g., 91a) in these figures show the probability of failure vs. thermal fatigue life of the BGA solders. The second graphs (e.g., 91b) provide the sensitivity level of the system to each variable (derivative of the probability function), while the third graph (e.g., 91c) indicate the importance level of the system variables. The importance level is indicative of relative ranking impact of the given variables at Most Probable Point (see detailed discussion provided in appendix C). The anomaly noted in figure 95a is associated with the interaction of theoretical methods used in predicting the reliability of failure in conjunction complex FEM models (singularity issue).Fig.

95 is an example of a case where NESSUS was unable to properly construct the probability density function graph using the AMV+ method. It is believed that use of importance sampling technique (AMV-AIS) in the levels with non-monotonic behavior (finding the system response for a given probability level) may resolve this issue [116].

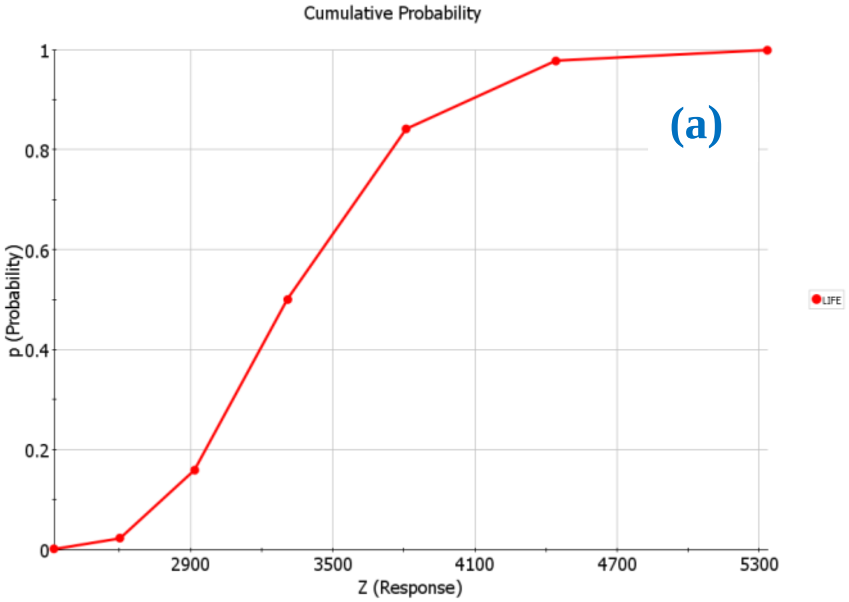

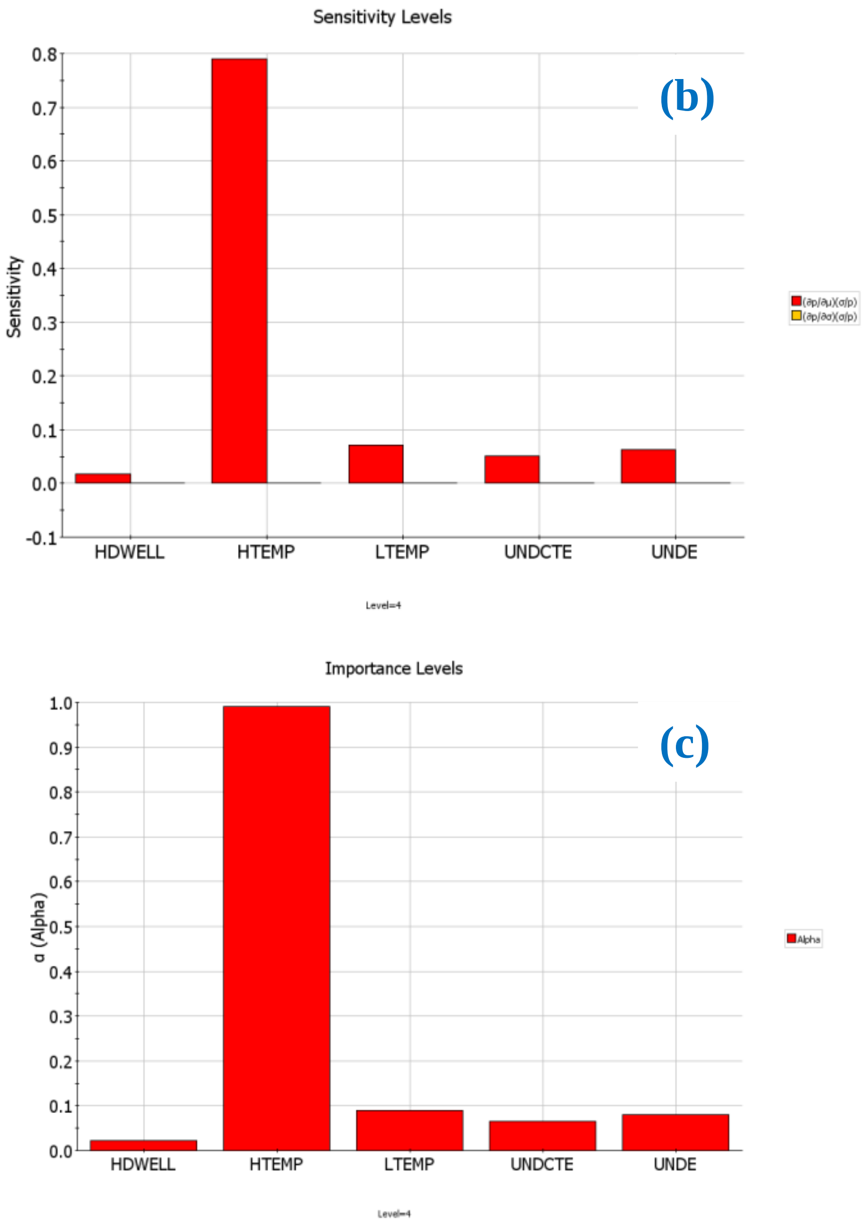

Fig. 91 Probability of failure (top) vs. cycle-to-failure N_f, Sensitivity at 50% probability (middle) and importance level at 50% probability (bottom) of the random variables used in the Run A

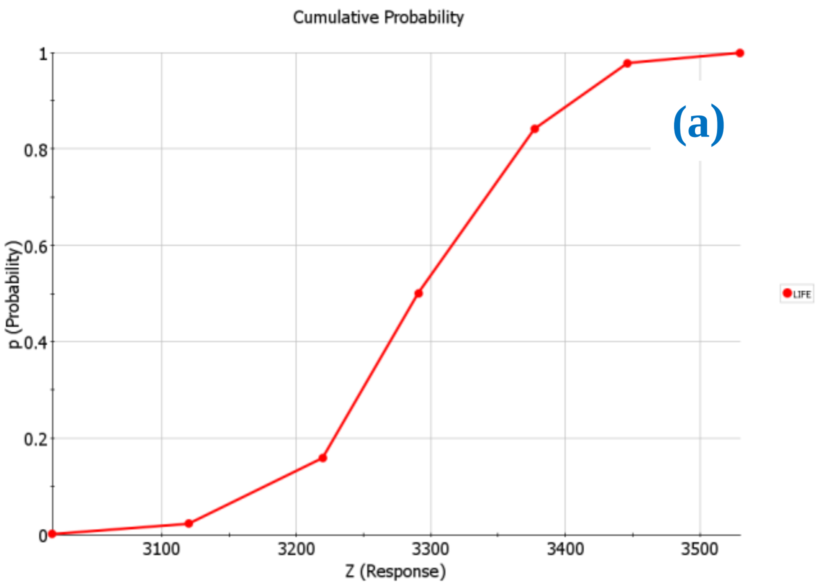
Cumulative Probability
(a)
1
0.8
0.6
0.4
0.2
0
p (Probability)
3100
3200
3300
3400
3500
Z (Response)
LIFE

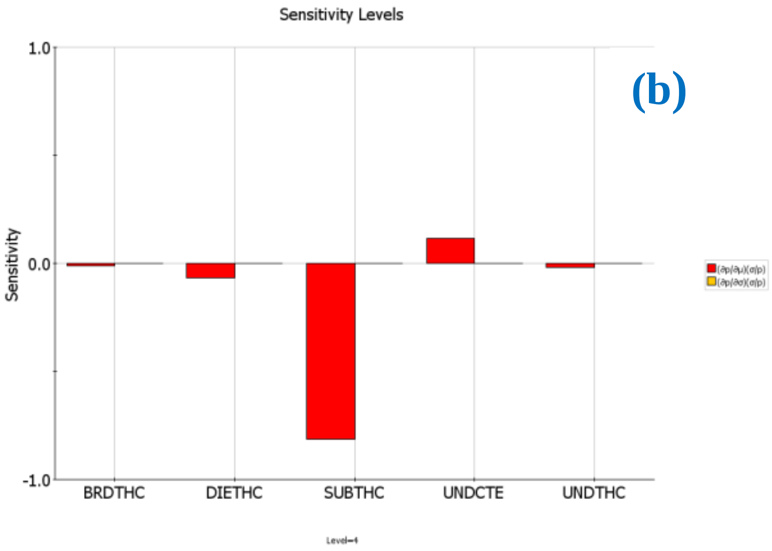
Sensitivity Levels
(b)
1.0
0.0
-1.0
Sensitivity
BRDTHC
DIETHC
SUBTHC
UNDCTE
UNDTHC
(∂p/∂μ)(σ/p)
(∂p/∂σ)(σ/p)
Level=4

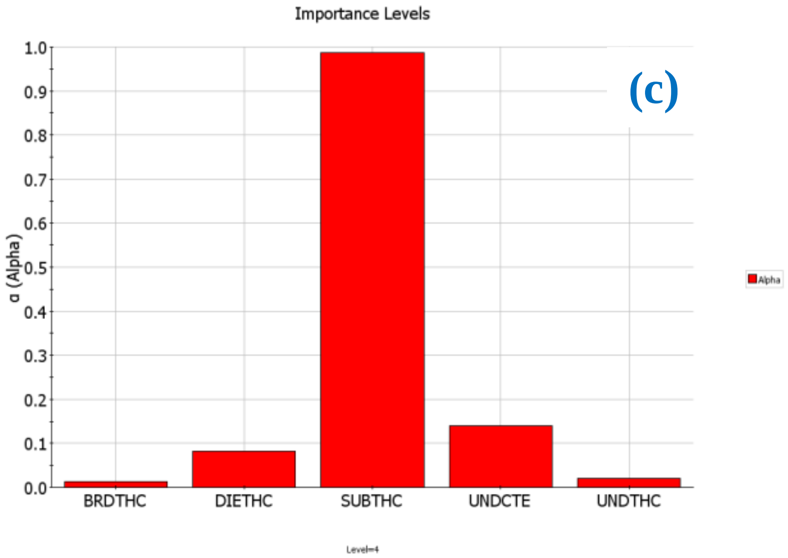

Fig. 92 Probability of failure (top) vs. cycle-to-failure N_f, Sensitivity at 50% probability (middle) and importance level at 50% probability (bottom) of the random variables used in the Run B

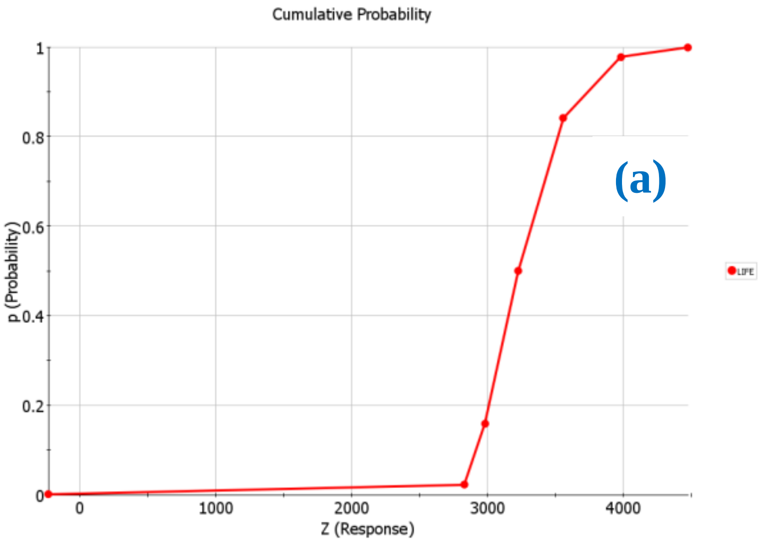

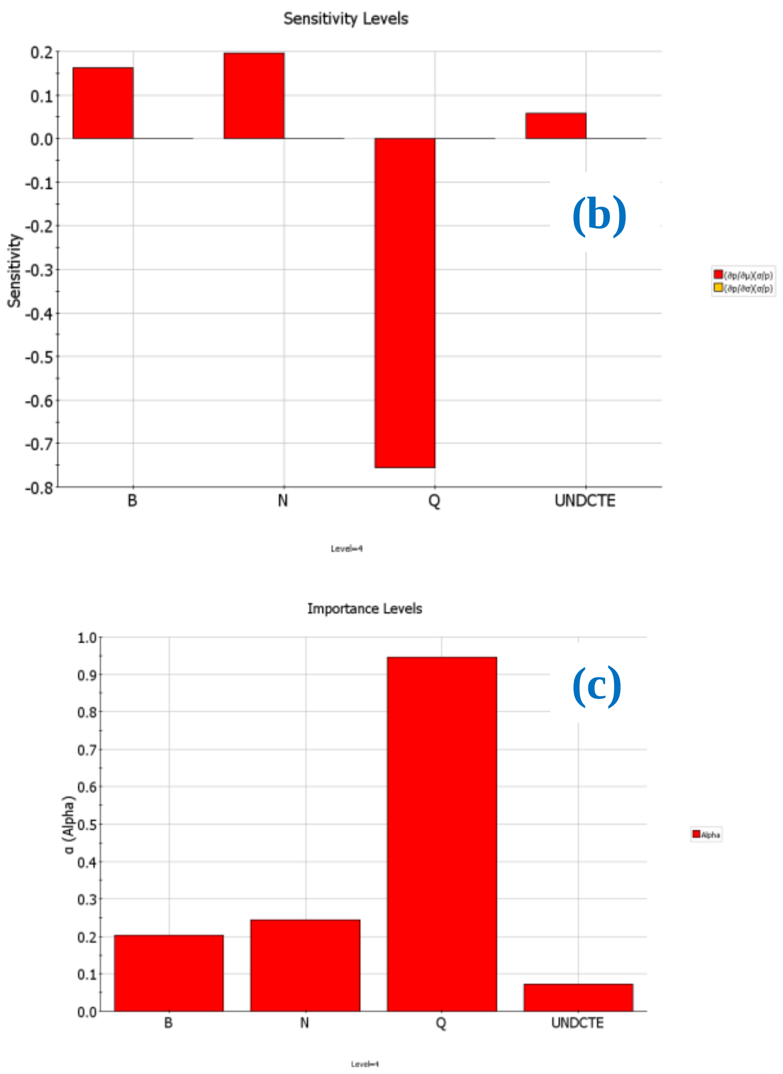

Fig. 93 Probability of failure (top) vs. cycle-to-failure N_f, Sensitivity at 50% probability (middle) and importance level at 50% probability (bottom) of the random variables used in the Run C

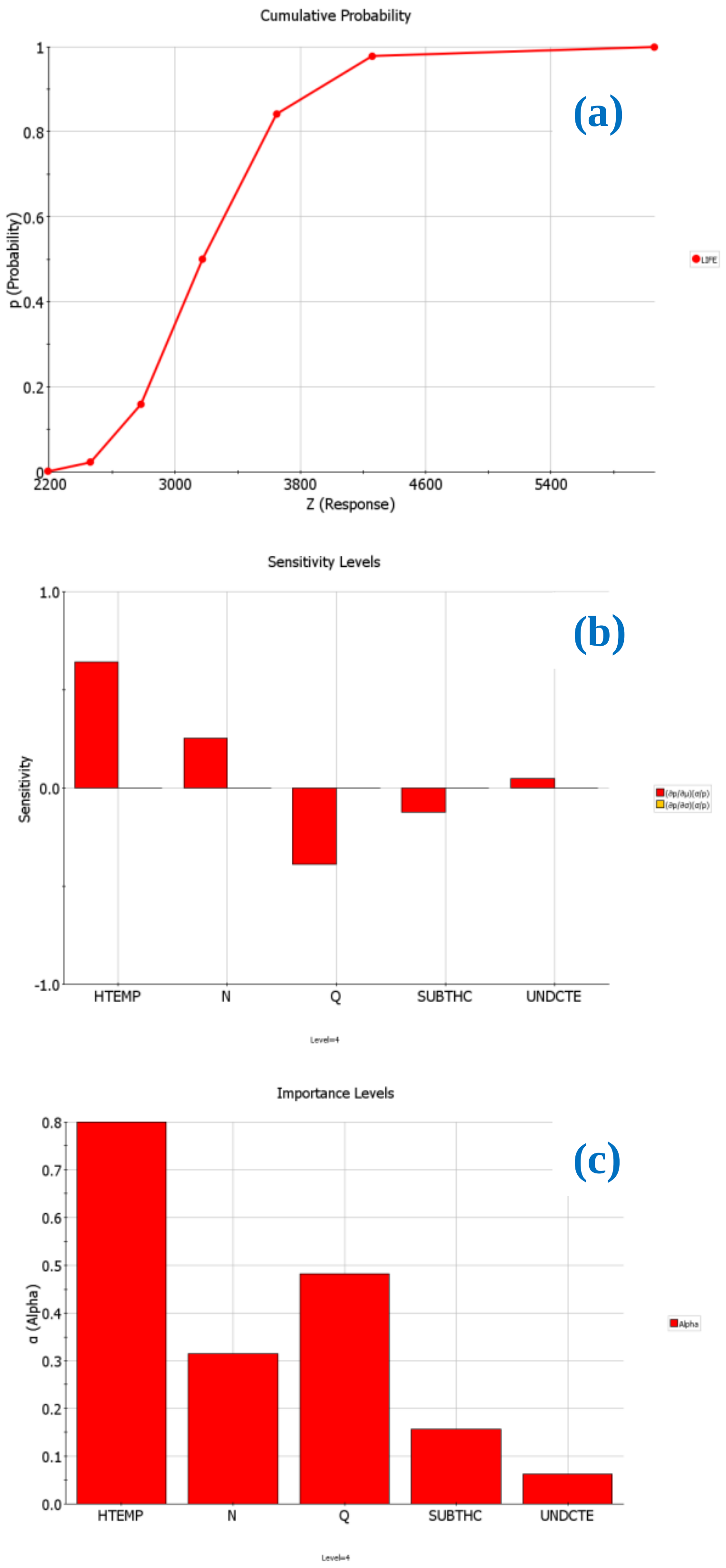
Cumulative Probability
(a)
1
0.8
0.6
0.4
0.2
0
p (Probability)
2200
3000
3800
4600
5400
Z (Response)
LIFE
Sensitivity Levels
(b)
1.0
0.0
-1.0
Sensitivity
HTEMP
N
Q
SUBTHC
UNDCTE
(∂p/∂μ)(σ/p)
(∂p/∂σ)(σ/p)
Level=4
Importance Levels
(c)
0.8
0.7
0.6
0.5
0.4
0.3
0.2
0.1
0.0
α (Alpha)
HTEMP
N
Q
SUBTHC
UNDCTE
Alpha
Level=4

Fig. 94 Probability of failure (top) vs. cycle-to-failure N_f, Sensitivity at 50% probability (middle) and importance level at 50% probability (bottom) of the random variables used in the Run D

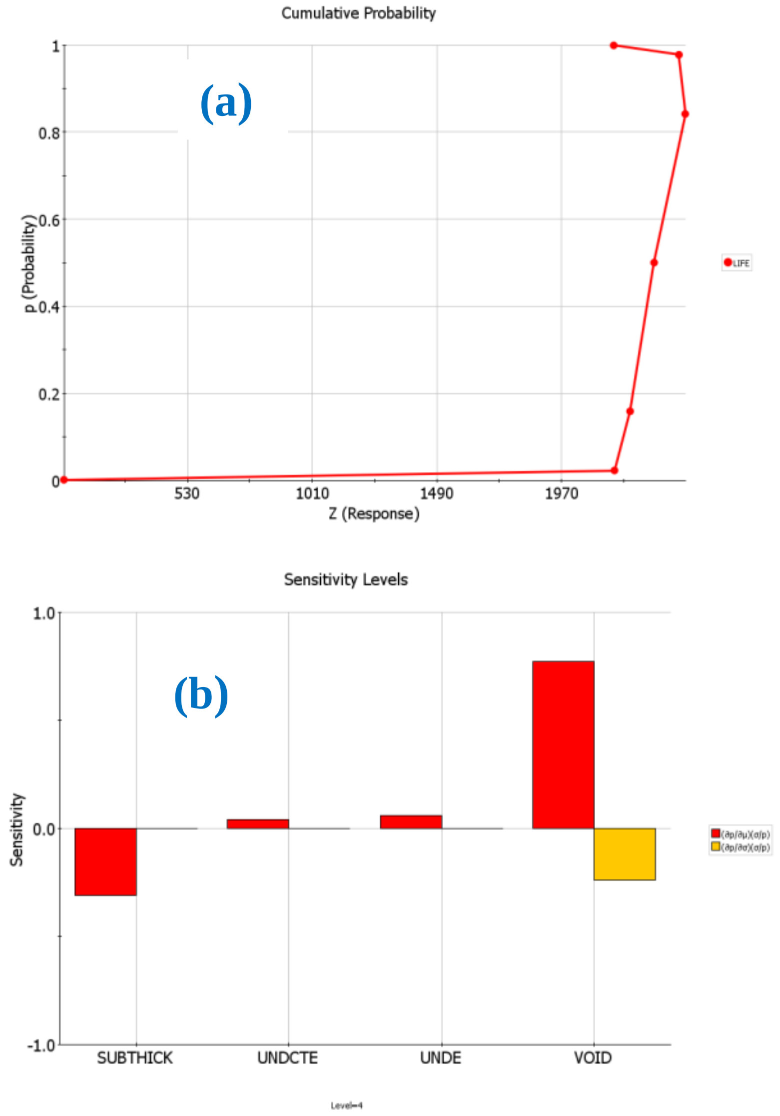

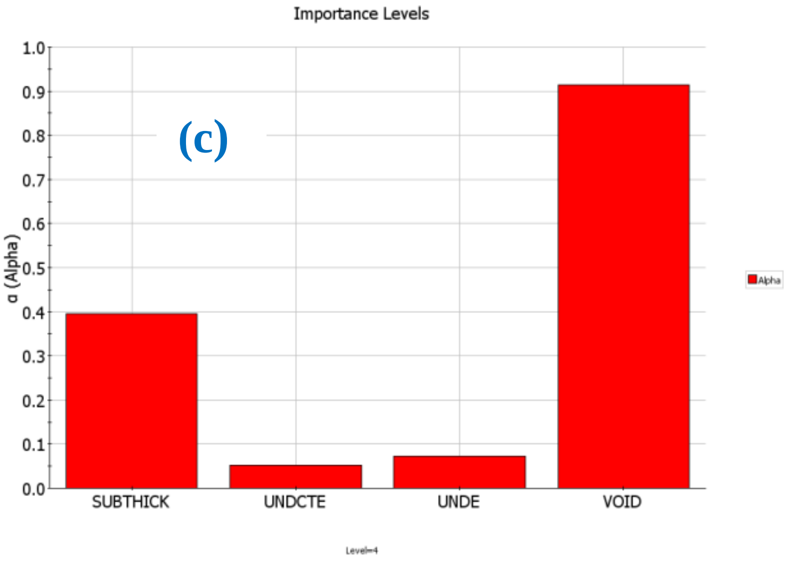

Fig. 95 Probability of failure (top) vs. cycle-to-failure N_f, Sensitivity at 50% probability (middle) and importance level at 50% probability (bottom) of the random variables used in the Run E

In all of these results the probability of failure is defined as the integral of the joint probability density function of the random variables of the system. Since the random variables used in IMPRPK are independent, therefore the probability density function will be equal to the product of the individual distributions. As it was mentioned before, the sensitivity is the derivative of the probability function with respect to mean (μ) and standard deviation (σ) of each random variable. Sensitivity results will demonstrate how sensitive is the reliability of the system with respect to the changes in means and standard deviations of the system variables.

The following conclusions could be conveyed by reviewing these probabilistic and sensitivity results:

- High dwell temperature, Substrate thickness, activation energy in creep constitutive model and internal void sizes seem to have the highest impact on the reliability of the SAC405 MCH packages.
- Various combinations of the system variables will result in different thermal fatigue life and sensitivity predictions. For instance the substrate thickness and activation energy in the hyperbolic sine creep model were the variables with high sensitivity in Run B and Run C respectively, but these variables in combination with High dwell temperature variable, were not as significant as high dwell temperature.
- Package life prediction is influenced by the random variables present in a system and their interaction with each other.

It should be noted that the sensitivity of each random variable could be different for various probability levels as shown in Fig. 96. This means that some variables may not be a significant reliability concern at lower probability levels and can become more important factor at higher probability levels.

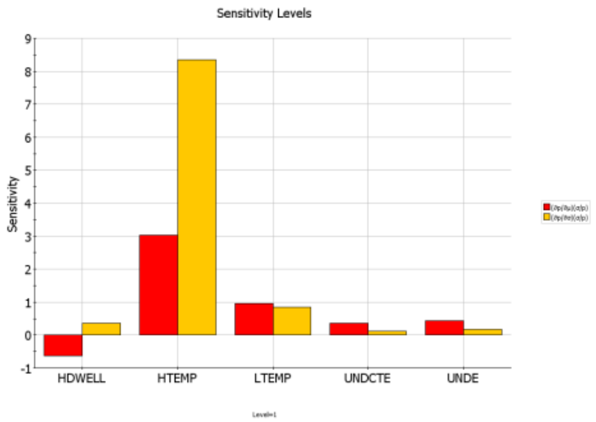

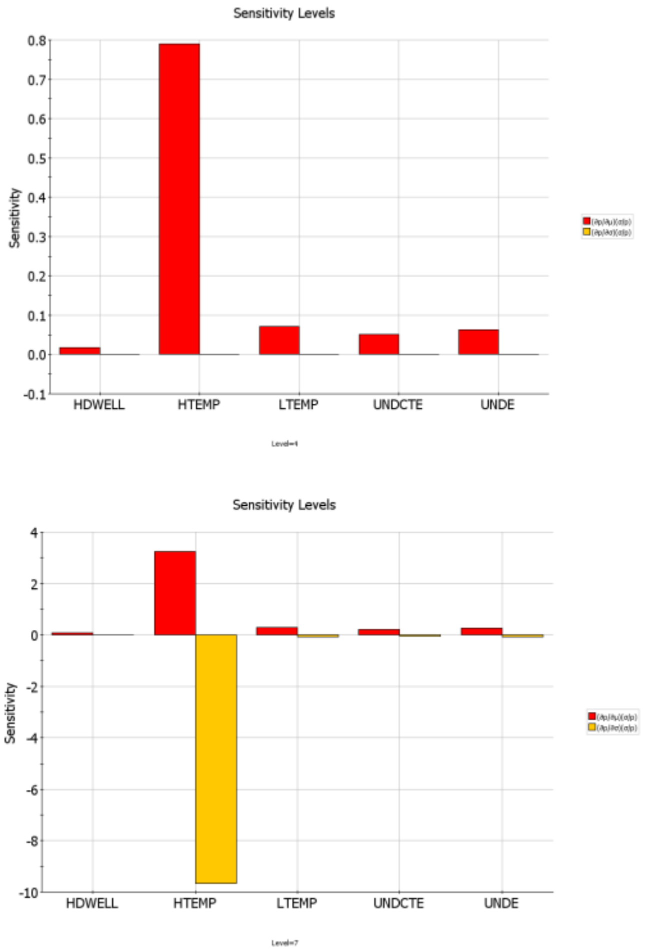

Fig. 96 Different sensitivity levels in Run A. (Top) sensitivity for very low probability (Center) sensitivity for 50% reliability (Bottom) sensitivity for very high reliability

Chapter 7

CONCLUSION

This chapter will review and summarize the IMPRPK tasks on microelectronic reliability and probabilistic analysis. The main purpose of this project was to investigate the applicability of probabilistic design to microelectronics packaging systems. Probabilistic methodology is used in incorporating the impact of system variabilities on system performance, reliability, etc. NESSUS probabilistic methodology developed by SwRI was identified as the most appropriate tool for application to complicated microelectronic package (MEP) system and due to its better efficiency and improved capabilities in solving complex limit state functions with multiple random variables, compared to other available probabilistic solutions, was adopted for use in IMPRPK.

We focused on BGA interconnect reliability in validating this approach. MEP System variabilities considered included natural variabilities such as material properties, design variabilities such as dimensional tolerances, variabilities related to the manufacturing and use condition (e.g. defect size distribution, operation temperature and dwell times).

Two package form factors, flip chip with underfill (MCH) & wire bonded with molding compound (ICH) were considered in this research.

The efficiency and applicability of the IMPRPK approach in microelectronic reliability was validated by conducting a wide range of analyses using the different parameters and their combinations. The effect of different combinations of the system variables on the reliability of the system was evaluated and parameters which highly influence the reliability of the overall system were identified.

Parameters such as use temperature, activation energy for creep Q, substrate thickness, and internal void size showed higher levels of impact on reliability compared to other parameters such as Underfill CTE, Underfill E and High temperature dwell time.

Results of the sensitivity analysis will help design engineers to come up with more reliable package designs. The sign and magnitude of these sensitivity results which are derivatives of the probability of failure function with respect to the mean and standard deviation of the system parameters, will dictate the impact of each parameter on overall system reliability.

IMPRPK study has shown that increasing the activation energy, as well as, increasing the thickness of package substrate, board and silicon die will improve the reliability of the package. This is revealed by IMPRPK prediction of reduced probability of failure and negative sensitivity values. It should be noted that the system variables where positive sensitivity values are predicted (e.g., use condition temperature, dwell time, underfill elastic modulus, underfill CTE and Void size) are indicative of decrease in the package reliability as a result of an increase in the mean and standard deviation of these package variables.

In conclusion, with IMPRPK results one should consider increasing the mean values of the parameters when negative sensitivity is predicted and decreasing those with positive sensitivity. It is important to mention that the sensitivity results are highly dependent on variable combinations. The sign and magnitude of the sensitivity results could be altered with different combination of variables. As an example, 7% increase in substrate thickness (equal to one standard deviation) will improve the reliability of BGAs by70%.

To reduce the simulation time, we used “segmentation” approach for sensitivity analysis, where NESSUS simulations were conducted using groups of various parameters, with one parammeter included in all runs for reference. This approach was considered appropriate in validating the IMPRPK-NESSUS capability in a timely manner. The idea was to use the sensitivity information from all the simulations and further consolidate them into one set for concurrent ranking of all parameters and identification of the key parameters. Such approach, and/or simulation considering the most critical parameters can be used in identifying the key parameters, to be considered in design, manufacturing, and/or establishing process control.

Examples of analysis results in this study were:

- Package substrate thickness has a more significant impact on reliability of both MCH & ICH package design in comparison to the board and die thickness

- The substrate thickness effect was insignificant in comparisson to the temperature effect (e.g., hold tempertaure, activation energy), and stress exponent, based on NESSUS analysis using these parameters.

Through this study the applicability of IMPRPK and probabilistic analysis for various package parameters was validated and the results were presented in detail (Chapter 6). It is recommended that followup work to be conducted through additional IMPRPK-NESSUS simulations using the key parameters identified in the “segmented” simulations performed in this study, and considering realistic variabilities that one may encounter with activation energies, srtress exponent, etc.. Synergistic effect and the Interaction of various paramters on the BGA reliability should also be further investigated.

Deterministic methodologies needed in predicting component reliabilities were developed and incorporated into IMPRPK. As such FEM models were developed for couple of BGA layouts and package form-factors (MCH and ICH designs), FEM models were validated by comparing the independent predictions of the model with the experimental data obtained through characterization effort in this research. The predicted strain energy density values using the FEM model were in agreement with BGA crack distributions. Higher cumulative strain energy predicted by FEM for solder joints residing under and outside of the die shadow region in MCH and ICH designs were in agreement with the observed failure pattern in these two package designs.

The noted difference in BGA solder failure distribution in these two designs is attributed to the thermal mismatch between the package components. According to the FEM results, the dissipated energy density values are higher for the Sn37Pb BGAs compared to the SAC405. Presence of molding compound and the accuracy in CTE and Tg values, as well as, the care in incorporating them in FEM models are of significant importance in obtaining the correct system response.

In addition to developing a probabilistic methodology for MEP, we were able to obtain package dimensions, material properties and BGA internal defects distributions through detailed characterization effort. ABAQUS “global” and “local” FEM models for MCH and ICH packages were developed and validated using the ATC test data. Potential inaccuracy in ICH model prediction of steady-state dissipated-strain-energy- density (e.g., 3rd cycle ECDDEN) was recognized and should be further investigated.

A crack growth based life prediction model (e.g. Darveaux’s model) was selected for use in IMPRPK. This model utilizes the FEM response (e.g. energy) to predict crack initiation and growth. The predicted thermal fatigue life using the Darveaux’s model with the steady-state energy density values from FEM was in line with the package life measure through accelerated thermal cycling tests.

REFERENCES

[1]. Reiff D, Bradley E. In: A novel mechanical shock test method to evaluate lead-free BGA solder joint reliability. Electronic components and technology conference, 2005. proceedings. 55th; IEEE; 2005. p. 1519-25.

[2]. Mishiro K, Ishikawa S, Abe M, Kumai T, Higashiguchi Y, Tsubone K. Effect of the drop impact on BGA/CSP package reliability. Microelectronics Reliability. 2002;42(1):77-82.

[3]. Teng SY, Brillhart M. In: Reliability assessment of a high CTE CBGA for high availability systems. Electronic components and technology conference, 2002. proceedings. 52nd; IEEE; 2002. p. 611-6.

[4]. Chan Y, Ju T, Hareb SA, Lee Y, Wu JS, Lii MJ. Reliability modeling for ball grid array assembly with a large number of warpage affected solder joints. Journal of Electronic Packaging(Transactions of the ASME).

[5]. Park S, Joshi R, Goldmann L. In: Reliability of lead-free copper columns in comparison with tin-lead solder column interconnects. Electronic components and technology conference, 2004. proceedings. 54th; IEEE; 2004. p. 82-9.

[6]. Meilunas M, Primavera A, Dunford SO. In: Reliability and failure analysis of lead-free solder joints. Proceedings of the IPC annual meeting; ; 2002.

[7]. CIech JP. Solder reliability solutions: A PC-based design-for-reliability tool*. Soldering & Surface Mount Technology. 1997;9(2):45-54.

[8]. Limaye P, Vandevelde B, Van de Peer J, Donders S, Darveaux R. In: Probabilistic design approach for package design and solder joint reliability optimization for a lead free BGA package. Thermal, mechanical and multi-physics simulation and experiments in micro-electronics and micro-systems, 2005. EuroSimE 2005. proceedings of the 6th international conference on; IEEE; 2005. p. 531-7.

[9]. Howieson M. In: CBGA to FR4 printed circuit board with no underfill thermal mismatch study. Electronic components and technology conference, 2001. proceedings., 51st; IEEE; 2001. p. 1487-95.

[10]. Perkins A, Sitaraman SK. In: Predictive fatigue life equation for CBGA electronic packages based on design parameters. Thermal and thermomechanical phenomena in electronic systems, 2004. ITHERM'04. the ninth intersociety conference on; IEEE; 2004. p. 253-8.

[11]. Farooq M, Goldmann L, Martin G, Goldsmith C, Bergeron C. In: Thermo-mechanical fatigue reliability of pb-free ceramic ball grid arrays: Experimental

data and lifetime prediction modeling. Electronic components and technology conference, 2003. proceedings. 53rd; IEEE; 2003. p. 827-33.

[12]. Zhang L, Patwardhan V, Nguyen L, Kelkar N, Sitaraman R. In: Solder joint reliability model with modified darveaux's equations for the micro smd wafer level-chip scale package family. Electronic components and technology conference; IEEE; 1999; 2003. p. 572-7.

[13]. Lau JH. Thermal fatigue life prediction of flip chip solder joints by fracture mechanics method. Eng Fract Mech. 1993;45(5):643-54.

[14]. Hacke P, Fahmy Y, Conrad H. Phase coarsening and crack growth rate during thermo-mechanical cycling of 63Sn37Pb solder joints. J Electron Mater. 1998;27(8):941-7.

[15]. Lall P, Islam MN, Singh N, Suhling JC, Darveaux R. Model for BGA and CSP reliability in automotive underhood applications. Components and Packaging Technologies, IEEE Transactions on. 2004;27(3):585-93.

[16]. Lai YS, Wang TH, Lee CC. Thermal–Mechanical coupling analysis for coupled power-and thermal-cycling reliability of board-level electronic packages. Device and Materials Reliability, IEEE Transactions on. 2008;8(1):122-8.

[17]. Lau JH. Solder joint reliability of flip chip and plastic ball grid array assemblies under thermal, mechanical, and vibrational conditions. Components, Packaging, and Manufacturing Technology, Part B: Advanced Packaging, IEEE Transactions on. 1996;19(4):728-35.

[18]. Engelmaier W. Generic reliability figures of merit design tools for surface mount solder attachments. Components, Hybrids, and Manufacturing Technology, IEEE Transactions on. 1993;16(1):103-12.

[19]. Lall P, Singh N, Suhling J, Strickland M, Blanche J. In: Thermal reliability considerations for deployment of area array packages in harsh environments. Thermal and thermomechanical phenomena in electronic systems, 2004. ITHERM'04. the ninth intersociety conference on; IEEE; 2004. p. 259-67.

[20]. Clech JPM, Langerman F, Augis J. In: Local CTE mismatch in SM leaded packages: A potential reliability concern. Electronic components and technology conference, 1990.., 40th; IEEE; 1990. p. 368-76.

[21]. Engelmaier W, Attarwala AI. Surface-mount attachment reliability of clip-leaded ceramic chip carriers on FR-4 circuit boards. Components, Hybrids, and Manufacturing Technology, IEEE Transactions on. 1989;12(2):284-96.

[22]. Kuo W, Prasad VR. An annotated overview of system-reliability optimization. Reliability, IEEE Transactions on. 2000;49(2):176-87.

[23]. Ghaffarian R. Area array technology for high reliability applications. Micro- and Opto-Electronic Materials and Structures: Physics, Mechanics, Design, Reliability, Packaging. 2007:283-312.

[24]. Engelmaier W. Solder joints in electronics: Design for reliability. Design and Reliability of Solders and Solder Interconnections, The Minerals, Metals & Materials Society. 1997:9-19.

[25]. Darveaux R, Reichman C. In: Ductile-to-brittle transition strain rate. Electronics packaging technology conference, 2006. EPTC'06. 8th; IEEE; 2006. p. 283-9.

[26]. Arulvanan P, Zhong Z, Shi X. Effects of process conditions on reliability, microstructure evolution and failure modes of SnAgCu solder joints. Microelectronics Reliability. 2006;46(2):432-9.

[27]. Qi Y, Lam R, Ghorbani HR, Snugovsky P, Spelt JK. Temperature profile effects in accelerated thermal cycling of SnPb and pb-free solder joints. Microelectronics Reliability. 2006;46(2):574-88.

[28]. Hugh Roberts, Sven Lamprech, Christian Sebald, Mark Bachman, John Osenbach, Kishor Desai, Ron Huemoeller, YoonHa Jung Robert Darveaux. Analysis of BGA solder joint reliability for selected solder alloy and surface finish configurations. IMAPS 5th internationalconference and exhibition on device packaging;

[29]. Newman K. In: BGA brittle fracture-alternative solder joint integrity test methods. Electronic components and technology conference, 2005. proceedings. 55th; IEEE; 2005. p. 1194-201.

[30]. Hacke P, Sprecher A, Conrad H. Microstructure coarsening during thermo-mechanical fatigue of pb-sn solder joints. J Electron Mater. 1997;26(7):774-82.

[31]. Song F, Lee SWR, Newman K, Sykes B, Clark S. In: Brittle failure mechanism of SnAgCu and SnPb solder balls during high speed ball shear and cold ball pull tests. Electronic components and technology conference, 2007. ECTC'07. proceedings. 57th; IEEE; 2007. p. 364-72.

[32]. Sharif A, Islam M, Chan Y. Interfacial reactions of BGA Sn–3.5% Ag–0.5% cu and Sn–3.5% ag solders during high-temperature aging with Ni/Au metallization. Materials Science and Engineering: B. 2004;113(3):184-9.

[33]. Tu KN, Zeng K. Tin‑lead (SnPb) solder reaction in flip chip technology. Materials Science and Engineering: R: Reports. 2001;34(1):1-58.

[34]. Song F, Lee SWR, Newman K, Sykes B, Clark S. In: High-speed solder ball shear and pull tests vs. board level mechanical drop tests: Correlation of failure mode and loading speed. Electronic components and technology conference, 2007. ECTC'07. proceedings. 57th; IEEE; 2007. p. 1504-13.

[35]. Chandran B, Goyal D, Thomas J. In: Effect of package design and layout on BGA solder joint reliability of an organic C4 package. Electronic components & technology conference, 2000. 2000 proceedings. 50th; IEEE; 2000. p. 1205-14.

[36]. Kanda Y, Kariya Y, Mochizuki Y. Effect of hold time on low cycle fatigue life of micro solder joint. Materials transactions. 2008;49(7):1524-30.

[37]. Syed AR. Creep crack growth prediction of solder joints during temperature cycling—an engineering approach. Journal of Electronic Packaging. 1995;117:116.

[38]. Lall P, Pecht M, Hakim EB. Influence of temperature on microelectronics and system reliability: A physics of failure approach. CRC; 1997.

[39]. Humpston G, Jacobson DM. Principles of soldering. ASM International; 2004.

[40]. Abtew M, Selvaduray G. Lead-free solders in microelectronics. Materials Science and Engineering: R: Reports. 2000;27(5):95-141.

[41]. Ostrom N, Wilson M, Frampton J. Draft lead report. State of California Department of Toxic Substances Control, Hazardous Waste Management Program, Regulatory and Program Development Division.Sacramento, CA. 2004.

[42]. Tummala RR. Fundamentals of microsystems packaging. McGraw-Hill New York:; 2001.

[43]. Ratchev P, Loccufier T, Vandevelde B, Verlinden B, Teliszewski S, Werkhoven D, et al. In: A study of brittle to ductile fracture transition temperatures in bulk pb-free solders. Proceedings of the 15th european microelectronics and packaging conference and exhibition; ; 2005. p. 248-52.

[44]. [Internet]. Available from: http://www.metallurgy.nist.gov/phase/solder/solder.html.

[45]. Zhao J, Miyashita Y, Mutoh Y. Fatigue crack growth behavior of 96.5 Sn‑3.5 ag lead-free solder. Int J Fatigue. 2001;23(8):723-31.

[46]. Kang S, Lauro P, Shih DY, Henderson D, Puttlitz K. Microstructure and mechanical properties of lead-free solders and solder joints used in microelectronic applications. IBM journal of research and development. 2005;49(4.5):607-20.

[47]. Vasudevan V, Fan X, Liu T, Young D. In: Slow cycle fatigue creep performance of pb-free (LF) solders. Electronic components and technology conference, 2007. ECTC'07. proceedings. 57th; IEEE; 2007. p. 116-23.

[48]. Shnawah DA, Sabri MFM, Badruddin IA. A review on thermal cycling and drop impact reliability of SAC solder joint in portable electronic products. Microelectronics Reliability. 2012;52(1):90-9.

[49]. Meyers MA, Mishra A, Benson DJ. Mechanical properties of nanocrystalline materials. Progress in Materials Science. 2006;51(4):427-556.

[50]. Arfaei B, Tashtoush T, Kim N, Wentlent L, Cotts E, Borgesen P. In: Dependence of SnAgCu solder joint properties on solder microstructure. Electronic components and technology conference (ECTC), 2011 IEEE 61st; IEEE; 2011. p. 125-32.

[51]. Masumura R, Hazzledine P, Pande C. Yield stress of fine grained materials. Acta Materialia. 1998;46(13):4527-34.

[52]. Shi X, Pang H, Zhou W, Wang Z. A modified energy-based low cycle fatigue model for eutectic solder alloy. Scr Mater. 1999;41(3):289-96.

[53]. Yunus M, Srihari K, Pitarresi J, Primavera A. Effect of voids on the reliability of BGA/CSP solder joints. Microelectronics reliability. 2003;43(12):2077-86.

[54]. Kim DS, Yu Q, Shibutani T, Sadakata N, Inoue T. In: Effect of void formation on thermal fatigue reliability of lead-free solder joints. Thermal and thermomechanical phenomena in electronic systems, 2004. ITHERM'04. the ninth intersociety conference on; IEEE; 2004. p. 325-9.

[55]. Date M, Shoji T, Fujiyoshi M, Sato K, Tu K. Ductile-to-brittle transition in Sn–Zn solder joints measured by impact test. Scr Mater. 2004;51(7):641-5.

[56]. Ren F, Nah JW, Tu K, Xiong B, Xu L, Pang JHL. Electromigration induced ductile-to-brittle transition in lead-free solder joints. Appl Phys Lett. 2006;89(14):141914,141914-3.

[57]. Yang SY, Jeon YD, Lee SB, Paik KW. Solder reflow process induced residual warpage measurement and its influence on reliability of flip-chip electronic packages. Microelectronics Reliability. 2006;46(2):512-22.

[58]. Suryanarayana D, Wu TY, Varcoe JA. In: Encapsulants used in flip-chip packages. Electronic components and technology conference, 1993. proceedings., 43rd; IEEE; 1993. p. 193-8.

[59]. Yin C, Alam M, Chan Y, Bailey C, Lu H. The effect of reflow process on the contact resistance and reliability of anisotropic conductive film interconnection for flip chip on flex applications. Microelectronics Reliability. 2003;43(4):625-33.

[60]. Zhong W, Chan Y, Alam M, Wu B, Guan J. Effect of multiple reflow processes on the reliability of ball grid array (BGA) solder joints. J Alloys Compounds. 2006;414(1):123-30.

[61]. Hao X, Qin L, Yang D, Liu S. In: Thermal-mechanical stress and fatigue failure analysis of A PBGA. Electronic packaging technology proceedings, 2003. ICEPT 2003. fifth international conference on; IEEE; 2003. p. 438-42.

[62]. Kang SK, Lauro P, Shih DY, Henderson DW, Gosselin T, Bartelo J, et al. In: Evaluation of thermal fatigue life and failure mechanisms of sn-ag-cu solder joints with reduced ag contents. Electronic components and technology conference, 2004. proceedings. 54th; IEEE; 2004. p. 661-7.

[63]. Conrad H, Guo Z, Fahmy Y, Yang D. Influence of microstructure size on the plastic deformation kinetics, fatigue crack growth rate, and low-cycle fatigue of solder joints. J Electron Mater. 1999;28(9):1062-70.

[64]. Ochoa F, Williams J, Chawla N. Effects of cooling rate on the microstructure and tensile behavior of a sn-3.5 wt.% ag solder. J Electron Mater. 2003;32(12):1414-20.

[65]. Mei Z, Morris J, Shine M, Summers TSE. Effects of cooling rate on mechanical properties of near-eutectic tin-lead solder joints. J Electron Mater. 1991;20(10):599-608.

[66]. Ochoa F, Deng X, Chawla N. Effects of cooling rate on creep behavior of a sn-3.5 ag alloy. J Electron Mater. 2004;33(12):1596-607.

[67]. Pang JHL, Xu L, Shi X, Zhou W, Ngoh S. Intermetallic growth studies on sn-ag-cu lead-free solder joints. J Electron Mater. 2004;33(10):1219-26.

[68]. Pang JHL, Tan KH, Shi X, Wang Z. Thermal cycling aging effects on microstructural and mechanical properties of a single PBGA solder joint specimen. Components and Packaging Technologies, IEEE Transactions on. 2001;24(1):10-5.

[69]. Towashiraporn P, Subbarayan G, McIlvanie B, Hunter B, Love D, Sullivan B. The effect of model building on the accuracy of fatigue life predictions in electronic packages. Microelectronics Reliability. 2004;44(1):115-27.

[70]. Norris K, Landzberg A. Reliability of controlled collapse interconnections. IBM Journal of Research and Development. 1969;13(3):266-71.

[71]. Pang JHL, Xiong B, Low T. In: Creep and fatigue characterization of lead free 95.5 sn-3.8 ag-0.7 cu solder. Electronic components and technology conference, 2004. proceedings. 54th; IEEE; 2004. p. 1333-7.

[72]. Lee W, Nguyen L, Selvaduray GS. Solder joint fatigue models: Review and applicability to chip scale packages. Microelectronics reliability. 2000;40(2):231-44.

[73]. Guo Z, Conrad H. Fatigue crack growth rate in 63Sn37Pb solder joints. Journal of Electronic Packaging. 1993;115:159.

[74]. Han C, Song B. Development of life prediction model for lead-free solder at chip resistor. Electronics packaging technology conference, 2006. EPTC'06. 8th; IEEE; 2006.

[75]. Clech JP. In: Solder joint reliability of CSP versus BGA assemblies. Proceedings, system integration in micro electronics, SMT ESS & hybrids conference, nuremberg, germany; ; 2000. p. 19-28.

[76]. Tasooji A. Reliability of area array package , literature review and applicability of current methodologies. Progress report - JPL NASA.

[77]. Wong T, Fenger H. In: Vibration and thermo-mechanical durability assessments in advanced electronic package interconnects. Electronic components and technology conference, 2004. proceedings. 54th; IEEE; 2004. p. 1080-7.

[78]. Barney MM. Microstructural coarsening during thermomechanical fatigue and annealing of micro flip-chip. Info:.

[79]. Schubert A, Dudek R, Auerswald E, Gollbardt A, Michel B, Reichl H. In: Fatigue life models for SnAgCu and SnPb solder joints evaluated by experiments and simulation. Electronic components and technology conference, 2003. proceedings. 53rd; IEEE; 2003. p. 603-10.

[80]. Zhang Q. In: A novel solder ball coating process with improved reliability. Electronic components and technology conference, 2005. proceedings. 55th; IEEE; 2005. p. 399-405.

[81]. Rodgers B, Flood B, Punch J, Waldron F. In: Experimental determination and finite element model validation of the anand viscoplasticity model constants for SnAgCu. Thermal, mechanical and multi-physics simulation and experiments in micro-electronics and micro-systems, 2005. EuroSimE 2005. proceedings of the 6th international conference on; IEEE; 2005. p. 490-6.

[82]. Yeo A, Lee C, Pang JHL. Flip chip solder joint reliability analysis using viscoplastic and elastic-plastic-creep constitutive models. Components and Packaging Technologies, IEEE Transactions on. 2006;29(2):355-63.

[83]. Varia R, Fan X. In: Reliability enhancement of wafer level packages with nano-column-like hollow solder ball structures. Electronic components and technology conference (ECTC), 2011 IEEE 61st; IEEE; 2011. p. 754-60.

[84]. Fan X, Pei M, Bhatti PK. In: Effect of finite element modeling techniques on solder joint fatigue life prediction of flip-chip BGA packages. Electronic components and technology conference, 2006. proceedings. 56th; IEEE; 2006. p. 9 pp.

[85]. Amagai M. Chip scale package (CSP) solder joint reliability and modeling. Microelectronics Reliability. 1999;39(4):463-77.

[86]. Syed A. In: Accumulated creep strain and energy density based thermal fatigue life prediction models for SnAgCu solder joints. Electronic components and technology conference, 2004. proceedings. 54th; IEEE; 2004. p. 737-46.

[87]. Pei M, Fan X, Bhatti PK. In: Field condition reliability assessment for SnPb and SnAgCu solder joints in power cycling including mini cycles. Electronic components and technology conference, 2006. proceedings. 56th; IEEE; 2006. p. 7 pp.

[88]. Wiese S, Wolter KJ. Creep of thermally aged SnAgCu-solder joints. Microelectronics reliability. 2007;47(2):223-32.

[89]. Ma H. Constitutive models of creep for lead-free solders. J Mater Sci. 2009;44(14):3841-51.

[90]. Wiese S, Schubert A, Walter H, Dukek R, Feustel F, Meusel E, et al. In: Constitutive behaviour of lead-free solders vs. lead-containing solders-experiments on bulk specimens and flip-chip joints. Electronic components and technology conference, 2001. proceedings., 51st; IEEE; 2001. p. 890-902.

[91]. Pao YH, Jih E, Artz BE, Cathey LW. A note on the implementation of temperature dependent coefficient of thermal expansion (CTE) in ABAQUS. Journal of Electronic Packaging. 1992;114:470.

[92]. Abaqus 6.11 user's manual.

[93]. Thacker BH, Riha DS, Fitch SHK, Huyse LJ, Pleming JB. Probabilistic engineering analysis using the NESSUS software. Struct Saf. 2006;28(1):83-107.

[94]. Riha D, Thacker B, Enright M, Huyse L, Fitch S. In: Recent advances of the NESSUS probabilistic analysis software for engineering applications. Proc. AIAA/ASME/ASCE/AHS/ASC 42nd structures, structural dynamics, and materials (SDM) conf., AIAA-2002-1268, denver, CO; ; 2002. p. 22-5.

[95]. Riha DS, Thacker BH, Hall DA, Auel TR, Pritchard SD. Capabilities and applications of probabilistic methods in finite element analysis. International Journal of Materials and Product Technology. 2001;16(4):358-69.

[96]. [Internet]. Available from: www.nessus.com.

[97]. [Internet]. Available from: www.darwin.swri.org.

[98]. Zeng K, Tu K. Six cases of reliability study of pb-free solder joints in electronic packaging technology. Materials Science and Engineering: R: Reports. 2002;38(2):55-105.

[99]. Tasooji A, Ghaffarian R, Rinaldi A. In: Design parameters influencing reliability of ccga assembly: A sensitivity analysis. Thermal and thermomechanical phenomena in electronics systems, 2006. ITHERM'06. the tenth intersociety conference on; IEEE; 2006. p. 1056-63.

[100]. Lara L. Electrical connectivity test - private communication.

[101]. Kari L. Dye and pry test - private communication.

[102]. Woodhams D. Dye and pry test - private communication.

[103]. Kang SK, Shih DY, Leonard D, Henderson DW, Gosselin T, Cho S, et al. Controlling ag 3 sn plate formation in near-ternary-eutectic sn-ag-cu solder by minor zn alloying. JOM Journal of the Minerals, Metals and Materials Society. 2004;56(6):34-8.

[104]. Shangguan D. Lead-free solder interconnect reliability. ASM International (OH); 2005. 2002;124(3):246-53.

[105]. Pelosi G. The finite-element method, part i: Rl courant [historical corner]. Antennas and Propagation Magazine, IEEE. 2007;49(2):180-2.

[106]. Synge JL, Rheinboldt W. The hypercircle in mathematical physics. Phys Today. 1957;10:45.

[107]. Duffin R. Distributed and lumped networks. Journal of Mathematics and Mechanics. 1959;8(5):793-826.

[108]. Szabo BA, Babuska I. Finite element analysis. Wiley New York; 1991.

[109]. Database for solder properties with emphasis on new lead-free solders (release 4.0) [Internet]. Available from: www.nist.gov.

[110]. Darveaux R. In: Effect of simulation methodology on solder joint crack growth correlation. Electronic components & technology conference, 2000. 2000 proceedings. 50th; IEEE; 2000. p. 1048-58.

[111]. Syed A. In: Predicting solder joint reliability for thermal, power, and bend cycle within 25% accuracy. Electronic components and technology conference, 2001. proceedings., 51st; IEEE; 2001. p. 255-63.

[112]. Nessus training manual.

[113]. Methods comparison document.

[114]. NESSUS theoretical manual.

[115]. Thacker BH, Riha DS, Fitch SHK, Huyse LJ, Pleming JB. Probabilistic engineering analysis using the NESSUS software. Struct Saf. 2006;28(1):83-107.

[116]. Private communication with Dr. John McFarland (SwRI)

[117]. Rosenblatt M. Remarks on a multivariate transformation. The Annals of Mathematical Statistics. 1952;23(3):470-2.

[118]. McKay MD, Beckman RJ, Conover WJ. Comparison of three methods for selecting values of input variables in the analysis of output from a computer code. Technometrics. 1979;21(2):239-45.

[119]. Maier HR, Lence BJ, Tolson BA, Foschi RO. First-order reliability method for estimating reliability, vulnerability, and resilience. Water Resour Res. 2001;37(3):779-90.

[120]. Hohenbichler M, Gollwitzer S, Kruse W, Rackwitz R. New light on first- and second-order reliability methods. Struct Saf. 1987;4(4):267-84.

[121]. Madsen HO. First order vs. second order reliability analysis of series structures. Struct Saf. 1985;2(3):207-14.

APPENDIX A

RANDOM VARIABLE DISTRIBUTION METHODS

- Normal (Gaussian) distribution:

The normal distribution is a continuous probability distribution that has a symmetric bell shape function (also known as Gaussian function). Equation (1) shows the mathematical relation for the normal distribution function.

$$f(x, \mu, \sigma^2) = \frac{1}{\sigma\sqrt{2\pi}}\, Exp\left[-\frac{1}{2}\left(\frac{x-\mu}{\sigma}\right)^2\right] \qquad (1)$$

In this function μ is the mean value of the measured data and σ represents the standard deviation.

One special case for the normal distribution (μ=0 and σ^2=1) is called standard normal distribution.

This distribution has the capability of taking any positive and negative real values and because of this fact majority of the random variables are categorized under the normal distribution function.

Fig.1 demonstrates the standard normal distribution.

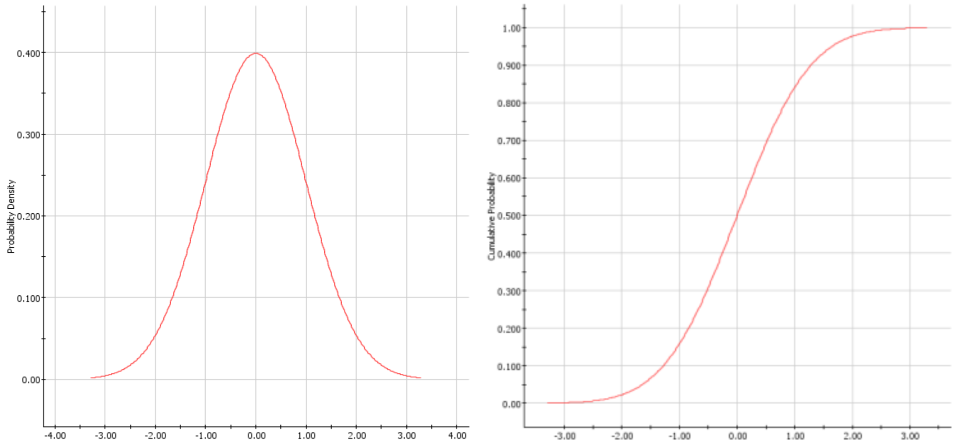

Fig 1. Probability density function (left) and Cumulative density function (right) representation for the standard normal distribution.

- Lognormal distribution:

The lognormal distribution is also a continuous distribution which has the following relation with the normal distribution.

If X is the lognormal with λ and ξ, then lnX would be a normal distribution with mean λ and standard deviation ξ. Equation (2) shows the relation between the above mentioned parameters.

$$\lambda = \ln \mu - \frac{1}{2}\xi^2 \quad \text{and} \quad \xi^2 = \ln(1+\sigma^2) \tag{2}$$

Equation (3) demonstrates the mathematic relation for the lognormal distribution function.

$$f(x) = \frac{1}{x\xi\sqrt{2\pi}}\, Exp\left[-\frac{1}{2}\left(\frac{lnx-\lambda}{\xi}\right)^2\right] \text{ for x} > 0 \tag{3}$$

As it could be seen from the Fig. 2, the lognormal distribution only takes the positive values (due to the log function).

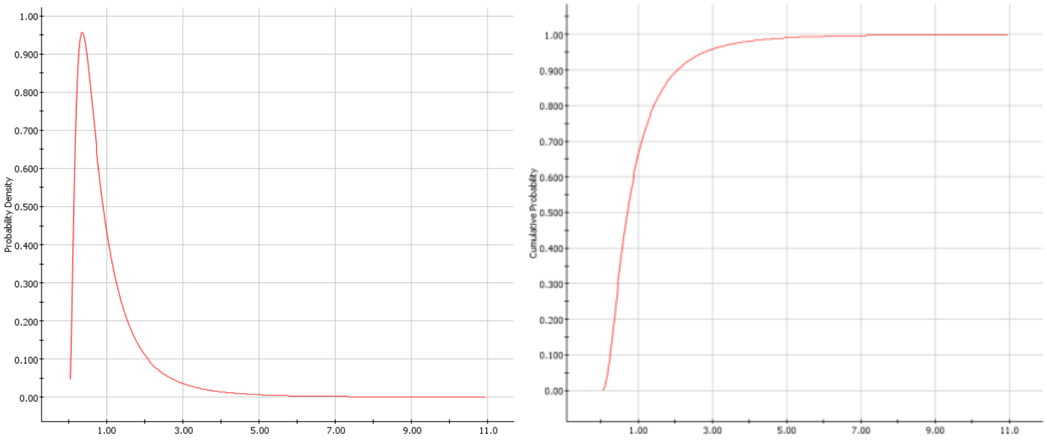

Fig 2. Probability density function (PDF) on the left and Cumulative density function (CDF) on the right for the lognormal distribution.

- Weibull distribution:

The Weibull distribution is a continuous distribution which is commonly used to define the particle and defect size distribution. Equation (4) shows the mathematical formulation for the Weibull distribution. The typical Weibull distribution has been presented in Fig. 3.

$$f(x) = \frac{\alpha}{\beta}\left(\frac{x}{\beta}\right)^{\alpha-1}\mathrm{exp}\left[-\left(\frac{x}{\beta}\right)^{\alpha}\right],\ x \geq 0 \tag{4}$$

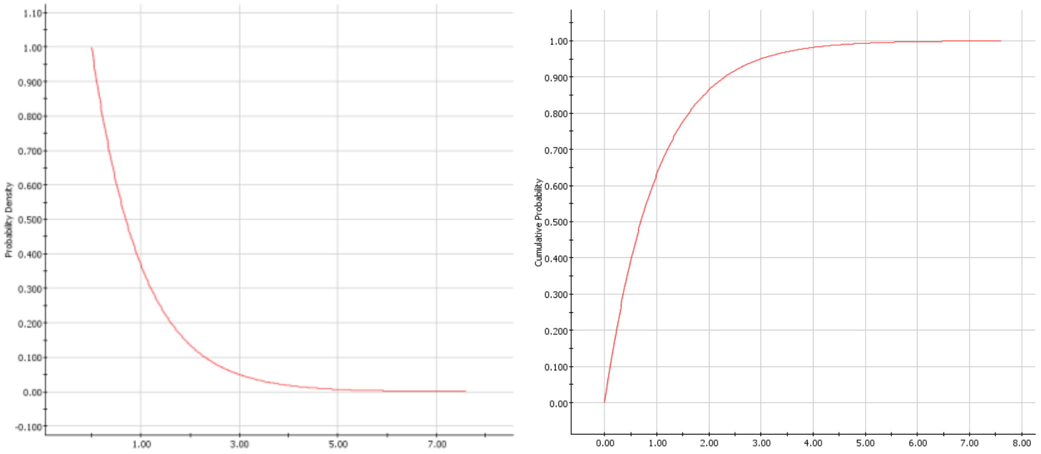

Fig 3. Probability density function (PDF) on the left and Cumulative density function (CDF) on the right for the Weibull distribution.

- Uniform distribution:

The uniform distribution (rectangular distribution) is a form of continuous distribution which has upper and lower bounds ([a] as lower bound and [b] as upper bound). Equation (5) shows the mathematical representations of the PDF and CDF distributions for uniform distribution.

$$a \leq x \leq b \quad PDF \Rightarrow\!\!> \; f(x) = \frac{1}{b-a} \quad and \quad CDF \Rightarrow\!\!> F(x) = \frac{x-a}{b-a} \tag{5}$$

The special cases of the uniform distribution occur when the value of the x is smaller or larger than the lower and upper bounds respectively.

Equation (6) shows these special cases:

$$\begin{aligned} &if\ x < a\ \ then\ \ f(x) = 0 \quad and \quad F(x) = 0 \\ &if\ x > b\ \ then\ \ f(x) = 0 \quad and \quad F(x) = 1 \end{aligned} \tag{6}$$

The mean and standard deviation of the uniform distribution will be calculated according to the following relations:

$$\mu = \frac{a+b}{2} \qquad\qquad \sigma = \frac{b-a}{2\sqrt{3}} \tag{7}$$

Fig. 4 shows the graphical representation of the uniform distribution.

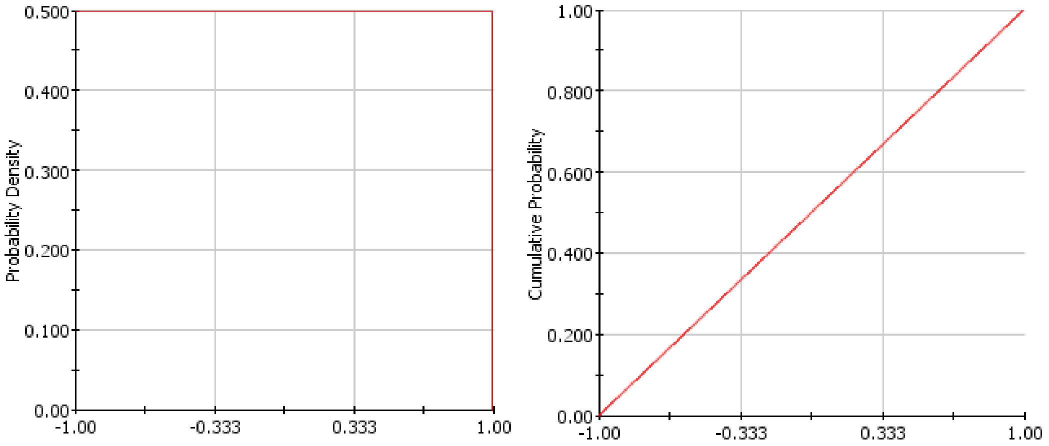

Fig 4. Probability density function (PDF) on the left and Cumulative density function (CDF) on the right for the uniform distribution.

APPENDIX B

DETAILS OF THE BOARDS AND MEP PACKAGES SUPPLIED BY INTEL CORPORATION FOR THIS STUDY

Board Number	Board Serial Number	Solder (EU/LF)	1st instance of electrical instability	Pull out cycle count	Result comment	(Dwell time) LD, min	Cycles	Remark
1	INV152600212 PBA C73302-200	Eutectic		2332		480	2332	
2	INV152600202 PBA C73302-200	Eutectic		200		480	2332	
3	INV152600208 PBA C73302-200	Eutectic		4412		60	6000	
4	INV152600236 PBA C73302-200	Eutectic		2332	pass	480	2332	
5	INV152600241 PBA C73302-200	Eutectic		2338		480	2332	
6	INV152600240 PBA C73302-200	Eutectic		150		240	4500	
7	INV152600197 PBA C73302-200	Eutectic						Time zero sample
8	INV152600231 PBA C73302-200	Eutectic		3526		240	4500	
9	INV152600200 PBA C73302-200	Eutectic		3075		240	4500	
10	INV152600074 PBA C69828-200	SAC405		6000	pass	60	6000	Missing smaller chip set
11	INV152600069 PBA C69828-200	SAC405		6000	pass	60	6000	
12	INV152600065 PBA C69828-200	SAC405		2332	pass	480	2332	
13	INV152600084 PBA C69828-200	SAC405		4000	pass	240	4500	Missing smaller chip set
14	INV152600201 PBA C73302-200	Eutectic		2171		60	6000	
15	INV152600053 PBA C69828-200	SAC405		2332		480	2332	
16	INV152600077 PBA C69828-200	SAC405		140		240	4500	Missing smaller chip set
17	INV152600238 PBA C73302-200	Eutectic		4412		60	6000	
18	INV152600188 PBA C73302-200	Eutectic	2243	4412		60	6000	
19	INV152600226 PBA C73302-200	Eutectic	4412	4412		60	6000	
20	INV152600194 PBA C73302-200	Eutectic						Time zero sample
21	INV152600219 PBA C73302-200	Eutectic						Time zero sample
22	INV152600221 PBA C73302-200	Eutectic						Time zero sample
23	INNB74800107 PBA E28048-100	SAC405						
24	INNB74800106 PBA E28048-100	SAC405						
25	INNB74800104 PBA E28048-100	SAC405						
26	INNB74800102 PBA E28048-100	SAC405						
27	INNB74800109 PBA E28048-100	SAC405						
28	INNB74800108 PBA E28048-100	SAC405						
29	INNB74800110 PBA E28048-100	SAC405						
30	INNB74800028 PBA E28048-100	SAC405						
31	INNB74800139 PBA E28048-100	SAC405						
32	INNB74800138 PBA E28048-100	SAC405						
33	INV152600086 PBA C69828-200	SAC405		2332	fail	480	2332	Missing smaller chip set
34	INV152600192 PBA C73302-200	Eutectic		2332	fail	480	2332	
35	INV152600211 PBA C73302-200	Eutectic		2332		480	2332	
36	INV152600198 PBA C73302-200	Eutectic	3400	4500		240	4500	
37	INV152600196 PBA C73302-200	Eutectic	3400	3187	pull 1_30_2007	240	4500	
38	INV152600073 PBA C69828-200	SAC405		4500	pass	240	4500	
39	INV152600078 PBA C69828-200	SAC405		4500	pass	240	4500	Missing smaller chip set
40	INV152600082 PBA C69828-200	SAC405		4500		240	4500	
41	INV152600085 PBA C69828-200	SAC405		4500		240	4500	
42	INV152600235 PBA C73302-200	Eutectic						Time zero sample
43	INV152600203 PBA C73302-200	Eutectic						Time zero sample
44	INV152600216 PBA C73302-200	Eutectic						Time zero sample
45	INV152600191 PBA C73302-200	Eutectic		2332	pass	480	2332	
46	INV152600063 PBA C69828-200	SAC405		2332	fail	480	2332	
47	INV152600060 PBA C69828-200	SAC405	1331	1522		480	2332	

Note: “Pull out cycle count” & “Cycle” columns represent the number of cycles prior to BGA failure and projected number of ATC cycles respectively.

APPENDIX C

PROBABILISTIC ANALYSIS - NESSUS OVERVIEW

1 Probabilistic analysis (Overview)

1.1 Commonly used Probabilistic Methods (Sampling Method)

Sampling methods because of their simplicity are widely used in probabilistic analysis. Beside the simplicity and accuracy of these methods their capabilities in analyzing the multiple limit state functions regardless of their condition (continuous or discrete functions) make them popular methods. In sampling technique the random variable distribution of each system variable will be divided in to certain number of increments or samples. Higher the number of samples will result in more accurate prediction of probability of failure. Since there are no simplifications or assumptions involved in definition of the limit state function in sampling methods, therefore these methods will work with any single or multiple limit state functions.

There are two major sampling methods:

1. Monte Carlo (MC)
2. Latin Hypercube Sampling (LHS)

The principals of these two methods are the same with the difference in sample distribution method (Fig. 1). In the Monte Carlo method, the samples are mostly populated around the center of the spectrum (around mean value) while the samples in LHS method are distributed more evenly throughout the spectrum (advantage over the Monte Carlo). Fig.1 below provides a schematic representation of this approach.

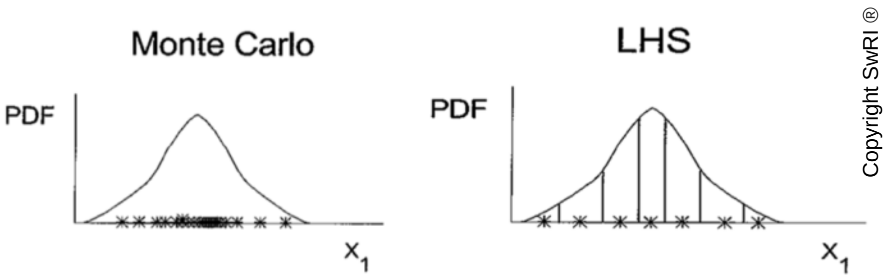

Fig. 1 Sample distribution comparison between the Monte Carlo and LHS sampling techniques.

In the sampling methods increasing the number of analyzed samples will lead to more accurate prediction. The main concern regarding the use of these common sampling methods is the long process time to obtain the system response, especially when a numerical code (e.g. ABAQUS, ANSYS finite element codes) is used in determining the system response. In some complex systems, the analysis of each sample could take few hours. Considering the large number (usually ~100,000 to 1,000,000 samples) of required samples to obtain an accurate prediction, the reliability analysis may take years to finish. With the use of analytical closed form equations in determining the system response, utilizing the sampling methods are recommended to achieve more accurate prediction. Sampling methods will be discussed more in detail in the rest of this chapter.

1.2 Theoretical Probabilistic Methods

Besides the advantages of the sampling methods, the large number of required samples is the main disadvantage of these methods. In order to address this concern, extensive amount of research has been conducted by the statisticians and reliability engineers to develop efficient and affordable solutions for system reliability and sensitivity predictions of complex systems with acceptable levels of accuracy. Majority of these efforts are focused in development of the theoretical and numerical techniques which are mainly used in probabilistic and reliability analysis of the complex systems. These theoretical methods will reduce the process cost and time by approximating the reliability of the systems to some acceptable confidence levels.

Some of the common theoretical methods which are widely used in the probabilistic analysis and are included in NESSUS [113-114] probabilistic methods are:

- First and second Order Reliability Methods (FORM and SORM): works based on the linear and parabolic expansion of the limit state function in the design point (Most Probable Point)
- Mean Value (MV), Advanced Mean Value (AMV) and Advanced Mean Value plus (AMV+) methods: works based on the first and second order mean value calculations and continuous corrections to achieve the acceptable confidence level.

Unlike the sampling methods (e.g., Monte Carlo and Latin Hypercube sampling) which require a large number of samples to provide the exact reliability, the theoretical methods such as those listed above are capable of approximating the probability of the failure P_f or more commonly the Reliability of the system (1- P_f) with relatively high accuracy & confidence levels using very low number of iterations.

1.3 Advantages and Disadvantages of Various Probabilistic Methods

Comparison between the efficiency and accuracy of the sampling and theoretical methods reveals the advantages and disadvantages of these models. The advantages of the sampling techniques are their high accuracy and ease of implementation in predicting the reliability of any system. The main disadvantages of these sampling methods are the large number of required samples. On the other hand, the main advantage of the theoretical methods over the sampling techniques is approximating the reliability of the system with much lower number of required samples and relatively high levels of accuracy. The disadvantage of the theoretical models is their limitation in the number of limit state functions which could be processed utilizing these methods. Convergence issue and non-monotonic probability functions are the other common problems associated with these techniques.

2 System response and limit state function

As discussed earlier in this chapter, the response or performance function “Z(X)” is basically the response of the system to the random variables (Equation 1) [114]. In the IMPRPK, the dissipated energy density is chosen to be the system response.

$$Z(X) = Z(X_1, X_2, ..., X_n) \qquad (1)$$

According to equation (1), the system response is function of random variables of the system. In this relation the X_i (i=1,2,…,n) represent the random variables of the system (e.g. temperature, dwell time, geometry, etc.).

The probabilistic analysis is a statistical study to predict the probability of the occurrence of a limit state function and the limit state function defines the limit for system failure.

3 Random variable distribution

In previous sections, the concepts of the system response and limit state functions were defined. The details of data processing and constructing the random variable distribution will be covered in this section. The standard mathematical forms of Probability Density Functions (PDF) and Cumulative Density Functions (CDF) are generally used to create the random variable distributions. Fig. 2 shows the difference between the PDF and CDF.

The definition of the PDF and CDF is presented below:

- PDF (Probability Density Function) = fX (X)
  - Which indicates how likely each value of X (random variable) is to occur (occurrence probability of each random variable)
- CDF (Cumulative Distribution Function) = FX (X)
  - Which measures the probability that the random variable X does not exceed the value x.

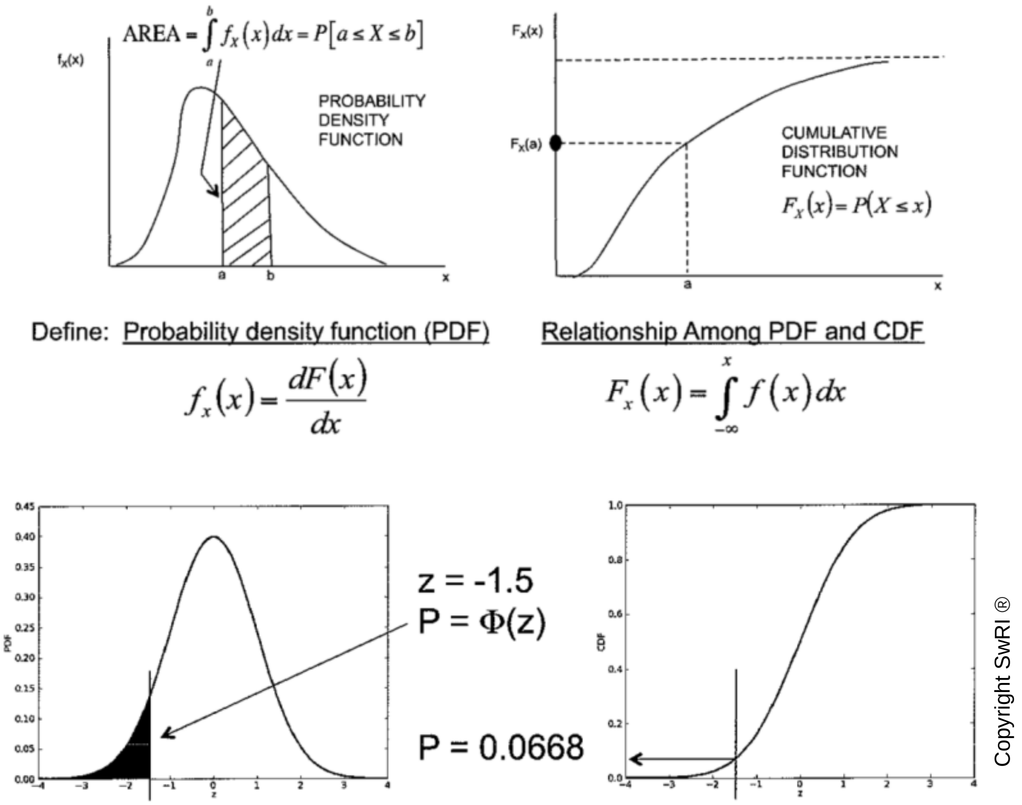

Copyright SwRI ®

Fig. 2 The relation between the PDF and CDF functions [112].

There are different statistical distribution functions (e.g. Normal distribution, lognormal distribution, Weibull distribution and uniform distribution) which are generally used in defining the random variables of the systems [112]. Depending on the type of the data, one of the above mentioned distribution functions could be selected (e.g. normal distribution is used for positive and negative values; log normal was used only for positive values, etc.). All of the random variables in IMPRPK are defined using the standard normal distribution except the void distribution which uses Weibull distribution.

Fig. 3 shows the typical shape of the normal Probability Density Function (PDF) and Cumulative Density Function (CDF) used in Probabilistic analysis.

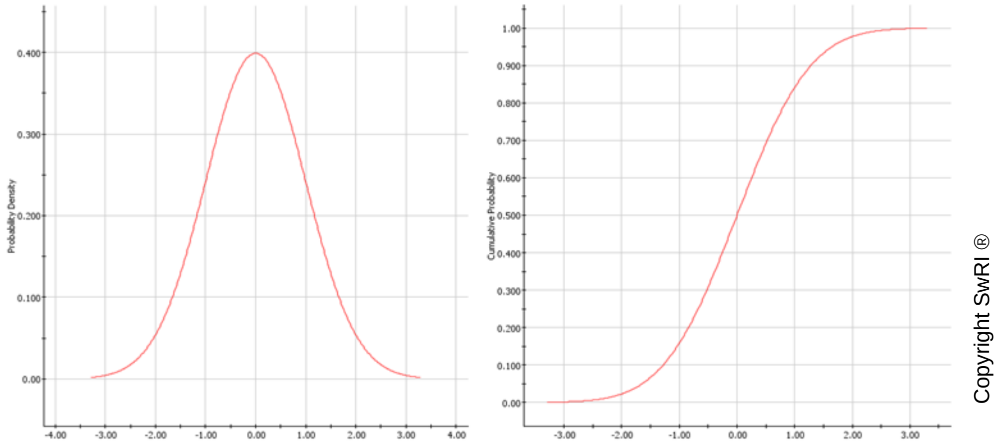

Fig. 3 Typical normal PDF (left) and normal CDF (right) distribution density functions used in the probabilistic analysis of the SAC405 MCH packages.

Details of different distribution density functions are discussed in Appendix (A).

Random variables could demonstrate different interactions. Here are some of the common distribution interactions:

In these relations X and Y represent random variables:

a. **Marginal distribution of X:** defines the probability density function (PDF) of X without regard to Y.

$$f_X(x) = \int_{-\infty}^{\infty} f_{XY}(x,y)\,dy \qquad (2)$$

b. **Conditional distribution of X for given Y:** defines the probability density function (PDF) of X for a specific Y.

$$f_{X|Y}(x|y) = \frac{f_{xy}(x,y)}{f_y(y)} \qquad f_y > 0 \tag{3}$$

c. **Independent random variables:** defines the probability density function (PDF) when X and Y are independent random variables.

$$f_{X|Y}(x,y) = f_X(x) \tag{4}$$

In the recent case (independent random variables), the conditional PDF becomes the marginal and the joint PDF becomes the product of the marginal distributions.

$$f_{XY}(x,y) = f_X(x) f_y(y) \tag{5}$$

Therefore, if we have (n) independent random variables $X=(X_1,X_2,\ldots,Xn)$ then the joint probability density function will be:

$$f_{\underline{X}}(\underline{x}) = \prod_{i=1}^{n} f_{X_i}(x) \tag{6}$$

As a summary, the joint probability density function (PDF) is equal to the product of the marginal distributions when all of the variables are independent.

4 Most Probable Point (MPP) concept and search methods

As it was mentioned in the introduction section of this chapter, the theoretical probabilistic methods are more efficient compared to the sampling techniques. The efficiency of the theoretical methods is due to the locating of the failed samples around the most probable point on the joint PDF. The Most Probable Point (MPP) or Design Point is the optimum point on the domain boundary [112], [114]. In order to find the MPP in a system, the coordinates of the probability density function (PDF) need to be transferred to the u-space (u is standard normal vector) [117]. By transferring the joint probability density function (PDF) to the standard normal distribution, the origin of the standardized distribution in u-space will move to zero. The values of the mean and standard deviation in the u-space will be zero and one respectively.

Fig. 4 shows the transformation steps from the uniform to standard normal distribution. In the new system (standard normal distribution) the MPP will be located in the shortest distance between the surface of the limit state function (g(u)=0) and the origin of the standardized normal distribution (zero).

Using the MPP concept will increase the analysis efficiency (particularly with the complex systems in combination with FEM analysis). The principal of the theoretical techniques used in NESSUS are based on locating the Most Probable Point (MPP) concept.

Fig. 5 shows the process of locating the most probable point (MPP) in normal standard distribution space (U space).

Definition of the importance level is demonstrated in Fig. 6.

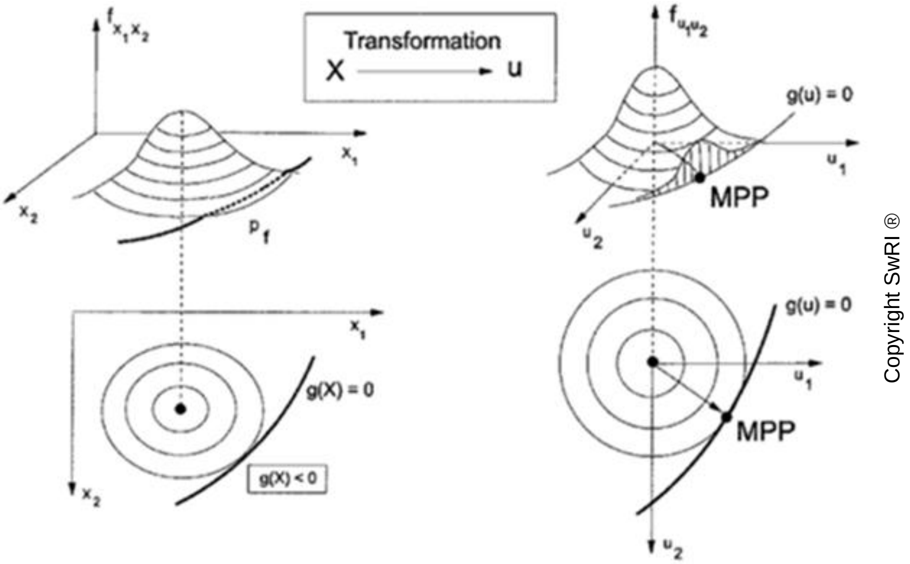

Fig. 4 Transformation from the uniform to standard normal distribution and locating the MPP [112]

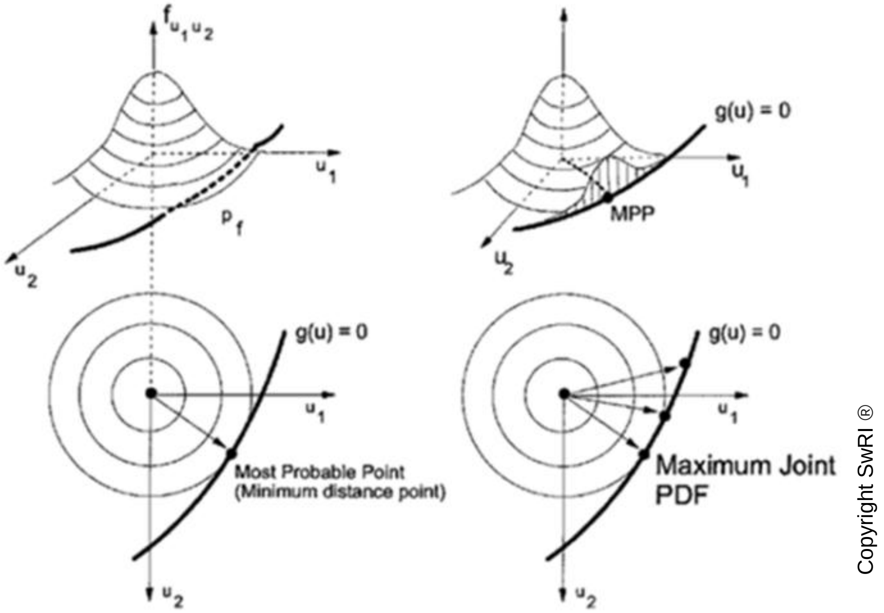

Fig. 5 Locating the MPP in standard normal distribution [112]

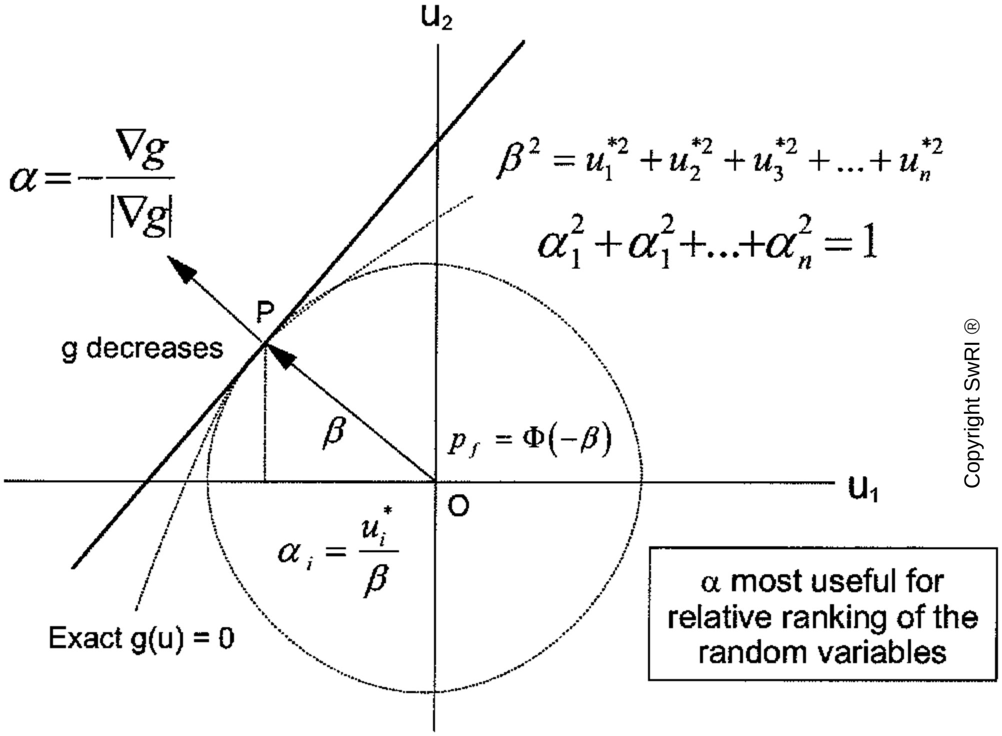

Fig. 6 Determining the importance level at MPP [112]

5 Probabilistic and reliability analysis techniques

The discussion provided in this section is based on SwRI training received during the course of this study. The information is mainly extracted from the SwRI documents [112-115] provided during the training.

As it was briefly described in introduction section of this appendix, there are different methods for probabilistic analysis which each one predicts the reliability of the system to some extent. Depending on parameters such as analysis time, complexity of the analysis (specially using the numerical techniques) and desired accuracy and confidence level, one of these probabilistic analysis techniques could be utilized.

Among these methods, the sampling approach is the most common technique for the probabilistic analysis of the complex systems with multiple limit state functions. Considering the benefits of the sampling methods such as simplicity of the analysis and accuracy of the results, the large number of required samples, long analysis time and high computing cost are the drawbacks associated with these techniques. In order to get an acceptable level of accuracy from a sampling based method (e.g. Monte Carlo) a number of samples between 100,000 to 1,000,000 are required to be analyzed and depending on the analysis time for each sample (this time could be as long as a couple of hours to days for some complex finite element models), this method could take a fairly long analysis time.

In order to avoid the long analysis time and reduce the CPU cost, the analytical methods were introduced. In these analytical methods, the process starts with identifying the most probable point (MPP) of failure. By using the analytical methods the CPU time and the number of required runs could be reduced significantly (see Fig. 86 presented in chapter 6). Beside the sampling and analytical techniques there is a third method which is called “Hybrid method”. This method uses the location of the MPP to focus the Monte Carlo sampling process around that point. By focusing the samples in the vicinity of the MPP we can get more failure points and efficient estimate of the probability compared to the standard Monte Carlo sampling. Fig. 7 shows the comparison between the basic and hybrid Monte Carlo methods.

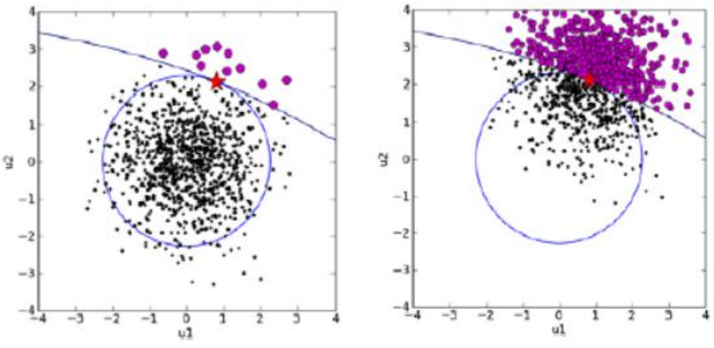

Basic Monte Carlo

MPP Based IS

Fig. 7 Comparison between the basic and hybrid Monte Carlo analysis [113] (the purple points represent the failed samples).

5.1 Sampling based probabilistic models

5.1.1 Monte Carlo (MC)

Monte Carlo is the most common sampling based method used in probabilistic analysis. Fig. 8 shows the steps of the Monte Carlo probabilistic analysis:

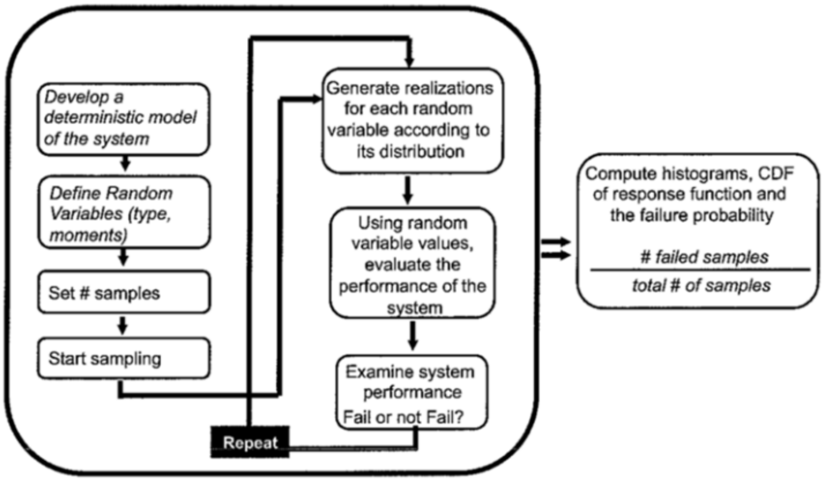

Fig. 8 Monte Carlo analysis flowchart [112]

One of the issues with the Monte Carlo method is the sample distribution order. In this method samples are not distributed evenly throughout the data range and mostly are populated around the mean value and by increasing the number of samples the distribution will slowly move towards the tails of the distribution profile. The tail regions are generally the most important regions in the probabilistic analysis since low and high probability values are important in decision making. Therefore a large number of samples are required to be processed to achieve an acceptable confidence level in sampling methods (with low number of samples, not enough samples would fall in the tail regions).

The probability of failure in Monte Carlo is defined by [114]:

$$p_f = \frac{N_f}{N} \tag{7}$$

Where N is the total number of evaluated samples and N_f is the number of the samples with negative g values or simply the number of failed samples.

Fig. 9 shows a typical PDF Vs. sample distribution graph for the Monte Carlo method.

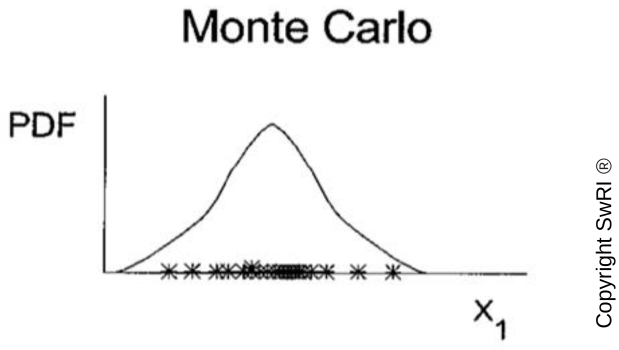

Fig. 9 PDF distribution for the Monte Carlo method [112]

The probability of failure is a random variable and as we get closer to the tail regions, the confidence level will ramp up (moving from the standard deviation of 1 to 2.6 will increase the confidence level from 68% to 99% (Fig. 10)).

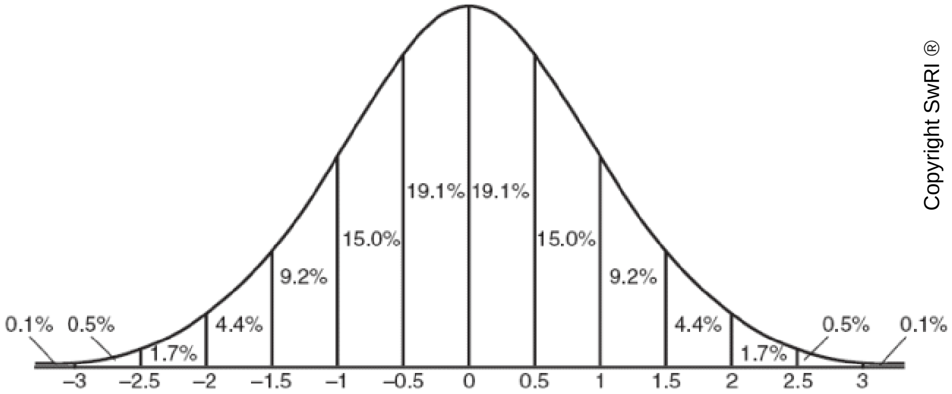

Fig. 10 Standard normal probability density function (PDF).

Some of the main advantages and drawbacks of the Monte Carlo are as follows [112-113]:

- Advantages:
    - It works with any model (e.g. FEM)
    - Simple to implement in existing software
    - The response does not need to be known in analytical form
    - Discontinuity in the model response is tolerable
    - It is used as benchmark to verify all other risk assessment methods
    - Multiple limit states are allowed
- Drawbacks:
    - Slow to estimate small probabilities with high confidence

- Large number of samples are required to be processed in order to estimate the small probabilities with relatively high confidence

5.1.2 Latin Hypercube Sampling (LHS)

In order to address the Non-equal sampling distribution in the Monte Carlo method, an alternative sampling method was introduced. This new method is called Latin Hypercube Sampling (LHS) and was introduced in 1979 [118]. Latin Hypercube Sampling technique works in the bases of the Latin square method which requires of having a square grid somehow that there is only one sample locates in each row and column of this grid (Fig. 11) [114].

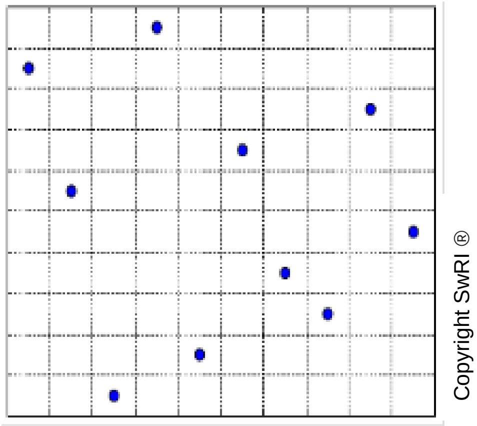

Fig. 11 Latin Hypercube sample in two dimensions of size N=10 [114]

In this technique, samples are distributed more evenly (arbitrarily) over each input variable probability distribution and the distance between the samples are maximized to improve the coverage (Fig. 12 & 13).

Using this technique will produce more failed samples compared to the standard Monte Carlo method for the same number of simulations. The efficiency of the

LHS with about 2000 samples is almost equivalent to 100000-1000000 Monte Carlo samples.

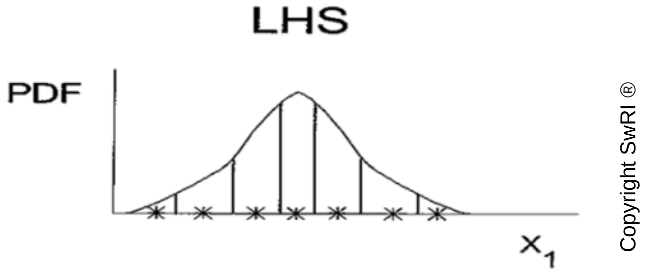

Fig. 12 Typical PDF distribution of the LHS method [112]

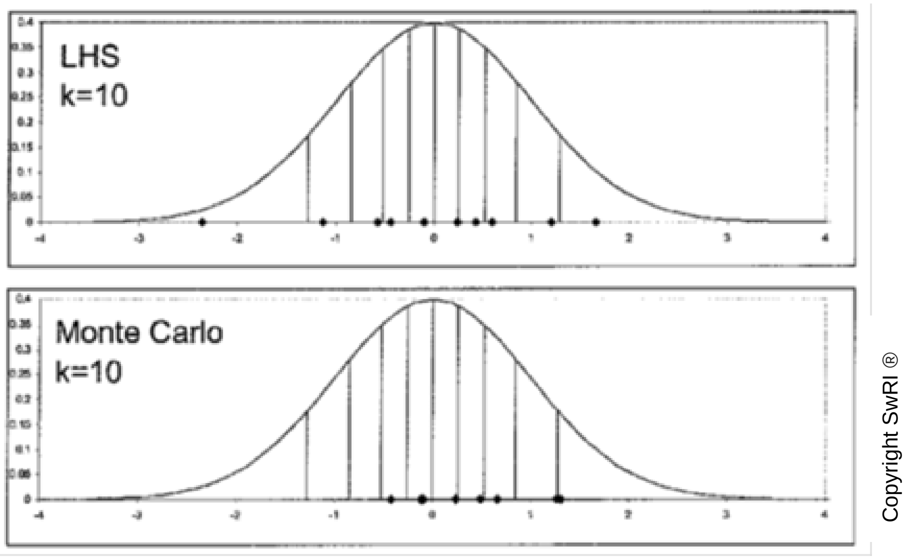

Fig. 13 Comparison between the Monte Carlo and LHS methods [112]

Some of the main advantages and drawbacks of the LHS are as follows [112-113]:

- Advantages:
    - Could be applied to any model

  - Samples are distributed more evenly compared to the standard Monte Carlo (Requires the small number of samples)
  - Typically is used for computing the mean, standard deviation and distribution of the response.
  - Supports multiple limit state functions
- Drawbacks:
  - Large number of samples are required to estimate the small probabilities

5.2 Analytical based probabilistic models

Although the sampling methods are accurate and simple to implement, but the efficiency of these type of methods are not great (Fig. 86 chapter 6). To improve the efficiency of the analysis and reduce the process time, the analytical techniques were considered. Most of these analytical methods are constructed based on the concept of "importance" sampling. Importance sampling provides the information about the failure region by targeting the most probable point (MPP). Construction of the limit state function around that MPP will minimize the computation time and will increase the efficiency of the analysis.

The First Order Reliability Method (FORM), Second Order Reliability Method (SORM), Mean value (MV), Advanced Mean Value (AMV) and Advanced Mean Value plus (AMV+) are developed using the above mentioned concept [112],[114]. The initial step of performing the analytical probabilistic analysis is locating the MPP by transformation from the uniform distribution to the standard normal distribution (Finding the MPP).

Fig. 14 and 15 display the process of transformation from uniform distribution to standard normal distribution.

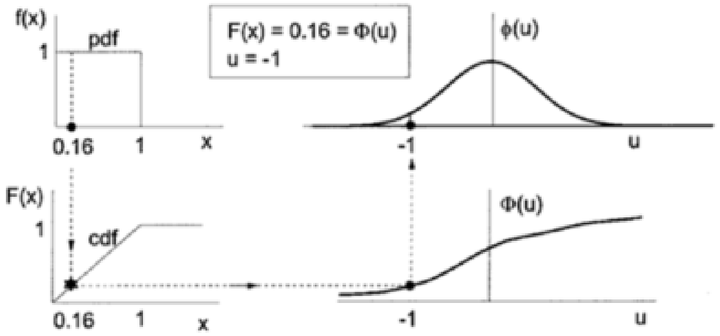

Fig. 14 Transformation from the uniform distribution to the standard normal distribution [112].

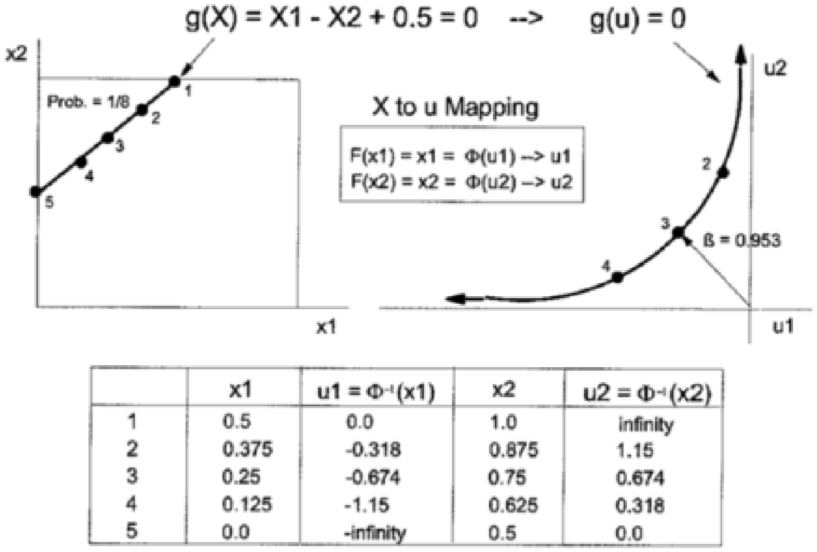

	x1	$u1 = \Phi^{-1}(x1)$	x2	$u2 = \Phi^{-1}(x2)$
1	0.5	0.0	1.0	infinity
2	0.375	-0.318	0.875	1.15
3	0.25	-0.674	0.75	0.674
4	0.125	-1.15	0.625	0.318
5	0.0	-infinity	0.5	0.0

Fig. 15 Process of transformation (mapping) from uniform to standard normal distribution [112].

5.2.1 First and Second Order Reliability Methods (FORM and SORM)

The first order reliability method (FORM) is constructed based on the linear expansion of the limit state or “g” function at the most probable point (MPP) in the u-space (Standard normal). First order reliability method (Fig. 16) was initially developed to be used in the reliability analysis of the structures [119].

In order to use the first order reliability method (FORM), the uniform distributions are required to be transformed to the standard normal space (u space):

Equation (8) shows the mathematical conversion between the uniform and standard distributions.

$$u = \Phi^{-1}[F_X(x)] \qquad x = F_X^{-1}[\Phi(u)] \tag{8}$$

The first order polynomial is in the form of:

$$g(u) = a_o + \sum_{i=1}^{n} a_i (u_i - u_i^*) \tag{9}$$

And therefore the probability of failure is a function of the minimum distance from the origin (in the u-space) and the plane formed by first order polynomial g(u).

Equation (10) demonstartes the probability of the failure in terms of the distance from the MPP.

$$p_f \approx \Phi(-\beta) \tag{10}$$

In this equation, β is the distance between the origin in u-space and the most probable point (MPP) which could be calculated using the following relation:

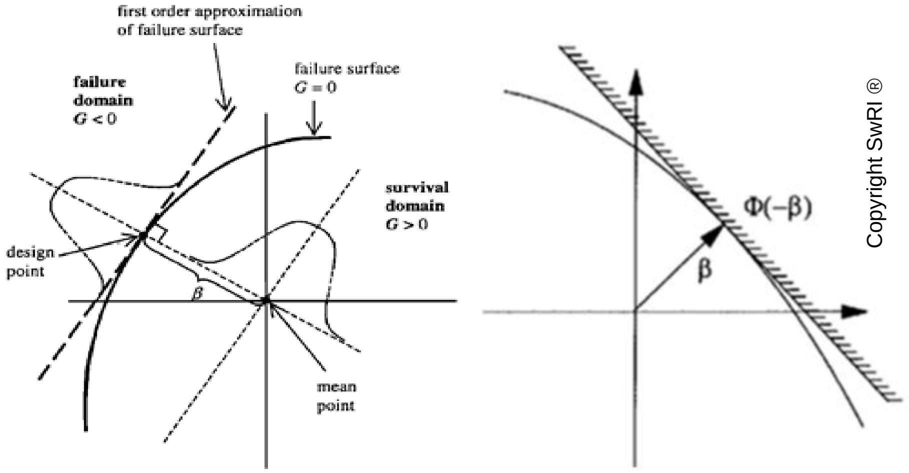

$$\beta = \frac{\mu_g}{\sigma_g} = \frac{a_o + \sum_{i=1}^{n} a_i \mu_i}{\sqrt{\sum_{i=1}^{n} a_i^{2} \sigma^{2}_{i}}}$$

Fig. 16 First order reliability method (FORM) setup [112]

Details of the First Order Reliability Method (FORM) has been reported by M. Hehenbichle [120].

Similar to the first order reliability method (FORM), the second order reliability method (SORM) is constructed based on second order polynomial expansion (quadratic approximation to g(u)).

$$g(u) = a_o + \sum_{i=1}^{n} a_i (u_i - u^*_i) + \sum_{i=1}^{n} b_i (u_i - u^*_i)^2 + \sum_{i=1}^{n} \sum_{j=1}^{i-1} c_{ij} (u_i - u^*_i)(u_j - u^*_j)$$

$$p_f \approx \Phi(-\beta) \prod_{i=1}^{n-1} (1 - \beta k_i)^{-1/2} \qquad (11)$$

The K_i is the principal curvature at the most probable point (MPP).

Fig. 17 shows the comparison between the first and second order reliability methods against the exact limit state function. The prediction from the second order reliability method is much closer to the exact limit state function. The details of the SORM are presented in reference [121].

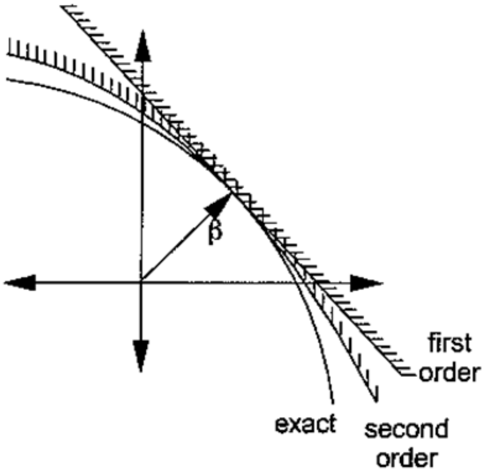

Copyright SwRI ®

Fig. 17 second order reliability method (SORM) [112]

Some of the main advantages and drawbacks of the FORM and SORM are as follows [112-114]:

- Advantages:
    - Relatively efficient for small probabilities of failure
    - Exact prediction for linear functions (FORM only) and exact prediction for parabolic surfaces (SORM only)
    - Accuracy of linear and parabolic approximations has improved for small probability of failure for FORM and SORM respectively.
- Drawbacks:
    - Locating of MPP may be difficult for non-linear functions

- Error in probability prediction for non-linear and non-parabolic limit state functions for FORM and SORM respectively.
- Applicable on single limit state function only

5.2.2 Advanced Mean Value methods (MV, AMV and AMV+)

For the systems with complex limit state functions, using the FORM and SORM would not be beneficial. In order to analyze these complex systems, the mean value based techniques were developed.

Assuming the exact response of the system as:

$$Z_{exact} = Z(X_1, X_2, X_3, \ldots., X_n) \tag{12}$$

The response of the first order mean value will be:

$$Z_{MV} = a_{\mathrm{o}} + \sum_{i=1}^{n} a_i x_i \tag{13}$$

And the mean value estimate will be:

$$\mu_z = E(Z) = a_{\mathrm{o}} + \sum_{i=1}^{n} a_i \mu_i \tag{14}$$

The estimate of the variance will be:

$$\sigma_z{}^2 = V(Z) = \sum_{i=1}^{n} a_i{}^2 \sigma_i{}^2 + \sum_{i=1}^{n} \sum_{j=1}^{n} a_i a_j \rho_{ij} \sigma_i \sigma_j \tag{15}$$

Similar calculations were done to determine the second order mean value. After obtaining the response for the mean value (Z_{MV}), this value was used to calculate the Advanced Mean Value (AMV).

$$Z_{AMV} = Z_{MV} + H(Z_{MV}) \qquad (16)$$

Where $H(Z_{MV})$ is the difference between the response of the mean value (Z_{MV}) and exact response of the system (Z_{Exact} is calculated in the most probable point of Z_{MV}).

Fig. 18 shows the steps involved in finding the response for Advanced Mean Value (AMV).

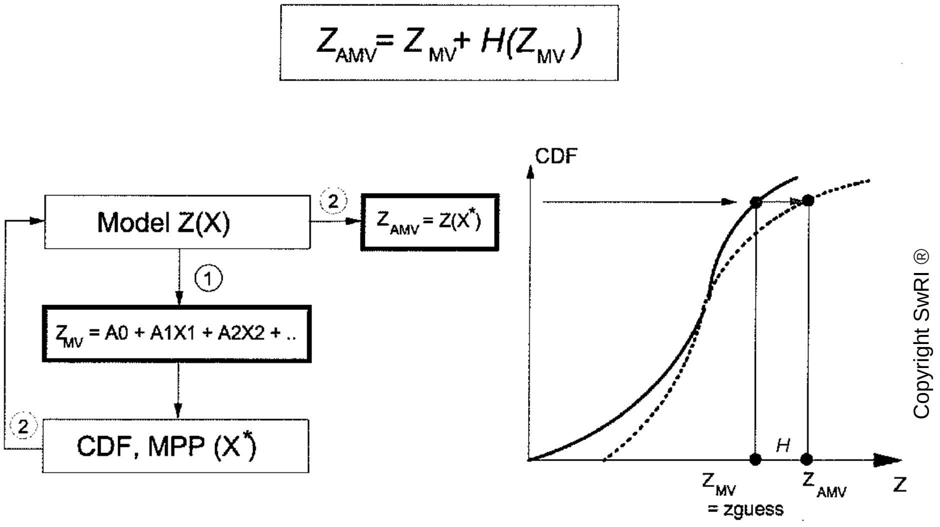

Fig. 18 Process of calculating the AMV [112].

The concept of the Advanced Mean Value plus (AMV+) is similar to the Advanced Mean Value (AMV) and is developed based on correcting the response of the Advanced Mean Value (Z_{AMV}) in the most probable point and repeating this process until the convergence of the response occurs. The final result of the Advanced Mean Value plus (AMV+) will be more accurate and close to the exact response of the system. Fig. 19 demonstrates the details of the AMV+ process.

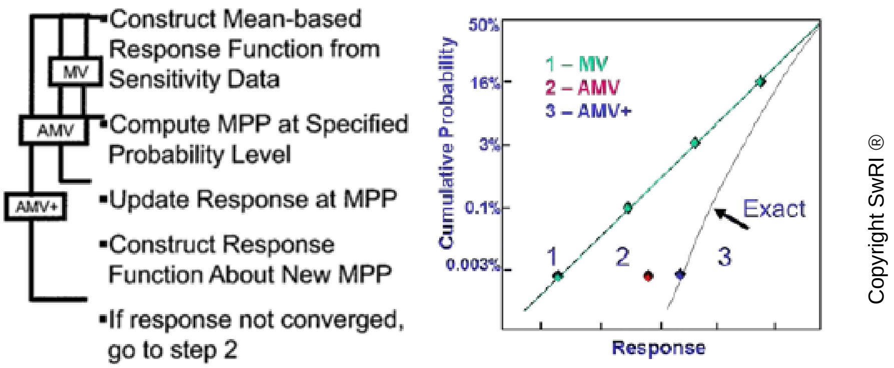

Fig. 19 Steps of the MV, AMV and AMV+ methods [112].

As a summary, the process of determining the response of the system using the (AMV+) is same as (AMV) with repetitive response correction in the most probable point until the convergence occurs.

Table. 1 Number of required FEM solutions for the MV, AMV and AMV+methods (N= number of random variables, M=number of CDF probability levels and i= number of iterations) [112].

Solution method	# FEM Solutions	Total FEM solutions
MV	N+1	N+1
AMV	M	N+1+M
AMV+	i*[(N+1)*M+M]	N+1+M+(N+2)*M*i

A simple comparison between the AMV+ and Standard Monte Carlo methods indicates relatively good efficiency and accuracy of the AMV+. AMV+ method provides detail information in the tail regions of the CDF (Cumulative Density Function) facilitating in prediction of very low and very high probability of failure. In the probability function graph, AMV+ covers the probability ranges from 1E-5 to 0.999 while the Monte Carlo only covers the ranges between the 0.01 to 0.99 [112]. The AMV+ also requires much less number of FEM runs compared to the standard Monte Carlo to generate the results (Fig. 89 chapter 6). Some of the main advantages and drawbacks of the MV, AMV and AMV+ are as follows [112-113]:

- Advantages:
    - More efficient than FORM (MPP search is performed on a fast running approximate function)
    - Exact result prediction for linear functions (composed of normal random variables)
    - Accuracy of linear approximation improves for small probability of failure
- Drawbacks:
    - Locating the MPP may be difficult for non-linear response functions
    - Applicable on single limit state function only